Development of Tools and Methods for the Characterization of the Groundwater-Surface Water Interface

By

Mackenzie M. Cremeans

Submitted to the Department of Geology and the
Graduate Faculty of the University of Kansas
in partial fulfillment of the requirements for the degree of
Doctor of Philosophy

Committee members

Dr. J.F. Devlin, Chairperson

Dr. Mary Hill

Dr. Daniel Hirmas

Dr. Leigh Stearns

Dr. Randy Stotler

Date defended: April 9, 2018

The Dissertation Committee for Mackenzie M. Cremeans certifies
that this is the approved version of the following dissertation :

Development of Tools and Methods for the Characterization of the Groundwater-Surface Water Interface

Dr. J.F. Devlin, Chairperson

Date approved: May 13, 2018

Abstract

This study focuses on water exchange, and associated processes, at the groundwater-surface water interface (GWSWI). The contributions of the study, as a whole, can be divided into two groups: scientific contributions and technical contributions. Scientifically, there are three main contributions. Firstly, the data presented below map a stream reach to show separate the effects of water flow and contaminant concentrations on contaminant mass discharge. The field demonstration of this concept, at the sub-meter scale, is novel. Secondly, the data included in the comparison of methods suggest the variability of flow across the GWSWI is large when compared with the differences related to replication of measurements. This suggests the importance of mapping in detail to ensure that all the controlling points of discharge are included. Thirdly, SBPVP measurements made a field-based mass loading calculation for a vertical flow bioreactor possible. It was found that the attenuation capacity of this system was about three orders of magnitude greater than the theoretical attentuation capacity suggested. Technically, there are five main contributions. Firstly, the design and validation of a new measurement tool to quantify flow across the groundwater-surface water interface (the streambed point velocity probe, or SBPVP). Secondly, a demonstration and comparison of the SBPVP in the field with three other, more commonly used methods. Thirdly, the development of a new method to quantify contaminant discharge into a stream using the SBPVP. Fourthly, a demonstration that the new approach can provide highly detailed information about the distribution of contaminant mass discharge, which could be of value to risk assessment and remediation design. Fifthly, the application of the SBPVP to the characterization of a vertical flow bioreac-

tor for the purpose of assessing its performance. Given these contributions, the study presents a new tool for investigating the groundwater-surface water interface and describes various applications (and their associated scientific advances) in detail.

Acknowledgements

As noted in 12th century, by John of Salisbury, new knowledge can only be discovered by "standing on the shoulders of giants" (*nanos gigantum humeris insidentes*). Nothing has proven that point to me more strongly than the daunting and formidable process of earning a Ph.D. over these last four years. As I reflect on these acknowledgments, I can't help but think of the many wonderful people who have guided me along the way. Thank you, to all of you, for your investment in me.

The availability of funding has been crucial to the completion of the work detailed in this dissertation. Over the past four years, I have been astounded by the generosity of many funding sources that have made my work possible. First and foremost, I'd like to thank the Madison and Lila Self Graduate Fellowship for providing incredible professional development experiences and great collaborative conversations, in addition to funding the entirety of my graduate research assistantship. To Dr. Stefani Buchwitz, Amy Benoit-Warlick, Tammie Zordel, and Dr. Michael Roberts, thank you for your tireless dedication to fulfilling the goals of Madison and Lila Self. The bulk of this research was conducted at the Grindsted site in Denmark. I'd like to thank GEOCON for funding this work in its entirety (Innovation Fund Denmark, contract no. 1305-00004B). Additional funding from the University of Kansas Doctoral Research Fund, the Kansas Geological Foundation, the American Geophysical Union, the Association for Women Geoscientists, and the Department of Geology was instrumental to the full completion of this research.

Scientific research is, by nature, an exercise in teamwork. I am fortunate to have started off well with my very first team I had at KU, my committee, who set the tone for the rest of the degree. To my advisor, Dr. Rick Devlin, thank you for the amazing opportunities you have afforded me throughout this process, and also, for working alongside me to ensure the success of these projects. To Dr. Mary Hill, Dr. Dan Hirmas, Dr. Leigh Stearns, and Dr. Randy Stotler: Thank you for initially agreeing to see me through this process, and for all the time and effort that followed. I've appreciated your insights, encouragement, and advice.

The idea of teamwork extends to the collaborative efforts at the Grindsted, Raadvad, and Commerce sites, where most of my dissertation work took place. To Dr. Ursula McKnight, Dr. Poul Bjerg, and Dr. Bob Nairn, thank you for numerous insightful conversations and fruitful partnerships. I have deeply appreciated your knowledge and input throughout. All three projects proved to be humbling, enlightening puzzles I truly enjoyed unraveling with you!

Of course, aside from the content of this dissertation, many hours of logistical and financial work went into making this study possible. Without the wonderful Department of Geology staff, the work of the past four years would never have been completed. Ramia, Ally, Cari, and Yolanda: Thank you all for your tireless efforts to keep projects running and your humor through everything from ridiculous travel antics to submitting this very document. You've made even the toughest experiences manageable.

Along the way, I also have been fortunate to have a few "unofficial" mentors. To Dr. Jen Roberts and Dr. Gwen Macpherson, thank you for your example, mentorship, and advice, which have truly made my experience at KU exceptional. Additionally, a heartfelt thank you to Dr. Marnie McInnes and Dr. Wayne Glausser, for being end-

lessly supportive and inspirational and to Dr. Jim Mills, Dr. Tim Cope, and Dr. Scott Wilkerson for encouraging me to pursue a Ph.D., in the first place.

Finally, I am grateful for the many wonderful friends I have made in Lawrence. Firstly, to Trevor Osorno, thank you for making the countless hours in the lab eventful and for, inevitably, reminding me that breaks are necessary and useful to productivity. To Leila Joyce, Blair Schneider, Sarah Morton, and Jeff Ross, for everything from "Wine and Whine" to breakfast to random conversations on any given day, thank you for helping to preserve my sanity. Additional thanks to Alyssa Rollando, Eileen Cadel, and Doug Orsi, for the weekly meetings of the "Self Fellow Coffee Club," which provided much laughter. And, lastly, to my "adoptive" families in Lawrence, the Struves, the Scholz, and the Gilmores, thank you for reminding me to relentlessly participate in the manifestations of my blessings.

Thanks, to all of you, for being the giants in my life.

Contents

List of Figures

List of Tables

Chapter 1

Introduction

1.1 Importance of groundwater-surface water exchange

Though groundwater is the largest source of liquid, potable drinking water on Earth (Shiklomanov, 1993), this reservoir has suffered from notable contamination from anthropogenic waste sources (Fetter, 2000). Anthropogenic waste includes, but is not limited to, industrial solvents (such as trichloroethylene and benzene) (Fusillo et al., 1985), fertilizers (nitrates and synthetic organic agricultural chemicals) (Flipse et al., 1984; Rothschild et al., 1982; Oliveira and Sitar, 1985), landfill leachate (McLeod, 1984), and, of course, emerging contaminants (such as crotamiton and carbamazepine) (Barnes et al., 2002; Lapworth et al., 2012; Richardson and Ternes, 2018). Because water can be exchanged between groundwater and surface water, waterborne contamination can travel between the two across the groundwater-surface water interface (GWSWI) (Winter et al., 1998). Therefore, understanding the details of groundwater-surface water interactions is central to understanding the fate and transport of contaminants in the overall environment (Cey et al., 1998; Winter et al., 2003; Kalbus et al., 2006; Derx et al., 2010; Anibas et al., 2012; Freitas et al., 2015). Further, characterizing the chemical interdependence of groundwater and surface water, which depends on water flux across the GWSWI, is crucial to the estimation of contaminant mass discharges for risk assessment and contaminated site monitoring (Harvey and Bencala, 1993; Conant, 2004; Weatherill et al., 2014).

Currently, groundwater (and, by extension, surface water) is legally protected by a variety of legislation. For example, the European Union passed Water Framework Directive (Directive 2006/118/EC of the European Parliament and Council) on December 12, 2006 and, to keep up with emerging contaminants, modified the original with Commission Directive 2014/80/EU in 2014. The equivalent legislation in the United States is the Safe Drinking Water Act (1974), which gives the Environmental Protection Agency authority to establish maximum contaminant level goals and maximum contaminant levels. The Safe Drinking Water Act is complemented by legislation such as the Resource Conservation and Recovery Act (RCRA) (1976) and the Comprehensive Environmental Response, Conservation, and Recovery Act (CERCLA or Superfund) (1980), which regulate hazardous waste site clean-up. As noted by Winter et al. (1998), the connection between groundwater and surface can lead to groundwater as a significant (and potentially long term) contributor to surface water contamination. With approximately 75% of RCRA and CERCLA sites located within a half mile of a surface water body (Tomassoni, 2000; Biksey and Gross, 2001), fully understanding that connection could be vital to remediation efforts.

Flow at the GWSWI is governed by a variety of factors including, but not limited to, hydraulic gradient (i), stream geometry, and hydraulic conductivity (K) distributions within the aquifer and streambed (Larkin and Sharp, 1992; Cey et al., 1998; Huggenberger et al., 1998; Woessner, 2000; Sophocleous, 2002; Fleckenstein et al., 2006; Kalbus et al., 2006; Allen et al., 2010; Binley et al., 2013; Flipo et al., 2014; Balbarini et al., 2017). These factors commonly have complex distributions at groundwater-surface water interfaces (e.g. a stream or lake beds). Therefore, distributions of flow across the groundwater-surface water interface should be expected to have an equally complex distribution. Nevertheless, exchange interfaces are often treated as uniform boundaries, for reasons of convenience, lack of data, limits on computing power, or numerical instability in models (Balbarini et al., 2017). The first step to improving the description of a streambed and its associated discharge zones, is to conduct measurements of flow across the GWSWI, to localize and quantify

the discharge zones in the greatest detail that can practically be achieved. Therefore, methods to quantify groundwater-surface water exchange quickly and accurately, and at an appropriately small scale, are desirable.

1.2 Methods of measuring flow across the GWSWI

1.2.1 Review of methods

A variety of methods have been developed to measure flow across the GWSWI. These methods include tools such as mini-piezometers, seepage meters, tracers, and temperature profilers, all of which have demonstrated cases of successful application. However, none of the existing technologies has proven universally applicable, with limitations arising from device design, or cost and time requirements as well as measurement sensitivity to physical and chemical conditions on the streambed (Dakin et al., 1985; Baxter and Hauer, 2000; Baxter et al., 2003; Rosenberry and Morin, 2004; Zamora, 2006; Schmidt et al., 2006, 2007; Rosenberry et al., 2008; Tyler et al., 2009; Vogt et al., 2010; Briggs et al., 2012; Matheswaran et al., 2014).

Darcy calculations, a relatively common method of quantifying discharge (Baxter and Hauer, 2000; Baxter et al., 2003; Rosenberry and LaBaugh, 2008), rely on accurate knowledge of hydraulic conductivity (K) and hydraulic gradient (i). K can be conveniently obtained *in situ* from slug tests using mini-piezometers to access the sediments (various methods of sediment testing in the laboratory are also commonly used, e.g., grain size analysis and permeametry). i must be measured in the field. Further details regarding Darcy calculations, and the associated methods, are given in Chapters 3 and 4.

Seepage meters are another commonly used, inexpensive tool to measure water flux across the GWSWI. This tool provides a "direct" measurement of flux across the GWSWI, which sets it apart from most other methods (i.e. a seepage meter takes a direct measurement of the volume of water

that crosses a known area of the streambed over time). Unfortunately, seepage meters cannot be easily installed in hard sediments or in deep water. Additionally, several design-related sources of error have been shown to sometimes lead to significant negative biases in the measurements (Murdoch and Kelly, 2003; Rosenberry, 2008). In some cases, these design-related biases have been overcome with adequate modifications (for example, Solder et al. (2016)).

Another approach to quantifying flow is to measure the progress of tracers. Originally, tracer tests were conducted in aquifers and several tracers have proven useful in this regard. For example, environmental tracers (such as ^{3}H, ^{2}H, ^{18}O) and injected tracers, have been used to estimate groundwater velocities in aquifers at a variety of scales since the late 1800s (Thiem, 1887; Slichter, 1902, 1905; Robertson and Cherry, 1989; de Souza et al., 2015). Most tests tend to focus on a scale of less than a few hundred meters, though spills have also been opportunistically exploited for larger scale investigations (Mackay et al., 1986; van der Kamp et al., 1994). As interest in groundwater-surface water exchange grew, tracer-based methods were adapted for GWSWI investigations. These methods include tracers that can be injected into the stream or streambed (lake or lakebed, etc.), and tracers such as ambient heat (which can vary with depth) (Harvey et al., 1996; Anderson, 2005). While tracer tests are expected to provide more velocity data that approach a 'direct' measurement than methods that depend on indirect metrics such as hydraulic head or heat gradients, they tend to be relatively time-intensive and cost-prohibitive for many projects.

To reduce the cost and time requirements of tracer tests, technologies were developed that focused on smaller scale measurements, in particular, those conducted from a single well. Interest in single-well groundwater velocity measurements began with the borehole dilution method, which equates the ambient groundwater velocity to the flushing time of a tracer from a borehole (or well) (Drost et al., 1968; Bernstein et al., 2007; Halevy et al., 1967). Other in-well techniques use proprietary commercial devices, and include the Geoflo® meter, the colloidal borescope, and the VECTOR® Groundwater Flowsensor (also known as the In Situ Permeable Flow Sensor or ISPFS) (Kerfoot

and Massard, 1985; Kearl, 1997; Su et al., 2006).

These tools have many advantages, relative to tracer tests, including generally being faster and less cost prohibitive. However, they also have some disadvantages, particularly notable error related to flow deviations associated with well screens and filter packs (Johnson, 1963; Kerfoot and Massard, 1985). While potentially useful for aquifer testing, these methods are not designed for use in stream and lake environments (i.e. installing multiple wells in streams or lakes would be costly and time intensive). Moreover, in-well methods utilize wells that extend vertically over some distance (commonly on the order of a meter). This scale of measurement could be too large to catch the details of flow in stream or lake bed, where patterns of discharge can be heterogeneous on a sub-meter scale. Because of these limitations, and the fact the in-well methods can only measure velocities in the vicinity of streams (not in streams themselves), the convenience of in-well devices is often offset by the potential measurement errors and the differences in flow between stream banks and stream beds.

Efforts to gain a multifaceted understanding of groundwater-surface water exchange have combined methods for a more complete characterization of groundwater discharge at a boundary. For example, in Becker et al. (2004), current meter measurements and temperature surveys were combined within a model to provide a detailed quantification of heterogeneous groundwater flow that was regarded as an enhancement to the individual methods. In another example, Ivkovic (2009) combined data from multiple scales, using five separate sources of data (groundwater and river channel base elevations from GIS databases, flow duration data, stream hydrograph data, vertical aquifer connectivity data from nested piezometers, and paired stream and groundwater hydrographs). Though these investigations, and others, represented advances in the field by improving data effectiveness, none of the studies resulted in datasets with the detail necessary to describe any single exchange zone (Conant, 2004; Freitas et al., 2015).

1.2.2 The streambed point velocity probe

The streambed point velocity probe (SBPVP), developed over the course of this dissertation, is designed to circumvent case-specific limitations of the above methods, or to serve as a complementary, independent source of flow information in cases where the other methods perform well (Cremeans and Devlin, 2017). Measurements with the SBPVP are not reliant on the estimated parameters required for Darcy's Law calculations (n and K), nor do they rely on the measurement of i. The device measures seepage velocity by timing the movement of a tracer across the probe surface, on the scale of about a centimeter. An advantage of such a small-scale test is that the time to complete a measurement is generally quite small – under two hours for seepage velocities of 0.5 m/d or greater. The slowest field measurement so far encountered was approximately 3.5 hours, corresponding to a seepage velocity of 18 cm/day. Another advantage of the tool is that it makes possible a high density of measurements in a relatively short period of time. Its primary limitation is that it is only tested for operation in sediments that are unconsolidated and soft enough for installation by hand. Thus far, this includes sandy stream bottoms (Grindsted, Denmark), interfaces made of primarily organic material (Commerce, Oklahoma). Preliminary testing has begun in mixed sediment settings (see Raadvad Preliminary Data, in the appendices) but further work is needed to determine the SBPVP's suitability for that setting.

1.3 The field sites as representative case studies

Over the course of this thesis, two field sites are the subjects of study. The main site is a reach of the *Grindsted Å* which flows from west to east through Grindsted, Denmark. The stream is naturally meandering (with few modifications) and groundwater-fed (median flow of 2000 L/s), ranging from 1 to 2.5 m deep and 8 to 12 m wide (Nielsen et al., 2014; Sonne et al., 2017). The upper aquifer includes 10 to 15 m of Quarternary sand underlain by 65 to 70 m of Tertiary sand which is hydrologically connected to the stream (Heron et al., 1998). A thick clay layer is beneath the Tertiary sand at approximately 80 meters below ground surface (Sonne et al., 2017). The stream is

contaminated by a complex mixture of compounds including chlorinated solvents, sulfonamides, barbituates, and BTEX (benzene, toluene, ethylbenzene, and xylene) (Holm et al., 1995; Kjeldsen et al., 1998; Hunkeler et al., 2011; Petersen, 2012). This study only considers the discharge of chlorinated solvents into the *Grindsted Å* (i.e. tetrachloroethene (PCE), trichloroethene (TCE), dichloroethene (DCE), and vinyl chloride (VC)). These compounds are expected to originate at a pharmaceutical factory site (in operation from 1914 to 1999) approximately 1.5 km north of the stream (Nielsen et al., 2014; Rasmussen et al., 2016; Balbarini et al., 2017; Sonne et al., 2017).

When contaminant plumes, such as the mass of chlorinated solvents in Grindsted, interact with surface water bodies, contaminants necessarily pass through groundwater-surface water interfaces (Kim and Hemond, 1998; Lorah and Olsen, 1999a,b; Yamamoto et al., 2001; Chapman et al., 2007; Ellis and Rivett, 2007; LaSage et al., 2008; McKnight et al., 2010; Rivett et al., 2012). As discussed earlier, flow across the GWSWI is likely a common occurrence at contaminated sites. Several factors, including notable heterogeneity, may affect the location and magnitude of inputs from the plume. Therefore, information regarding the influence of that heterogeneity on flow (and, by extension, mass discharge) could be useful for the design of remediation and monitoring plans (Balbarini et al., 2017). Chapter 4 of provides a case study demonstrating the potential usefulness of the SBPVP at sites where contamination is discharging into a stream.

As mentioned above approximately 75% of hazardous waste sites regulated by CERCLA, or Superfund, have the potential for exchange of contaminants across the groundwater-surface water interface. In Commerce, Oklahoma, spring water originating in the Tri-State Superfund area (southeastern Kansas) rises to the surface under artesian flow conditions and is collected in a manmade passive treatment system (described in more detail in Chapter 5). The pond evaluated in this study was designed to serve as a vertical flow bioreactor (VFBR). As such, its performance was expected to depend on loading rates and residence times of the water in the reactive pond bed material (primarily organic matter, underlain by a geotextile liner). This site is a case study representative of

engineered systems, and the application of the novel methods developed here to study them.

In summary, both of the study sites that were visited in this work fall within the range of typical geological (and geo-engineered) settings, and therefore provide data that can be used to infer general conclusions that may apply to other sites.

1.4 Outline of the study

1.4.1 Statement of goals and objectives

This study expands the knowledge of water exchange across the GWSWI by using high-density datasets (from measurements in the GWSWI itself) to evaluate these flows. This study focuses, in part, on characterizing a contaminated field site where natural groundwater-surface water exchange involves measurable levels of contaminants. To broaden the settings examined, a geo-engineered system is also included.

To accomplish this task, a new tool was needed to effectively and rapidly characterize fluxes at the groundwater-surface water interface. Therefore, the first objective of this study is to develop and laboratory validate a new device capable of generating high-density datasets at the groundwater-surface water interface in a time-efficient and cost-effective way, while also minimizing potential sources of error. This tool is called the streambed point velocity probe (SBPVP).

The second objective of this study is to apply the fully developed and laboratory validated SBPVP to the *Grindsted Å* field site, to determine if the device worked in field settings. Data from the SBPVP will be gathered alongside data from conventionally used methods, such as Darcian calculations and temperature profiling to make this assessment in a preliminary fashion while also addressing the third and fourth objectives, below.

The third objective of this study is to fully evaluate the SBPVP against established tools for measuring flow across the GWSWI. For comparative purposes, co-located measurements using mini-piezometers, streambed point velocity probes, temperature profilers, and seepage meters will be directly compared to determine the technologies that provide the most accurate and precise estimations of flow across the GWSWI. Furthermore, this assessment will address the range of seepage velocity estimates that the various technologies can handle.

The fourth objective of this study is to apply the high-density datasets to field problems to gain further insight into patterns of groundwater-surface water exchange and their influence on contaminant mass discharges. These applications occurred at the Grindsted site and a second site at Commerce, Oklahoma. At Grindsted, datasets from SBPVPs, mini-piezometers, and temperature profilers were used in concert with pore water concentration data to describe the spatial distribution of contaminant mass discharge. At the Commerce site, data from the SBPVP will be used to calculate a theoretical contaminant removal rate in a vertical flow bioreactor.

1.4.2 Overview of the dissertation

This dissertation is presented in six chapters.

Chapter 1, as presented above, contains a literature review of relevant technologies, advances, and importance of the groundwater-surface water interface. Additionally, chapter 1 outlines the objectives of this study and introduces the topic of this dissertation by presenting the structure of the remaining chapters below.

Chapter 2 addresses the first objective of this dissertation: to develop and laboratory validate the SBPVP. This chapter describes the design and preliminary testing of the streambed point velocity probe (SBPVP) in a Nested Storage Tank (NeST). Comparison of theoretical and measured velocities, injection styles, injection depth, variable pumping velocity, and variable installation depths

will be included in the discussion of the suitability of the SBPVP for measuring centimeter-scale groundwater velocities at simulated groundwater-surface water interfaces.

Chapter 3 compares the SBPVP with other tools applied at the *Grindsted Å* along a transect running parallel to the north shore of the stream. The methods discussed include mini-piezometers, SBPVPs, temperature profilers, and seepage meters. Aside from discussing the differences between each of the estimates of seepage velocity, the advantages and disadvantages of using each method are discussed as they are compared with each other.

Chapter 4 discusses the field application of the SBPVP in the *Grindsted Å*. In this chapter, high-density datasets from three tools (mini-piezometers, temperature spears, and the SBPVP) are presented and mapped to show the spatial distribution of discharge into the stream. This data is then paired with pore water concentration data to map the spatial distribution of contaminant mass discharge of chlorinated ethenes (PCE, TCE, cDCE, and VC), lending insight to the areas of high and low contaminant discharge within the streambed. Such information could be important to the design of monitoring and remediation programs at this site.

Chapter 5 discusses the use of the SBPVP in a new environment, a vertical flow bioreactor (VFBR) in Commerce, Oklahoma. The substrate in the VFBR is largely composed of organic material, which is a departure from the sandy streambed of the *Grindsted Å*. A preliminary study was conducted and the data was used to calculate a water balance as well as a removal rate of harmful constituents in the minewater passing through the VFBR.

Chapter 6 is discusses the general conclusions of the work in the preceding chapters, as well as future directions and recommendation for the continuation of this line of research.

Chapter 2

Validation of a new device to quantify groundwater-surface water exchange

As published in the Journal of Contaminant Hydrology, 2017

2.1 Abstract

Distributions of flow across the groundwater-surface water interface should be expected to be as complex as the geologic deposits associated with stream or lake beds and their underlying aquifers. In these environments, the conventional Darcy-based method of characterizing flow systems (near streams) has significant limitations, including reliance on parameters with high uncertainties (e.g., hydraulic conductivity), the common use of drilled wells in the case of streambank investigations, and potentially lengthy measurement times for aquifer characterization and water level measurements. Less logistically demanding tools for quantifying exchanges across streambeds have been developed and include drive-point mini-piezometers, seepage meters, and temperature profiling tools. This project adds to that toolbox by introducing the streambed point velocity probe (SBPVP), a reusable tool designed to quantify groundwater-surface water interactions (GWSWI) at the interface with high density sampling, which can effectively, rapidly, and accurately complement conventional methods. The SBPVP is a direct push device that measures *in situ* water velocities at

the GWSWI with a small-scale tracer test on the probe surface. Tracer tests do not rely on hydraulic conductivity or gradient information, nor do they require long equilibration times. Laboratory testing indicated that the SBPVP has an average accuracy of $\pm$ 3% and an average precision of $\pm$ 2%. Preliminary field testing, conducted in the *Grindsted Å* in Jutland, Denmark, yielded promising agreement between groundwater fluxes determined by conventional methods and those estimated from the SBPVP tests executed at similar scales. These results suggest the SBPVP is a viable tool to quantify groundwater-surface water interactions in high definition in sandy streambeds.

Keywords: groundwater-surface water; exchange; technology; tracer test

Highlights:

-A new point measurement tool, the streambed point velocity probe (SBPVP) is presented.

-The tool quantifies groundwater-surface water exchanges on the basis of a tracer test.

-The SBPVP measures with an accuracy of $\pm$ 3% and a precision of $\pm$ 2% in the lab.

2.2 Introduction

For decades, it has been recognized that humans create more waste than the environment can absorb (Freeze and Cherry, 1979; Hiscock and Bense, 2014). Unfortunately, groundwater is often the receptacle for anthropogenic waste, in spite of its importance as the largest source of accessible, potable water on Earth. Because surface water and groundwater are connected systems, understanding solute exchange at the groundwater-surface water interface (GWSWI) is important in contaminant transport studies. In hydrogeologic investigations, Darcy calculations are commonly used to quantify discharge rates between groundwater and surface water. However, these calculations are subject to errors from uncertainties in hydraulic conductivity (K) and other scale-related aspects of the analysis, e.g., difficulties may exist obtaining accurate hydraulic gradients in streambeds, where physical and chemical changes can occur over very short distances (Harvey et al., 2013; Post and von Asmuth, 2013; Devlin and McElwee, 2007; Butler et al., 2002; Zemansky

and McElwee, 2005; Molz et al., 1989). Alternative technologies have been developed to supplement Darcy calculations and circumvent these problems. For example, seepage meters measure specific discharges across the groundwater-surface water interface (GWSWI) without reference to K or hydraulic gradient (Lee, 1977; Solder et al., 2016). However, they are not easily installed in deep streams, or in streambeds with complex topography. Additionally, they are subject to biases if the devices do not seal well with the streambeds or if streambed permeability is susceptible to alteration during installation. In addition, seepage meters are subject to head losses associated with the various parts of the apparatus, which may cause underestimations of seepage flux (Rosenberry, 2008; Rosenberry and LaBaugh, 2008; Murdoch and Kelly, 2003).

An alternative method that has gained recent popularity is temperature profiling (Keery et al., 2007). While temperature-based water flux estimations have been gaining acceptance for over a decade, they are subject to possible biases in some cases. For example, vertical temperature gradient measurements may be affected by horizontal hyporheic flow, which can vary in magnitude and depth on a site-specific basis (Schmidt et al., 2007; Bhaskar et al., 2012; Irvine et al., 2016). However, errors associated with heat-flux analytical solutions are typically equal to, or less than, those associated with Darcy-flux (Lautz, 2010).

Point velocity probes (PVPs) were developed to provide direct, centimeter-scale measurements of groundwater velocity without the sources of error associated with wells, or other pre-existing tools and methods. Based on previous experiences measuring groundwater velocities in a variety of aquifer settings, the PVP was considered suitable, with modifications, for use measuring flow across the GWSWI (Labaky et al., 2007, 2009; Berg and Gillham, 2010; Schillig et al., 2011; Kempf et al., 2013; Devlin et al., 2012). The aim of this work was to adapt the PVP probe design for rapid deployments in stream settings, for the purpose of measuring water exchanges across the GWSWI. As a first step toward this goal, the new tool was validated in a laboratory setting and then deployed for preliminary comparative tests against conventional methods, in a natural stream.

2.3 Methods

2.3.1 Probe design

The streambed point velocity probe (SBPVP), an adaptation of the original PVP, is designed to measure vertical flow through a streambed. To effectively work in a streambed environment, the SBPVP is a smaller diameter tool than the PVP, with only vertical detectors (as opposed to horizontal and vertical detectors), and is a re-deployable tool (as opposed to a tool installed in a dedicated borehole) (Labaky et al., 2007; Walter and Devlin, 2017). The SBPVP was designed as a small-diameter direct-push device to facilitate the deployment of the probe in the top few centimeters of the streambed sediments (Figure 2.1). Measurements are made by performing a mini-tracer test, *in situ*, on the probe surface. To prevent horizontal hyporheic flow from flushing the tracer away from the probe (preventing breakthrough at the detectors), a shield was designed to surround the probe and effectively isolate the vertical component of flow in the streambed for the SBPVP to measure (Figure 2.1B). The injected tracer is transported to detectors by ambient groundwater flow producing breakthrough curves (BTCs) from which seepage velocities can be estimated. Modeling and experimental field trials suggest that the transition from ambient flow to purely vertical flow inside the cylinder occurs over a relatively short distance compared to the probe placement in Figure 2.1A. Flow direction (upward or downward) is indicated by the location of the detector that registers the response to the tracer. In the current design, the detectors are sensitive to contrasts in electrical conductance, as described by Labaky et al. (2007). Therefore, in freshwater systems, a chloride salt tracer is typically used (up to 1 g/L). For each test, only a small volume of tracer solution is injected (0.05 mL to 0.5 mL).

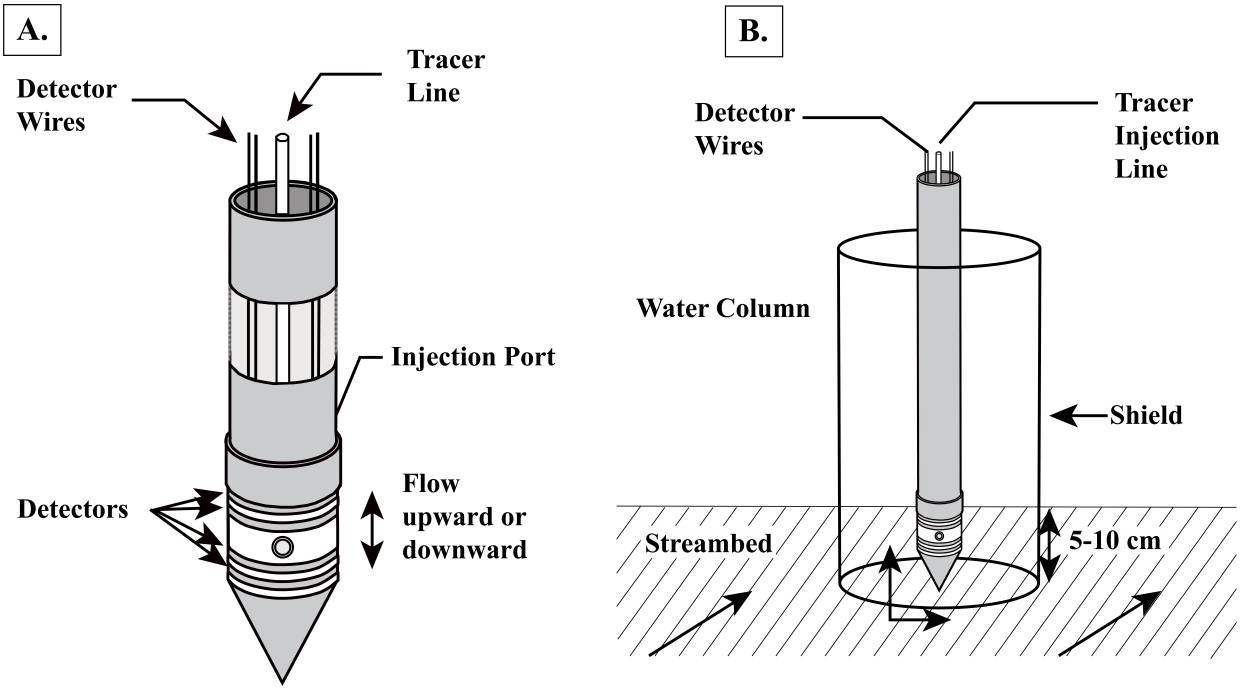

Figure 2.1: (A) A schematic view of the streambed point velocity probe (SBPVP). The measuring component of the SBPVP is a drive point with two detector pairs (four metal rings) separated by ABS plastic rings and an injection port. The SBPVP has a 3.6 cm outer diameter. A 12-strand copper core cable and an injection line connect the device to a datalogger and carry tracer to the surface of the probe, respectively. (B) A schematic of the SBPVP with the shield (outer diameter 22 cm), as installed in a streambed. The shield separates the potentially non-vertical flow (angled arrows) into horizontal and vertical vectors (horizontal and vertical arrows) for measurement purposes.

In this study, the progress of the tracer was recorded with a Campbell Scientific CR1000 datalogger programmed to collect data points at 1 s intervals. The BTCs generated by each tracer test were processed with the free software, VelProbePE (Schillig, 2012). The software generates an estimate of the velocity by fitting the BTCs with either a one-dimensional solution to the advection-dispersion equation (fit on velocity and dispersivity) or by the method of moments (Freyberg, 1986).

2.3.2 NeST streambed simulator

The SBPVP was tested in laboratory tanks that were constructed using the Nested Storage Tank (NeST) design described by Bowen et al. (2012). The NeST comprised a water-filled compartment that served as the source reservoir, a saturated sand compartment, and an outer housing tank that served as a precaution against leakage. To adapt the NeST to mimic vertical flow through a streambed, water was directed from the source tank through a customized flow distribution box in the bottom of the saturated sand tank, through the sand medium to an overlying pond of water (Figure 2.2). The flow distribution box was constructed of ABS plastic that was printed with a U-Print 3D printer by Dimensions. The floor comprised 16 interlocking pieces, which were printed at the maximum size allowed by the 3D printer (17 cm by 14.5 cm). The connected segments established a near-uniform constant head boundary on the floor of the sand-filled tank. The interlocking segments comprising the top of the flow distribution floor were fabricated with 70 perforations each. The purpose of these perforations was to direct flow upward into the sand. All seams between segments were sealed with waterproof epoxy to ensure flow out of the floor only occurred through the perforations. The water flowed upward through the sand into a standing pool of water, simulating groundwater discharge through a streambed (with no horizontal hyporheic flow) into a channel. A peristaltic pump recirculated the water from the pool back into the reservoir compartment to maintain a constant hydraulic gradient across the sand (Figure 2.2). Pumping rate was measured before and after each test period to verify constant flow rates and provide the data needed to calculate an 'expected' velocity through the tank.

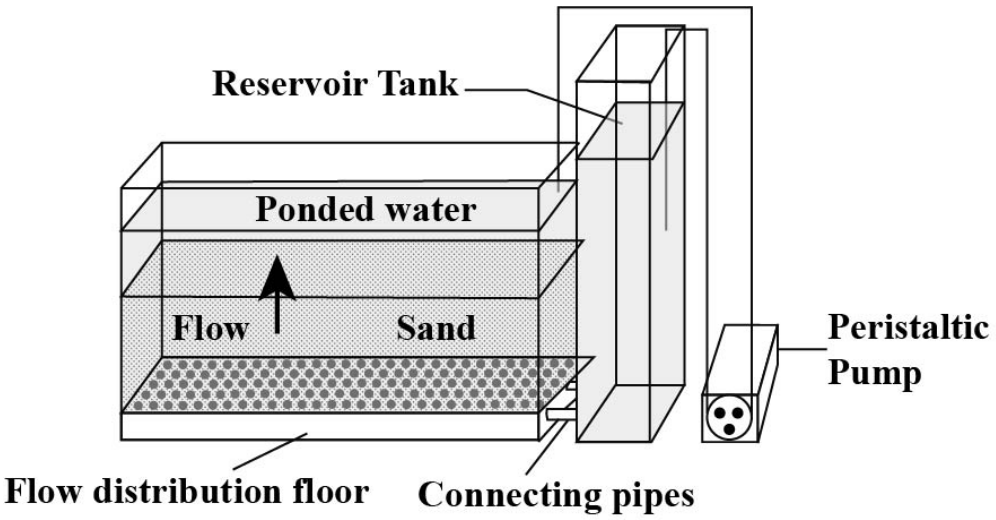

Figure 2.2: The schematic of the NeST, showing water flowing from the high head reservoir tank into flow distribution floor, which directed the water upward into the saturated sand tank and eventually into the ponded water. A peristaltic pump operating at a constant pumping rate serves to maintain the head difference between the sand tank and the reservoir tank.

Flow rates through the sand could be adjusted by varying the pumping rate. Quantitative estimates of seepage velocity in the sand were obtained from:

$$v_{expected} = \frac{Q}{nA} \tag{2.1}$$

where $v_{expected}$ is the expected seepage velocity of the water in the sand, Q is the pumping rate – which is also the total discharge rate of water through the sand, n is the effective porosity of the sand, and A is the horizontal cross-sectional area of the sand-filled tank. The probe was assessed for accuracy and precision over a range of groundwater velocities between about 50 and 450 cm/day, selected based on both equipment limitations and range of expected flow rates at a field site selected for later testing of the device (see the Preliminary Field Assessment section). However, based on the measurement range of the original PVP, it is expected that the SBPVP should have a lower limit on the order of a few centimeters per day. Field testing has shown the instrument can also measure velocities in excess of 10 m per day (Figure 2.7A). Therefore, the full range of measurement for this device is yet to be determined and should be addressed in future work. Total porosity was assumed

equal to the effective porosity and was estimated gravimetrically from a core of the saturated sand collected at the end of the testing. An estimation of porosity (specific to the tank) was derived from:

$$n = \frac{\frac{M_{wetsed} - M_{drysed}}{p_w}}{V_{core}} \tag{2.2}$$

where n is porosity, M_{wetsed} is the mass of saturated core sediment (M), M_{drysed} is the mass of dry core sediment (M), p_w is the density of water (M/L^3), and V_{core} is the volume of the saturated core (L^3). In all tests, tracer injections were conducted manually using 1.0 mL syringes. The best results were obtained when the tracer injections were 0.3 mL in volume, delivered over 15 to 25 s with a tracer concentration of 0.5 g/L NaCl.

2.3.3 Modeling

The design of the experimental apparatus lent itself well to the use of simple models to simulate the flow through the sand. Some complexity was introduced by the presence of seams between the floor panels, which created non-uniformities in flow at the bottom of the sand. To gain insight into the extent of vertical influence the seams had on flow in the tank, a two-dimensional (2D) steady-state flow simulation was executed. The model was constrained with no-flow boundaries on the left and right sides, a constant head boundary on the top, and a repeating series of constant flux nodes (representing the floor perforations), separated by no flow nodes (the seams), along the bottom. Homogeneous, isotropic, steady-state conditions were assumed throughout the sand. The model grid was 21 nodes vertically by 36 nodes horizontally, with $\Delta x = \Delta y = 1$ cm. The results of the modeling assessment were subsequently compared to experimental measurements of vertical flow with the SBPVP in the NeST, at vertical distances of 1.5 cm, 3.0 cm, 7.5 cm, 9.5 cm, 11.5 cm, and 13 cm above the tank floor, directly above a seam. Further details about this model can be found in the appendices.

2.4 Results and discussion

2.4.1 Determination of best deployment depth

To facilitate the visualization of locations where flow was most affected by the floor seams in the tank, the calculated vertical gradients from the model were normalized to the gradients calculated at the top of the sand, i.e., the furthest distance from the tank floor. The normalized gradients ($grad_{normalized}$) took values > 1 where flow entered the sand – over the floor perforations – and < 1 in the no-flow zones above the seams (Figure 2.3A). The modeling indicated that at 8 cm above the bottom of the tank, the gradient was 99% of that at the top, suggesting that SBPVP measurements made above this position would be unaffected by non-idealities at the lower boundary. Since the tank was generally packed to a total depth of about 20 cm, the critical depth was predicted to be 12 cm. Additional modeling conducted to determine the influence of the SBPVP shield on measurement quality suggested no biases would result from its use.

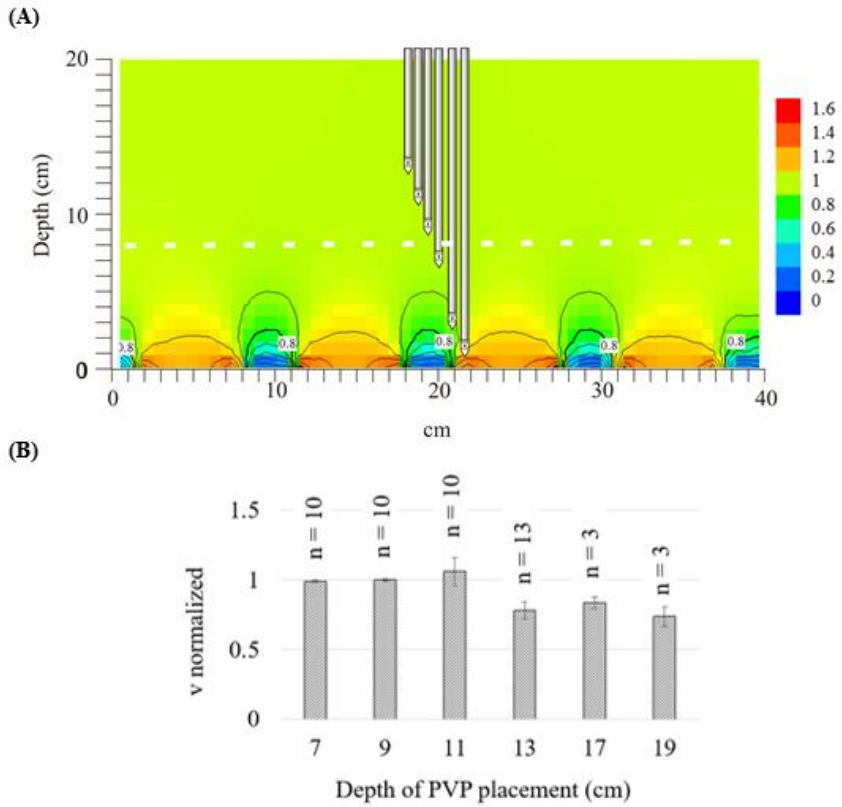

Figure 2.3: (A) Cross-section of the modeled relative to hydraulic gradient (across the NeST, with the depths of SBPVP measurements superimposed. The white dotted line shows the depth below which measurements underestimated seepage velocities compared to the expected seepage velocities. All SBPVP tests were conducted directly over a floor seam (indicated by low relative gradients); the offsets in the SBPVP placements are shown for clarity of presentation only. (B) Normalized velocities as a function of installation depth, as determined experimentally. The total sand depth in the tank is 20 cm. Measured velocities were biased low at depths > 13 cm.

2.4.2 Variable depth tests

To discern if installation depth has an effect on measurement accuracy in the tank experimentally, a series of tests were conducted to determine the depth range over which the SBPVP could be installed without introducing biases to the velocity measurements. As discussed above, the numerical simulations suggested that boundary effects would not measurably influence upward flow in the tank at depths less than about 12 cm (measured downward from the GWSWI). In practice, negative biases up to 20% from expected velocities occurred when the probe was pushed to depths > 11 cm, exceeding the biases predicted by the modeling (Figure 2.3B). This result indicated that experimental artifacts not related to the floor seams were present. The source of the artifacts is not known for certain, but it is likely that they are a result of changes to the porous medium induced by pushing the probe into place. Labaky et al. (2009) observed biases of a similar nature when direct push techniques were used to install a PVP in the C.F.B. Borden aquifer. On this basis, all subsequent testing was limited to depths < 9 cm from the GWSWI, where biases were apparently less than the resolution of the probe.

2.4.3 Variable velocity tests

In total, ninety tests were conducted (in 10 sets of 9 replicates) to assess the SBPVP's performance over a range of velocities (50 to 450 cm/day) at installation depths between 7 and 9 cm from the top of the sand (11 to 13 cm from the bottom of the tank). The tests lasted between 7 and 40 min for this velocity range. The conditions of the NeST testing were such that flow was expected to be entirely vertical. Therefore, the shield apparatus was not expected to be necessary to ensure the integrity of SBPVP measurements. This expectation was verified in tests conducted with and without the shield (from 50 to 300 cm/day). Excellent agreement was observed between these two conditions (Figure 2.4). All subsequent testing was conducted with the shield in place.

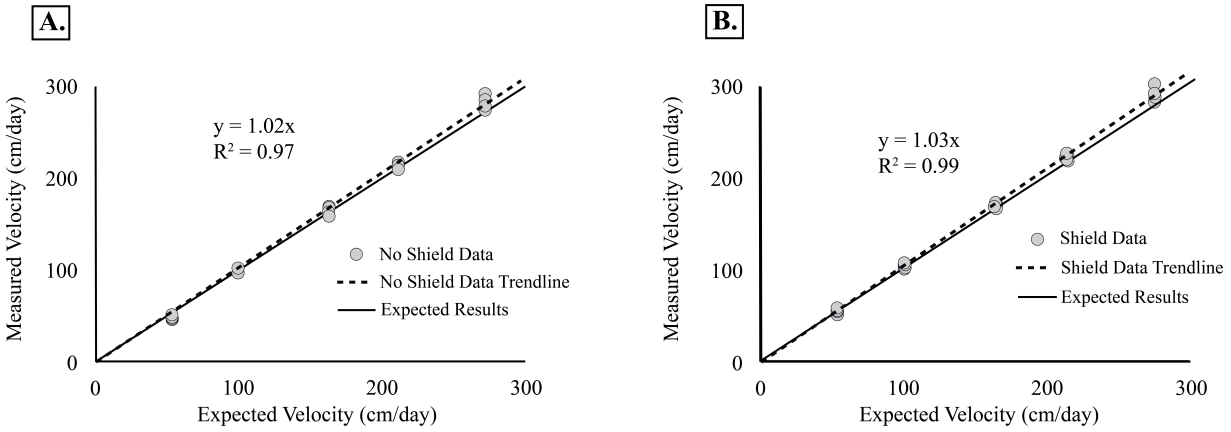

Figure 2.4: (A) The results of the variable velocity tests with an unshielded SBPVP. Test velocities ranged from 50 cm/day to 300 cm/day. (B) The results of the variable velocity tests with a shielded SBPVP. Test velocities ranged from 50 cm/day to 300 cm/day. The near identical outcomes of these experiments indicate the shield exerted no effect on the measurements.

The overall accuracy of the SBPVP measurements in the laboratory setting was generally within $\pm$ 8% of expected values, with an average accuracy of $\pm$ 3%. The overall precision of the SBPVP measurements in the laboratory setting did not exceed $\pm$ 4% with an average precision of $\pm$ 2%. These results showed that the probe performs satisfactorily over the range of velocities tested under the laboratory conditions of these tests.

2.4.4 Tracer injection

In most tests, a slight shoulder on the early-time side of the tracer BTCs was noted. The effect of the shoulder was to shift the fitted curve, from which the velocity parameter was estimated, slightly to earlier times, causing a small overestimation of the velocity. To evaluate the possibility that the shoulder was due to injection factors, tests with a typical tracer volume (0.3 mL) were performed with fast (< 10 s), medium (10–25 s), and slow (> 25 s) injections for comparison. Fast injections were found to result in repeatable, distinct, early-time "peaks" that preceded the main portion of the BTCs. These were thought to be caused by a thin plume of tracer that was forced along the probe surface during the injection phase (Figure 2.5). Slow- and medium-injection rates resulted in BTCs with weak or absent early-time shoulders. All injections maintained well-formed BTCs that could be fitted easily with the analytical solution in VelProbePE (Figure 2.5). The data quality

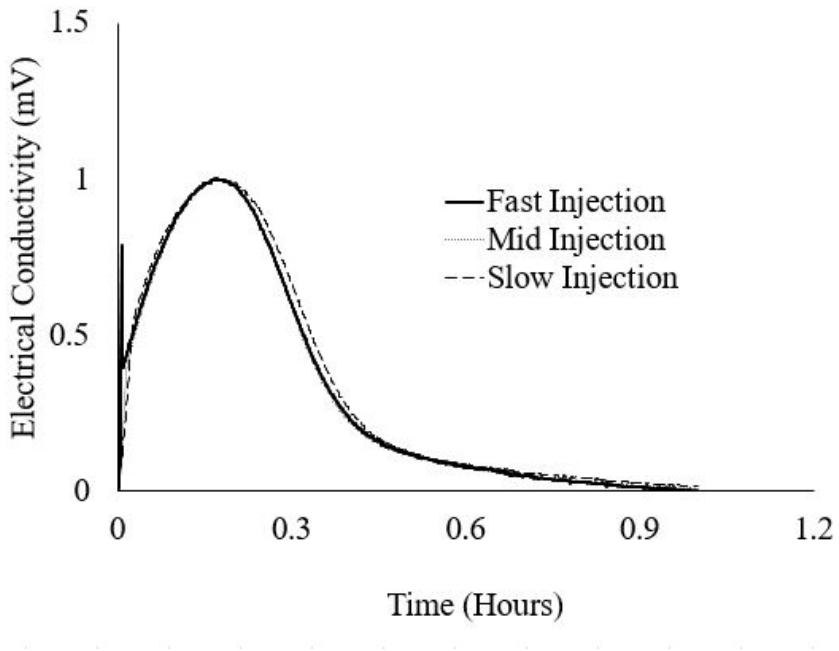

Figure 2.5: A comparison of tests at three different injection speeds, fast (< 10 s), medium (10–25 s), and slow (> 25 s). As shown above, the curves from all three injections at this velocity are very similar, yielding velocities that are within a reasonable span of error. The only significant difference is in the fast injection, where an early time peak appears because tracer is pushed onto the detectors by the injection (instead of being carried there by ambient flow). This early time peak becomes an early time slight injection shoulder in the mid and slow injection speeds.

of injections was found to be generally good as long as the signal strength was strong. On the basis of these findings, all subsequent tests were conducted with injection times between 10 s and 25 s, with a tracer solution of 0.5 g/L, and a tracer solution volume of 0.3 mL per injection. The resulting velocity estimates were in excellent agreement with the expected tank velocities estimated from pumping rates (Figure 2.4A and B).

2.4.5 Preliminary field assessment

Given the promising results of the SBPVP assessment in the laboratory, preliminary field testing was conducted in the field. The site selected was located in Grindsted, Denmark, on a meander of the *Grindsted Å* (Figure 2.6). The SBPVP was first tested in the streambed without the shield. In these tests, no signals were recorded at the probe detectors, suggesting horizontal flow was carry-

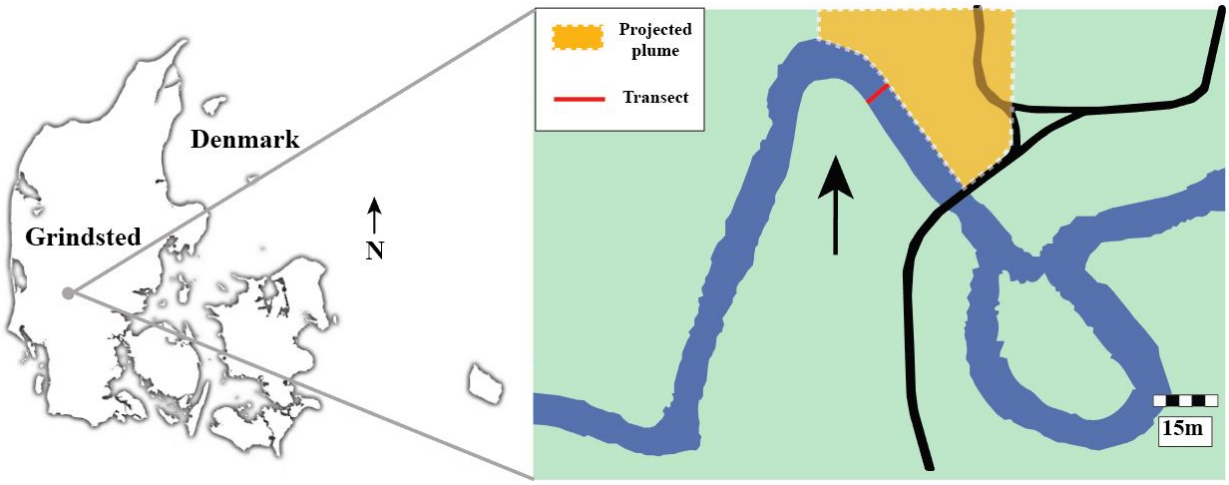

Figure 2.6: The location of the field testing in Grindsted, Denmark. The site was a specific meander of *Grindsted Å*. The transect presented in this preliminary study is marked in red. This transect is of interest because it assesses an area where a contaminant plume (orange) enters the stream. High concentrations, relative to other parts of the stream, were noted in this location.

ing the tracer off the probe before it could reach the detectors. The shield was then mounted on the probe and tracer BTCs were recorded normally.

The SBPVP was subsequently deployed in the stream, with the shield, and compared with measurements from mini-piezometers and temperature profiling spears taken in the same locations. The total time required to complete the SBPVP measurements across the transect was 1.5 h. The temperature measurements were completed in 0.5 h. The deployment, equilibration and head level measurements of the piezometers took 26 h. It should be noted that of the three methods utilized here, only the piezometers were suitable for repeated monitoring in time, which is an advantage over the other methods that may offset the installation time in some cases. At the Grindsted site, the piezometer transects could not be left in place for much longer than a day, due to boat traffic on the water. The three methods agreed well in identifying the locations of high and low fluxes (Figure 2.7B).

However, the magnitudes of the fluxes described by the temperature data were an order of magnitude lower (or more) than those described by the other two methods (Figure 2.7A). This disagreement in measured values is potentially explainable as the effect of horizontal hyporheic

flow on the temperature data, as reported by others and discussed in the Introduction section above. In this case, the effect may have been to bias temperature gradients low as channel water passed through the top 0.5 m of the streambed (the maximum depth that channel water may have reached in the streambed is not known). The *Grindsted Å* is known to be affected by a discharging plume of chlorinated solvents. The notable variability of the measured velocities across the streambed strongly suggests the need for a detailed characterization of the flow through the streambed at site, to achieve the best mass flux estimates for risk assessment purposes.

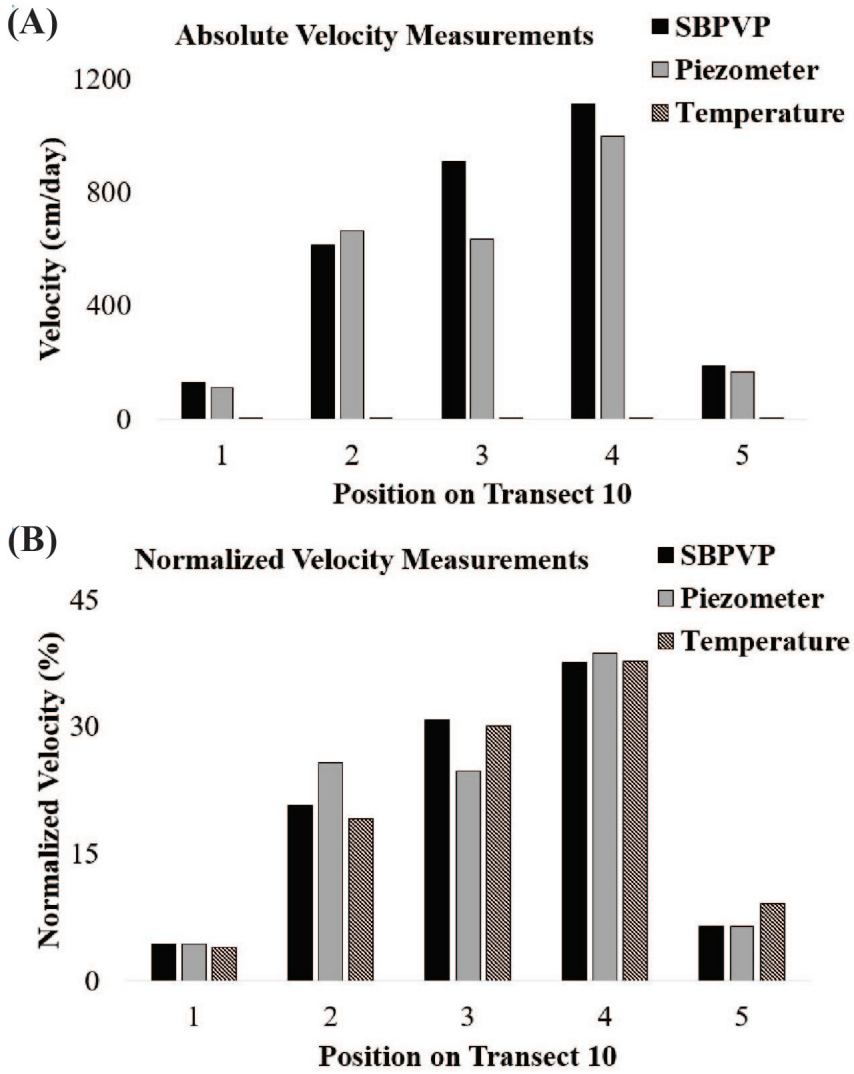

Figure 2.7: (A) Transect 10, with velocity measurements normalized to the total of velocity valued measured across the transect, shows good relative agreement between SBPVP measurements, mini-piezometer measurements, and temperature measurements. (B) Transect 10, displaying absolute velocity values, shows good absolute agreement between the SBPVP and mini-piezometer measurements and poor agreement with temperature measurements, which are biased low by an order of magnitude or more.

2.5 Conclusions

To complement existing tools and methods for assessing GWSW interactions, there is a need for a device that can rapidly and accurately estimate groundwater-surface water exchange rates. Laboratory testing with a NeST-based physical model of a streambed suggests that the SBPVP is a viable device for quantifying these exchange rates. Accurate measurements of water exchange across the GWSWI were found to be possible experimentally when the probe was deployed between 9 and 11 cm depth from the sediment-water interface. Comparisons of experimental data with a numerical model simulations suggested that artifacts related to sediment compaction might become important when the probe is pushed to greater measurement depths.

In these tests, the SBPVP was able to measure vertical fluxes with an accuracy within $\pm$ 3%, and a precision of $\pm$ 2%, on average, over a groundwater velocity range of 50 to 450 cm/day, without the need for calibration. The performance of the probe was such that its anticipated full range of measurement is greater than this, and further work is required to fully assess that range. To accommodate for natural conditions of streambeds, a hyporheic-flow shield was designed to isolate the vertical component of flow for the SBPVP measurements. The shield was found to exert no effect on the quality of the SBPVP measurements in the laboratory tests, and was found to be essential to obtain data in the field tests. A limited field trial of the SBPVP indicated that it performed as well as the Darcy-based method, using closely spaced mini-piezometers in the shallow streambed. K values for the piezometer calculations were estimated from slug tests performed in the streambed across a representative sample of the stream bottom sediments. Results from temperature profiles collected in the top 20 cm of the streambed, and taken in the same locations as the mini-piezometer measurements, did not compare as well possibly due to the effects of horizontal hyporheic flow in the streambed.

The work presented here shows that the SBPVP has the potential to provide a means of acquiring high density flux data from streambeds with less labor and time than is required for similarly

scaled Darcy methods. In addition, SBPVP measurements are based on tracer movement, which is a more direct indication of groundwater flow rates than methods based on hydraulic or temperature gradients. Given the results of this study, the SBPVP shows promise as an independent, complementary tool for quantifying groundwater-surface water exchange.

2.6 Acknowledgements

The authors would like to extend thanks to the Madison and Lila Self Graduate Fellowship for support of Mackenzie Cremeans and GEOCON for supporting the work. Allen Hase is acknowledged for assistance in equipment fabrication, Allison Grady is acknowledged for her assistance in the laboratory, Poul Bjerg and Ursula S. McKnight are acknowledged for valuable discussions and assistance with field work. Bent Skov and Flemming Møller are acknowledged for their assistance in the field.

Chapter 3

A comparison of tools for estimating groundwater-surface water exchange

Prepared for submission to Groundwater Monitoring & Remediation

3.1 Abstract

A comparison of tools for measuring discharge rates from groundwater to the *Grindsted Å* (stream) was conducted along a transect near the north bank of the stream. Four tools were evaluated at six locations spaced 3 m apart along an east-west transect near the north bank of the stream: mini-piezometers, streambed point velocity probes (SBPVPs), temperature profilers, and seepage meters. When data from the four methods are compared, it is found that all methods show a similar trend of low to high discharges westward along the transect. However, the magnitudes of estimated discharge did not fully agree. It was found that discharges estimated from mini-piezometer data were statistically the same, at the 90% confidence level, as those determined from seepage velocity measurements using the stream bed point velocity probe (SBPVP) at all locations tested. The same was true at four of the six locations for the seepage meter discharges. SBPVP data were, on average, within 29 cm/day and seepage meter data are, on average, within 45 cm/day of the seepage velocities predicted by mini-piezometer data. In contrast, discharges estimated from temperature

profiling to a depth of 40 cm into the streambed were found to be an order of magnitude, or more, less than those determined with the other methods. Where the methods produced statistically different discharge estimations at the same location, it is hypothesized that the differences arose from method specific sources of bias. That such biases were not of equal magnitude at all locations suggests that comparable measurements are possible by all methods under appropriate conditions. Thus, any of these tools could be used in a complementary fashion, on a site specific basis, to take advantage of their relative strengths.

Keywords: groundwater-surface water, comparison, tools, technology

3.2 Introduction

3.2.1 Review of methods of estimating groundwater-surface water exchange

Interest in estimating flow across the groundwater-surface water interface (GWSWI) is important for water resource management, including issues pertaining to water pollution and water supply (Fleckenstein et al., 2010; Rønde et al., 2017). With the advent of legislation that protects groundwater dependent ecosystems (such as the EU Water Framework Directive), interest in the GWSWI has intensified (Fleckenstein et al., 2010). Though much effort has been expended to understand groundwater-surface water interactions, the spatial patterns and temporal dynamics of hyporheic flow processes are not adequately understood (Krause et al., 2014). In large part, gaps in understanding are due to the spatial and temporal heterogeneity of the sediments at the GWSWI, leading to complexities in flow patterns that can be difficult to fully describe (Keery et al., 2007; Käser et al., 2009; Hatch et al., 2006; Rosenberry et al., 2013). To satisfy the need for more detailed information at the GWSWI, several tools have been developed to quantify and delineate water exchange zones. Unsurprisingly, few (if any) of these methods are universally suitable for use across the wide range of conditions found in streambeds.

The choice of method for characterizing flow at the GWSWI depends on the needs and challenges of the projects and sites. For example, in-well tools and methods (Halevy et al., 1967; Ballard, 1996; Kearl, 1997; Su et al., 2006), tracer tests (McCallum et al., 2012; Haria et al., 2013; de Souza et al., 2015), and synoptic flow gauging (Harte and Kiah, 2009) are among the approaches used to investigate flow at the GWSWI. The goal of this work is to compare and contrast the performances of three well-established tools, and one relatively new tool, along a transect in a stream. The methods used include mini-piezometers, temperature profilers, seepage meters, and streambed point velocity probes (SBPVPs), respectively. Previously, these methods were compared in a preliminary fashion to assist in the validation of PVP technology (Cremeans and Devlin, 2017; Cremeans et al., 2018). In this work, that comparative assessment was expanded to provide a more detailed dataset from which to identify strengths and weaknesses of the various methods in a sandy-bottomed stream.

One important outcome of this work is the extended field assessment of the SBPVP, relative to the more established methods. The SBPVP is an adaptation of the point velocity probe (PVP) which estimates groundwater velocity on the basis of a mini-tracer test on the probe surface (Labaky et al., 2007). The technology, in its various forms, has been validated in laboratory studies as well as several field settings (Devlin et al., 2009; Labaky et al., 2009; Berg and Gillham, 2010; Schillig et al., 2011; Devlin et al., 2012). Preliminary testing provided encouraging evidence that the SBPVP was a viable tool with potential advantages over alternative approaches (Cremeans and Devlin, 2017; Cremeans et al., 2018). The advantages of the SBPVP include rapid, simple deployment, the ability to quantify flow over wide range of magnitudes (at least 18 to 2700 cm/day), and circumvention of Darcy's Law and its associated sources of uncertainty, in particular hydraulic conductivity K (Cremeans et al., 2018). The SBPVP is limited to use in unconsolidated material, and is expected to be most effective in sandy sediments.

TThe technology assessment began with a side-by-side comparison of measured upward flows

through the streambed at the Grindsted stream, in Jutland, Denmark, determined from Darcy's Law, using mini-piezometers (Baxter et al., 2003; Rosenberry and LaBaugh, 2008). This approach has advantages including wide acceptance, relative simplicity, low materials cost, and the potential for the measurement of time-series data. Mini-piezometer surveys can be conducted with a high measurement density, allowing for high-resolution characterization of the GWSWI (as in Cremeans et al. (2018)). However, the use of Darcy's Law has some limitations, such as high potential error related to uncertainties in hydraulic conductivity (K) and challenges related to obtaining accurate hydraulic gradients over small distances, in some cases (Devlin and McElwee, 2007; Harvey et al., 2013; Post and von Asmuth, 2013).

Another technology that has gained notable recognition over the past decade is the use of temperature profiles in the streambed to delineate and quantify exchange rates (Krause et al., 2012). Temperature-based methods are advantageous because they offer a fast and efficient way to delineate and estimate water flux, as with the temperature spear tool (Schmidt et al., 2006, 2007; Lautz, 2010; Bhaskar et al., 2012; Irvine et al., 2017, 2016). They also offer the possibility of obtaining high spatiotemporal resolution (as with fiber-optic distributed temperature sensing) (Selker et al., 2006a,b; Tyler et al., 2009; Hausner et al., 2011; van de Giesen et al., 2012; Krause et al., 2012). Although temperature-based methods rely on a contrast between the temperature of groundwater and the temperature of surface water, which can vary seasonally (Krause and Blume, 2013; Rose et al., 2013), they have been shown to effectively quantify and delineate exchange zones in field studies (Westhoff et al., 2011; Lu et al., 2017).

Seepage meters have been in use for examining GWSW interactions since the late 1970s (Lee, 1977). Prior to that, they were developed to monitor water loss from irrigation canals (Israelsen and Reeve, 1944). They operate by isolating a fixed area of the streambed, usually using the top section of a steel barrel, and either collecting water that discharges upward across the GSWSI, or delivering water for infiltration downward across the interface. The collected or delivered water is

temporarily stored in a plastic bag connected to the barrel section via plastic tubing. The change in water volume in the bag over time (per area) can be used to estimate a seepage flux. The design of seepage meters inherently leads to time-averaged flow measurements. Like mini-piezometers, seepage meters are inexpensive and relatively simple to construct. They have the added advantage of measuring seepage rates directly, which has led to their common use (Murdoch and Kelly, 2003; Rosenberry, 2005; Rosenberry and LaBaugh, 2008; Rosenberry, 2008; Kennedy et al., 2010; Solder et al., 2016). Seepage meters have been employed to great advantage in field studies, but care must be taken to avoid biases associated with early construction designs and their deployment in deep or fast-moving water. Seepage meters are poorly suited for deployment in streambeds composed of hard substrates (Erickson, 1981; Brock et al., 1982; Woessner and Sullivan, 1984; Shaw and Prepas, 1990; Zamora, 2006; Blanchfield and Ridgway, 1996).

3.2.2 Field site

Groundwater-surface water exchange was investigated in the *Grindsted Å* (stream), Denmark, using mini-piezometers, temperature profilers, seepage meters and SBPVPs. All technologies were deployed at six equidistant measurement locations, spaced 3 m apart, along the north shore of the stream (Figure 3.1). The locations were selected based on the criterion that all instruments could be deployed to full advantage. This limited the study to the relatively shallow portions of the stream (<1.2 m deep) where the bed was essentially horizontal. Two sediment types were found to be present along this transect, silty sand and sand, as determined by visual inspection. The change from silty sand to sand occurred gradationally along the stream bottom, with the most abrupt change occurring between the fourth and fifth sampling locations, counting northward along the transect. Based on observations made during the equipment installation, and prior experience at the site (Sonne et al., 2017), the sediments observed at the top of the bed generally prevailed to a depth of 40 cm, leading to a relatively homogeneous shallow bed. Slug testing was conducted in four locations across the stream to characterize three sediment types (Figure 3.1). For the purposes of this study, locally isotropic conditions (regarding K) were assumed throughout this 40 cm zone.

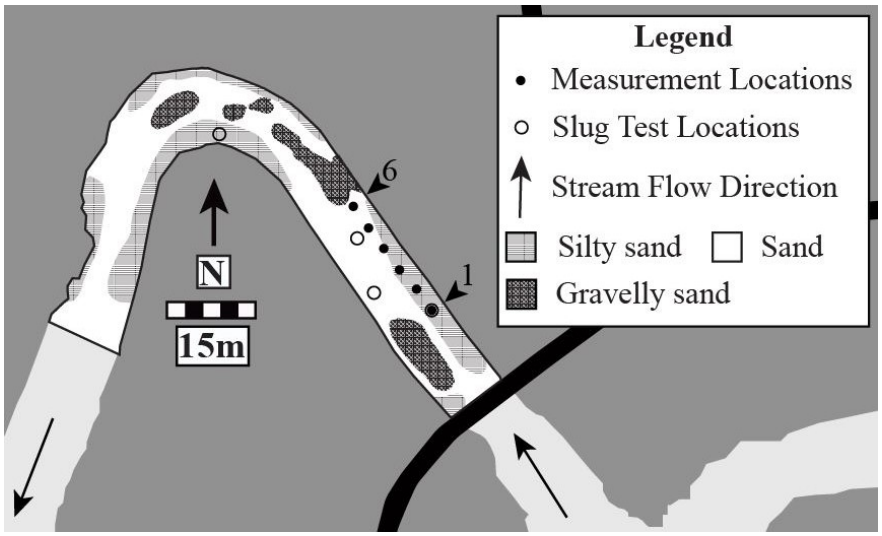

Figure 3.1: Map of the *Grindsted Å* streambottom. The distribution of three observed sediment types, silty sand, sand, and gravelly sand, are shown. The 6 measurement locations in the where mini-piezometers, the SBPVP, temperature spears, and seepage meters are shown as small solid circles. Slug test locations are indicated with open circles. Location 1 (large solid circle) was subjected to testing by the four methods and a slug test.

Based on prior investigations of this site, flow rates through the streambed were expected to be on the order of 100 cm/day on average. In the streambank sediments, local variations between 4 and 200 cm/day were estimated (Rønde et al., 2017).

3.3 Methods

3.3.1 Mini-piezometers

Hydraulic head data were collected from the *Grindsted Å* streambed using mini-piezometers constructed from open-ended clear polyvinyl chloride pipes with 2 cm inner diameters. The piezometers were installed with a drive-point to a depth of 40 cm (Figure 3.2) and allowed to equilibrate for 24 hours before data were collected with a Solinst Model 101 Water Level Meter. The water meter allowed gradient measurements to be taken within $\pm$ 1 cm of actual values. Hydraulic gradients across the GWSWI were calculated from the head data, using a stilling well to obtain the hydraulic head of the stream channel water (Baxter and Hauer, 2000; Baxter et al., 2003).

Hydraulic conductivity (K) values were obtained by slug testing based on the recommendations of Butler Jr (1997) (including recommendations such as making sure wells are properly developed). Four locations were chosen to represent the two observed sediment types in the transect examined: silty sand and sand. Two slug tests were conducted at each measurement location, resulting in eight total tests (all in situ at 40 cm depth) (Figure 3.1, Table 3.1). Butler Jr (1997) suggests three replications; only two replications were completed due to the similarity in slug test results between all pairs of measurements (Table 3.1). A drive point piezometer, with a 10 cm screen, was installed in each of the measurement locations with a pressure transducer (programmed to gather data every 0.5 s). After the system had been left to equilibrate for 8 hours, 1 m water slugs were introduced to the piezometer and the falling head response was recorded. Data from these tests were processed in AQTESOLV, where the K for each sediment type was calculated with the Hvorslev method (Hvorslev, 1951; Inc., 2016). Two slug tests were performed in each of the sediment types identified within the study transect. All tests exhibited a straight line overdamped response, and the reproducibility of responses within a given sediment type was good (see Results and Discussion). Porosity (n) was taken from previous work at the site that suggested an effective value of 0.3 (Rügge et al., 1999; Lønborg et al., 2006). Seepage velocities, v, in the streambed were subsequently calculated from the following version of Darcy's Law:

$$v = -\frac{Ki}{n} \tag{3.1}$$

where v is the seepage velocity (LT^{-1}), K is the hydraulic conductivity (LT^{-1}), i is the hydraulic gradient (unitless), and n is the porosity (unitless).

3.3.2 Temperature gradient method

In this study, the temperature gradient method described in Schmidt et al. (2007) was applied using an Ebro TFN-520 Type K handheld thermometer was deployed using a steel spear to measure the

temperature gradients. Temperatures could be measured to two decimal places with the available equipment. This approach relies on the one-dimensional analytical solution:

$$q_z = -\frac{k_{fs}}{p_f c_f z} ln \frac{(T_Z - T_L)}{(T_0 - T_L)} \tag{3.2}$$

where q_z is Darcy flux in the vertical direction (ms^{-1}), k_{fs} is the thermal conductivity of the solid-fluid system ($Js^{-1}m^{-1}K^{-1}$), $p_f c_f$ is the volumetric heat capacity of the fluid ($Jm^{-3}K^{-1}$), z is the depth of measurement (m), T_z is the temperature at depth z (^{o}C), T_L is the temperature of the groundwater which is fixed for all calculations (^{o}C), and T_0 is the temperature at z = 0 (^{o}C). For the calculations in this study, z (depth of measurement) is 40 cm, k_{fs} was assumed to be 2.2 $Js^{-1}m^{-1}K^{-1}$ (Hopmans et al., 2002) and $p_f c_f$ was 4.19 x 10^6 $Jm^{-3}K^{-1}$. T_L, the temperature of groundwater is 8.6 ^{o}C and was determined by averaging samples collected from streambank wells. T_0 is the temperature at the sediment-water interface. This value was measured along with a surface water measurement (T_{sw}) and a measurement at depth z (T_z) at every measurement location (Figure 3.2). T_z is the measurement of temperature at depth z, which was also taken at each measurement location by inserting the temperature spear into the sediment at 40 cm depth, the deepest a probe could be installed without damage. The 40 cm depth was selected in an effort to reach a zone beneath active horizontal hyporheic flow. More detailed descriptions of the use of temperature profilers and processing of temperature data in the *Grindsted Å* is given in Schmidt et al. (2007) and in Cremeans and Devlin (2017), respectively.

3.3.3 Seepage meters

Seepage meters were constructed in accordance with recommendations from Murdoch and Kelly (2003) and Rosenberry (2008). Briefly, the devices used in this study were fabricated from plastic buckets with diameters of about 30 cm, and installed to a depth of about 12 cm (Figure 3.2). The collection bag (with a maximum volume of 1 L) was connected to the bucket with 1.1 cm inner diameter tubing. To avoid head losses at the bag due to the movement of water in the stream

channel, the bag was placed inside a container where the water surrounding it was held stationary. Each test began with 250 mL of water in the bag. Since water was discharging upward across the GWSWI in this case, the bag gained water over the 30 to 90-minute period of a test. In each case, the bag was filled to a total volume not exceeding 750 mL, to minimize head losses related to resistance of bag inflation. The seepage meters were left to equilibrate for 24 hours prior to conducting flux measurements. Measurements of volume were accurate to the $\pm$ 2 mL and times were measured to the $\pm$ 1 s.

3.3.4 Streambed point velocity probes

In each of the six measurement locations, the SBPVP was installed 5-10 cm below the streambed with a hyporheic shield in place to prevent any influence from horizontal flow on the upward velocity measurements (Cremeans and Devlin, 2017) (Figure 3.2). Tests were conducted with tracer injection volumes ranging from 0.1 mL to 0.4 mL and with tracer concentrations ranging from either 1 g/L NaCl or 2 g/L NaCl, which have been shown to little or no effects of density flow in PVP tests in sandy media (Schillig et al., 2014). The tests required between 30 minutes and 180 minutes to complete. Data collection was accomplished using a PC connected to a Campbell Scientific CR1000 datalogger running LoggerNet® software set up to collect data at 2 second intervals. Data were processed using the software package VelProbePE (Schillig, 2012).

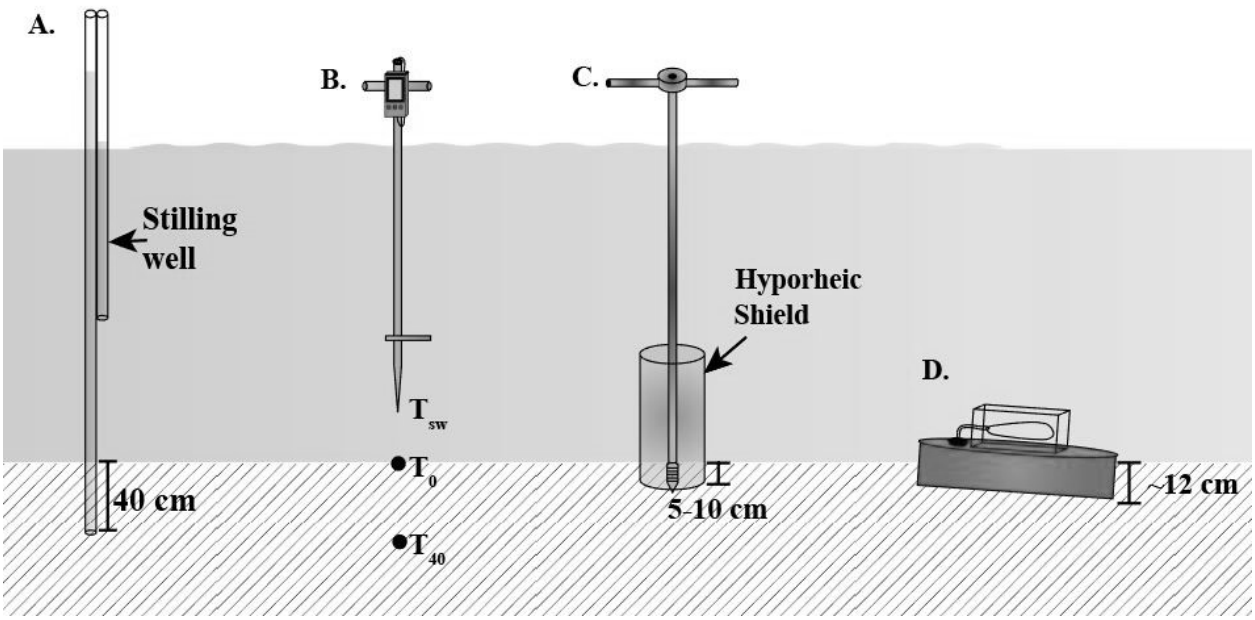

Figure 3.2: Schematic representations of the four methods compared in this study. A. The mini-piezometer. B. Temperature profiling. C. The SBPVP. D. Seepage meters. See text for details.

3.4 Results and discussion

Initially, data were examined to determine if the methods suggested similar trends in discharge. This was done by plotting the 6 discharge estimates from each method on a line graph to observe trends. At this time, it was noted that the methods used in this study did not always provide estimates of discharge that were comparable in an absolute sense, meaning that, while the trends could agree the magnitude of estimated discharge might not agree between the methods. The discrepancies in absolute discharge were explored in scatterplots comparing the methods directly, including plots with 1:1 and best fit lines. These plots include larger datasets from Cremeans et al. (2018) to allow for a more in-depth discussion.

In these analyses, all four methods tested revealed a qualitatively consistent trend in which lower seepage velocities were found at the eastern end (location 1) of the transect, and larger flow rates at the western end (location 6) (Figure 3.3, Table 3.1). This trend is consistent with the sediment types mapped on the streambed (Figure 3.1); the eastern end of the line was characterized by silty

sand and the western end by sand. The difference in upward seepage velocities ranged more than two orders of magnitude across the test zone, from a few centimeters per day at location 1 to 100 cm/day or more, depending on the method used, at locations 5 and 6.

Each of the techniques was implemented in duplicate (back to back measurements) at every location to assess measurement reproducibility. With the exception of two pairs of seepage meter measurements ($\pm$4.1% and $\pm$9.8%), all replicate pairs (n = 34) agreed to within $\pm$3% (see Table 3.1), establishing that the observed differences in values of seepage velocities from one method to another (visible in Figure 3.3) were due to either biases inherent to the methods, or variations arising from slight differences in placement of the instruments on the streambed, i.e., differences arising from sediment variability on the streambed. A standard deviation was calculated using four of the six measurement locations (locations 5 and 6 were omitted due to the change in geology at these locations) and plotted on Figure 3.3. These suggest similarity between the velocity estimations of the SBPVP, mini-piezometers, and seepage meters. The temperate profiler estimated notably smaller velocities and could not be compared in the same way.

Table 3.1: Part 1, Summary of K values and replicated velocity(cm/day) results with standard deviations for each measurement pair

Location	**Applied K**	**SBPVP 1**	**SBPVP 2**	**Mini-Piezometer 1**	**Mini-Piezometer 2**
1	$4.826x10^{-5}$	18.1 ± 0.0	18.1 ± 0.0	0.0 ± 0.0	0.0 ± 0.0
2	$4.826x10^{-5}$	47.0 ± 0.1	47.2 ± 0.1	110.8 ± 0.0	110.8 ± 0.0
3	$4.826x10^{-5}$	50.0 ± 0.0	50.0 ± 0.0	27.6 ± 0.1	27.8 ± 0.1
4	$4.826x10^{-5}$	45.8 ± 0.3	45.2 ± 0.3	56.0 ± 0.6	54.8 ± 0.6
5	$1.047x10^{-4}$	173.1 ± 0.1	172.9 ± 0.1	110.8 ± 0.0	110.8 ± 0.0
6	$1.047x10^{-4}$	149.8 ± 0.1	150.0 ± 0.1	138.4 ± 0.0	138.4 ± 0.0
Location	**Applied K**	**Temperature 1**	**Temperature 2**	**Seepage 1**	**Seepage 2**
1	$4.826x10^{-5}$	0.088 ± 0.002	0.091 ± 0.002	13.5 ± 0.7	13.5 ± 0.7
2	$4.826x10^{-5}$	0.085 ± 0.0008	0.084 ± 0.0008	25.4 ± 0.2	24.8 ± 0.2
3	$4.826x10^{-5}$	0.46 ± 0.003	0.46 ± 0.003	19.4 ± 0.2	19.1 ± 0.2
4	$4.826x10^{-5}$	0.53 ± 0.002	0.53 ± 0.002	25.8 ± 0.6	26.9 ± 0.6
5	$1.047x10^{-4}$	0.47 ± 0.003	0.48 ± 0.003	55.5 ± 0.3	56.1 ± 0.3
6	$1.047x10^{-4}$	1.58 ± 0.003	1.58 ± 0.003	62.1 ± 0.3	61.5 ± 0.3

Briefly, the measurement standard deviation for the median SBPVP velocity (48.5 cm/day) was $\pm$7.4% for the median mini-piezometer derived velocity (83 cm/day) was $\pm$43%; for the median seepage meter derived velocity (25.7 cm/day) the measurement standard deviation was $\pm$15%; for the median temperature gradient derived velocity (0.47 cm/day) the measurement standard deviation was $\pm$20%.

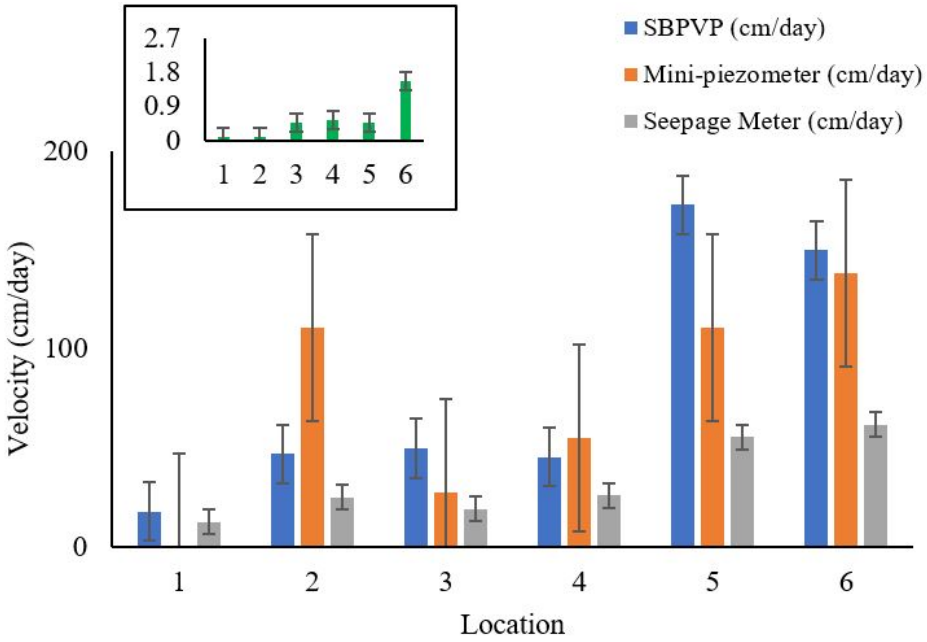

Figure 3.3: An absolute comparison of methods. As noted in the text, the temperature method estimates notably lower velocities than the other three methods. The error bars shown are one standard deviation, calculated from 4 of 6 locations (those with similar geology). For the SBPVP, mini-piezometers, seepage meters, and temperature profilers, one standard deviation is 14.8 cm/-day, 47.2 cm/day, 6.2 cm/day, and 0.23 cm/day, respectively.

The standard for comparison of flow estimations is, arguably, the method based on the measurement of Darcy parameters (K, i) and a Darcy calculation (equation 3.1). Therefore, a further assessment of the methods compared in this work was made by plotting seepage velocity estimates against the associated Darcy values at the same locations (Figure 3.4). Good agreement is indicated by a linear relationship between the measured values, with a slope of 1.0. The SBPVP data from this study plot the same way (slope = 1.0 $\pm$ 0.4 with 90% confidence) (Figure 3.4A). This finding also applies to the extended dataset collected over 92 locations within a 70 m reach of the *Grindsted Å*, which included the transect studied in detail here (Figure 3.4B).

In contrast, a weaker linear relationship was observed between the mini-piezometer data and the temperature gradient data (slope = 0.007 $\pm$ 0.004 with 90% confidence) (Figure 3.4C). Inspection of the extended dataset from Cremeans et al. (2018) suggests an improvement in the linearity of the relationship (slope = 0.015 $\pm$ 0.003 with 90% confidence) (Figure 3.4D), but the negative bias in the values discussed above persists. Finally, a linear relationship also appeared to exist between the mini-piezometer data and the seepage meter data, though the slope was significantly below 1 (slope = 0.41 $\pm$ 0.1 with 90% confidence) (Figure 3.4E), suggesting a systematic bias possibly related to the construction or deployment of the seepage meters used in the study.

This analysis supports two insights. First, the differences in bed conditioned-derived uncertainties between the various methods suggests different inherent capabilities between the methods at this site. In particular, the mini-piezometer method was characterized by a considerably higher uncertainty in velocity estimates than the other methods ($\pm$43% vs. $\pm$7 to $\pm$15%), possibly reflecting the challenges of ascribing accurate Darcy parameters (K, n, i) to each monitoring location. For example, measurement footprint sizes varied between the methods and could have contributed to different effective values of K within the same sediment type – both for different methods at the same location and the same method at different locations. Supporting this notion is the fact that seepage meter measurements had the largest footprint (750 cm^2) and exhibited the smoothest transition from low v to high v along the tested transect (Figure 3.3). Second, both the temperature gradient data and the seepage meter data produced velocity estimations that were consistently low compared to the other methods. As suggested in Figure 3.4A, the SBPVP derived velocities compared well with the mini-piezometer derived velocities. The systematic bias associated with the temperature gradient measurements may be associated to the effects of horizontal hyporheic flow, as discussed in Cremeans et al. (2018).

A further difference between the methods relates to the duration in time of each measurement.

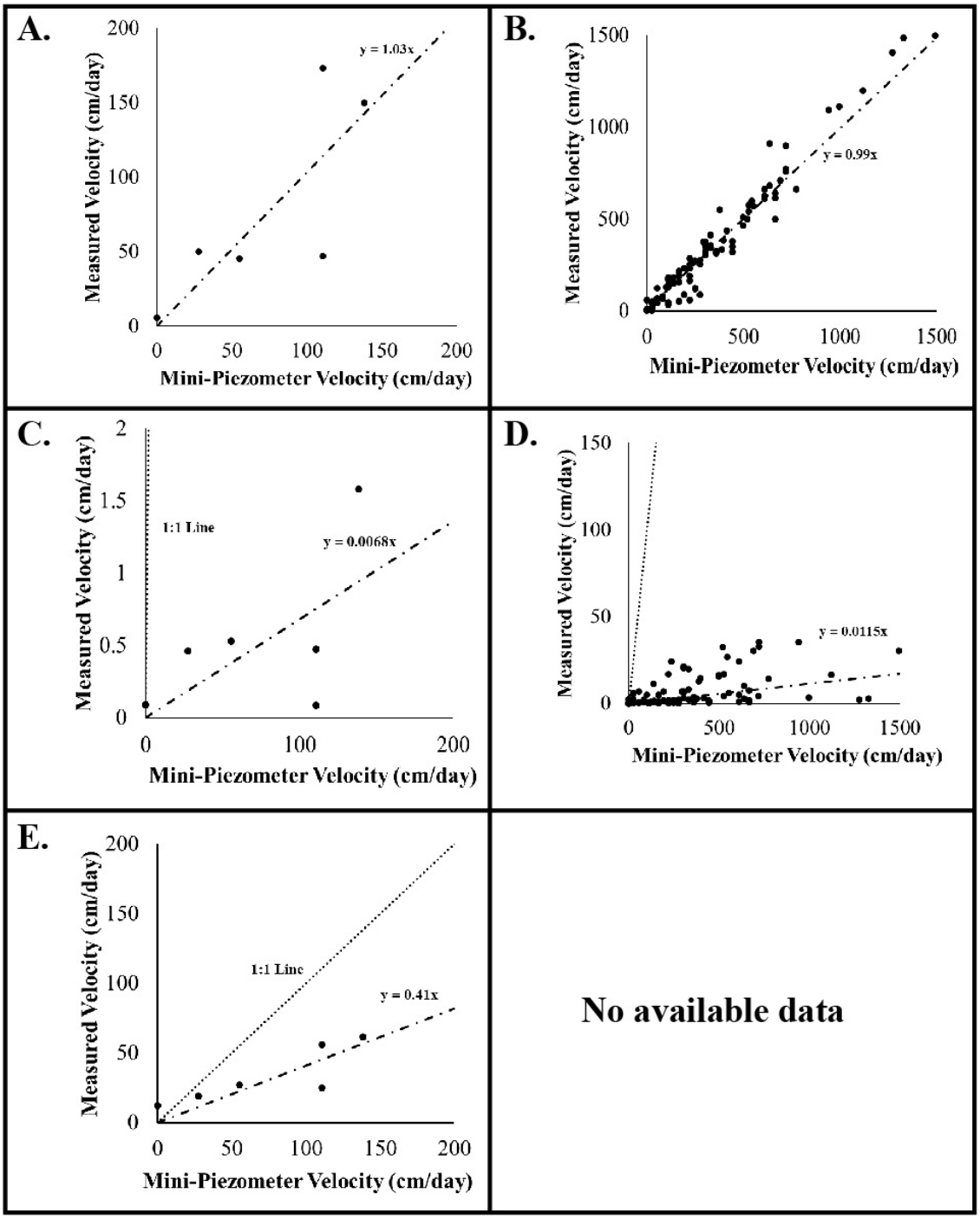

Figure 3.4: Comparisons of seepage velocities measured by each method with those estimated from Darcy calculations. Comparisons of seepage velocities measured by each method with those estimated from Darcy calculations Some plots also include a dotted 1:1 line. A) SBPVP within the transect B) SBPVP and Darcy-estimated seepage velocities determined over a 70 m reach of the stream, including zones of high velocity. Note near 1:1 correspondence between the SBPVP velocities with the Darcy-estimates, C) temperature profiling within the transect D) temperature and Darcy-estimated seepage velocities over the same 70 m reach, E) seepage meters along the transect.

For example, the mini-piezometer and temperature measurements presented in this study can offer an estimate of discharge at a particular point in time while seepage meter and SBPVP measurements offer average discharge estimates over discrete time periods (30 to 90 minutes or 30 to 180 minutes, respectively). In this study, steady state flow was assumed to permit direct comparisons. There were no observable reasons to doubt the assumption, but if it were violated during testing, the comparability of the methods could be compromised to some extent that was not quantified in this work.

3.5 Conclusions

All four methods tested identified a general trend of increasing seepage velocities in the *Grindsted Å* streambed, from the south end of the test transect to the north. However, of the methods tested, only the seepage velocities derived from the mini-piezometer and SBPVP datasets were statistically the same. Using these values as the benchmark for comparison, seepage meter data tended to underestimate the velocities by an average of about 40%, over a total measured range (by the seepage meters) of about 12 to 60 cm/day. The apparent bias was not statistically significant from the mini-piezometer-derived velocity estimates in 4 of the 6 locations tested. The differences are thought to be related to several possible causes, including the effects of measurement footprint size, and possibly issues related to the construction or deployment of the seepage meters.

The temperature data exhibited a strong negative bias of about an order of magnitude compared to the piezometer and SBPVP datasets. This bias is thought to be due to the influence of horizontal hyporheic flow in the streambed sediments at this site.

It is concluded from the above that for sandy bottom streams, like the *Grindsted Å*, the SBPVP tool provided the seepage velocity estimates that were most reliable, making this the preferred technology for quantifying flow across the GWSWI. In this study, mini-piezometer data contained relatively high uncertainties, likely arising from Darcy parameter estimation, seepage meter data

suffered from a slight negative bias, and temperature gradient data – collected as simple vertical profiles of temperature – suffered from significant negative biases. In addition to the performance issues above, the SBPVP was comparatively fast to deploy and the measurements fast to complete – only the temperature gradient method was faster. Thus, if the purpose of a site characterization is simply to identify the locations of prominent discharge zones, temperature profilers may be the preferred technology. It should be noted that the mini-piezometers and seepage meters used in this study were less expensive to fabricate, and produced data that were simpler to interpret. Mini-piezometers also offer the best chance to obtain time series data. Overall, these four tools all provide useful and complementary information and the tool of choice largely depends on the needs of a project.

3.6 Acknowledgements

The authors would like to extend thanks to the Madison and Lila Self Graduate Fellowship for support of Mackenzie Cremeans as well as the University of Kansas Doctoral Research Fund, Kansas Geological Foundation, and GEOCON (Innovation Fund Denmark, contract no. 1305-00004B) for supporting the work. From the Technical University of Denmark, Bent Skov is acknowledged for assistance in the field. From the Kansas Geological Survey, Geoff Bohling is acknowledged for his assistance with the statistical analysis.

Chapter 4

Application of new point measurement device to quantify groundwater-surface water interactions

As published in the Journal of Contaminant Hydrology

4.1 Abstract

The streambed point velocity probe (SBPVP) measures *in situ* groundwater velocities at the groundwater-surface water interface without reliance on hydraulic conductivity, porosity, or hydraulic gradient information. The tool operates on the basis of a mini-tracer test that occurs on the probe surface. The SBPVP was used in a meander of the *Grindsted Å* (stream), Denmark, to determine the distribution of flow through the streambed. These data were used to calculate the contaminant mass discharge of chlorinated ethenes into the stream. SBPVP data were compared with velocities estimated from hydraulic head and temperature gradient data collected at similar scales. Spatial relationships of water flow through the streambed were found to be similar by all three methods, and indicated a heterogeneous pattern of groundwater-surface water exchange. The magnitudes of estimated flow varied to a greater degree. It was found that pollutants enter the stream in lo-

calized regions of high flow which do not always correspond to the locations of highest pollutant concentration. The results show the combined influence of flow and concentration on contaminant discharge and illustrate the advantages of adopting a flux-based approach to risk assessment at the groundwater-surface water interface. Chlorinated ethene mass discharges, expressed in PCE equivalents, were determined to be up to 444 kg/yr (with SBPVP data) which compared well with independent estimates of mass discharge up to 438 kg/yr (with mini-piezometer data from the streambed) and up to 372 kg/yr crossing a control plane on the streambank (as determined in a previous, independent study).

Keywords: groundwater-surface water interactions; contaminant mass discharge; chlorinated ethenes; groundwater velocity; site characterization; streambed

4.2 Introduction

4.2.1 Groundwater-surface water interactions and solute exchange

The importance of groundwater-surface water exchanges across the groundwater-surface water interface (GWSWI) is well recognized for a variety of hydrological problems (Warnick, 1951; Lee, 1977; Winters and Lee, 1987; Winter et al., 2003; Kalbus et al., 2006; Krause et al., 2009, 2011, 2012). Even a small exchange between groundwater and surface water can deliver a noteworthy contribution of solutes to a surface water body. For example, if a surface water body is gaining, the contribution from groundwater can sometimes affect the flow and chemistry of surface water strongly (Schwartz and Gallup, 1978; Hurley et al., 1985; LaBaugh et al., 1995; Moore, 1999; Holmes, 2000). In principle, the converse can also be true, i.e., losing streams may exert notable effects on groundwater flow and chemistry. Thus, the chemical and physical properties of surface and groundwater are strongly interdependent.

Recently, contaminant mass discharges into a Danish stream, the *Grindsted Å*, estimated from

the analysis of concentration data and groundwater velocities at the stream bank using point velocity probes (PVPs), was compared to mass fluxes in the stream channel water (Rønde et al., 2017). Also, recently, a new method of measuring flow across the GWSWI was introduced and evaluated in laboratory tests, based on PVP technology (Cremeans and Devlin, 2017). In this article, the newly adapted PVP probes, temperature gradient measurements, and Darcy calculations are used to conduct a detailed survey of contaminant mass fluxes into the *Grindsted Å* along a reach receiving groundwater contaminated by chlorinated ethenes.

4.2.2 Methods of measuring flow across the GWSWI

In this work, a goal is to measure flow across the groundwater-surface water interface at the meter scale or less. To achieve this objective, two general approaches have been adopted (1) measuring indirect metrics that can be converted to discharge rates (e.g. hydraulic heads, temperature profiles, or salinity profiles) (Winter et al., 1988; Bartolino and Niswonger, 1999) and (2) measuring water flux across the GWSWI directly (e.g. with seepage meters) (Lee, 1977; Solder et al., 2016). These methods operate on a variety of scales. For example, seepage meters describe flux over the area of a drum (which can be any size but is usually on the order of about a meter in diameter). Mini-piezometers (often used in applications of Darcy's Law) approach point measurements in scale. Both of these methods focus on specific, small areas of the stream with each measurement. Synoptic gauging (as in Harte and Kiah (2009)), which measures the total change in discharge over a defined reach of a river or stream, gives a much larger scale view of discharge (one that would require many measurements from seepage meters or mini-piezometers to make comparison possible) but does not identify the locations of discrete discharge zones.

In general, the indirect methods, which can provide detailed spatial patterns of flow, are subject to errors and biases related to the conversion of the measured quantities to flow rates. For example, to obtain accurate estimates of discharge, Darcy calculations rely on accurate estimates of hydraulic conductivity (K) and hydraulic gradient (i) values, both of which are associated with high potential

error (Molz et al., 1989; Butler et al., 2002; Zemansky and McElwee, 2005; Devlin and McElwee, 2007; Post and von Asmuth, 2013). Several tools and methods for measuring water exchanges across streambeds have been developed using temperature gradients. These commonly rely on analytical solutions that assume one-dimensional flow (Bredehoeft and Papaopulos, 1965; Stallman, 1965) and, sometimes, are restricted to gaining streams (as in Schmidt et al. (2007)). Solutions have also been developed to use temperature in two- and three-dimensions and in losing streams (as discussed fully in Anderson (2005)).

The available direct methods of measuring flow across the GWSWI offer independent means of estimating exchanges across the GWSWI, and circumvent many of the sources of error mentioned above. In these cases, estimations of flux tend to depend on calculations involving easily measured properties with comparatively low uncertainties. For example, seepage meters measure discharge (Q) into a well-defined cross-sectional area (A) (usually, a steel drum) to permit the direct calculation of specific discharge ($q = Q/A$). Naturally, these methods come with their own sources of uncertainty, which tend to arise from the measurements themselves, which can be affected by local heterogeneity of the streambed material and biases introduced during equipment installation. For example, some investigators have seen agreement between measurements made by seepage meters and other methods in flowing streams (Rosenberry and Pitlick, 2009; Kennedy et al., 2010) while others have reported large uncertainties for measurements made in streambeds, or were unable to operate seepage meters at all in these settings (Cey et al., 1998; Zamora, 2006). The reasons for these uncertainties have been attributed to design limitations of the devices (Isiorho and Meyer, 1999; Murdoch and Kelly, 2003; Simpkins, 2006; Rosenberry, 2008), disturbance of flow paths due to instrument installation (Hutchinson and Webster, 1998), velocity heads imposed by waves and moving water interfering with seepage meter operation (Shinn et al., 2002), gas release in bed sediments (Kennedy et al., 2010), improper seals between the drums and the beds (Cey et al., 1998), small-scale spatial heterogeneities (Robinson et al., 1998; Bokuniewicz et al., 2004), and the combined effect of slow seepage rates with a moving streambed, causing scour or burial of the seepage

meters (Zamora, 2006). Other methods, such as multiple tracer injections in streambeds (Zellweger, 1994) and the measurement of isotopic and temperature signatures to infer groundwater inflows into streams (Cook et al., 2003) may be similarly influenced by streambed heterogeneity, difficult installation, and the challenges of working in a continuously evolving system (due to the transport of sediment, temporal variability of flow, etc.).

To gain a better picture of groundwater-surface water exchange, several studies have recommended a combination of two or more methods and datasets to characterize the sediment water interface (Becker et al., 2004; Verruijt, 2007; Ivkovic, 2009; De Smedt, 2014). Nevertheless, there are only a few examples of datasets sufficiently detailed to properly establish the nature of any single exchange zone and to address hydrological and contaminant fate issues (e.g., Conant (2004); Freitas et al. (2015)).

To help address the need for reliable, time-efficient, and cost-effective measurements of groundwater velocity, point velocity probe (PVP) technology was developed. The original PVPs were designed to measure centimeter-scale *in situ* groundwater velocities in aquifers. This technology has been field validated in sand aquifers, a glacial outwash aquifer, and along a stream bank (Labaky et al., 2007; Schillig et al., 2011; Devlin et al., 2012; Rønde et al., 2017). The goal of this work was to adapt PVP technology to measure exchange at the GWSWI for the purpose of estimating contaminant mass discharge. The tool created to meet this goal is referred to as the SBPVP (Cremeans and Devlin, 2017). Previously, the SBPVP was validated in laboratory tests (Cremeans and Devlin, 2017). In this study, the SBPVP was used for high-resolution characterization of flow patterns at the GWSWI of a stream where physical documentation of the interface was necessary to determine the mass discharge of chlorinated ethenes.

4.2.3 Field site

The *Grindsted Å* (stream) is located in Jutland, Denmark, proximal to an industrial site from which a plume of dissolved chlorinated solvents originates and subsequently discharges to the stream (Figure 4.1). Further information about the site and the stream is reported in Rasmussen et al. (2016), Balbarini et al. (2017), and Sonne et al. (2017). In this study, all measurements were gathered in the streambed of the *Grindsted Å*, over a reach of the stream instrumented with 26 transects, situated approximately 3 m apart, and oriented perpendicular to the stream flow direction (Figure 4.1). The transects each comprised three to five evenly spaced measurement locations. The stream bottom consisted of three observed sediment types: silty sand, sand, and gravelly sand, as determined by visual inspection at each measurement location. Mini-piezometers, temperature spears, and the SBPVP were used to estimate groundwater velocity at the GWSWI, at each location.

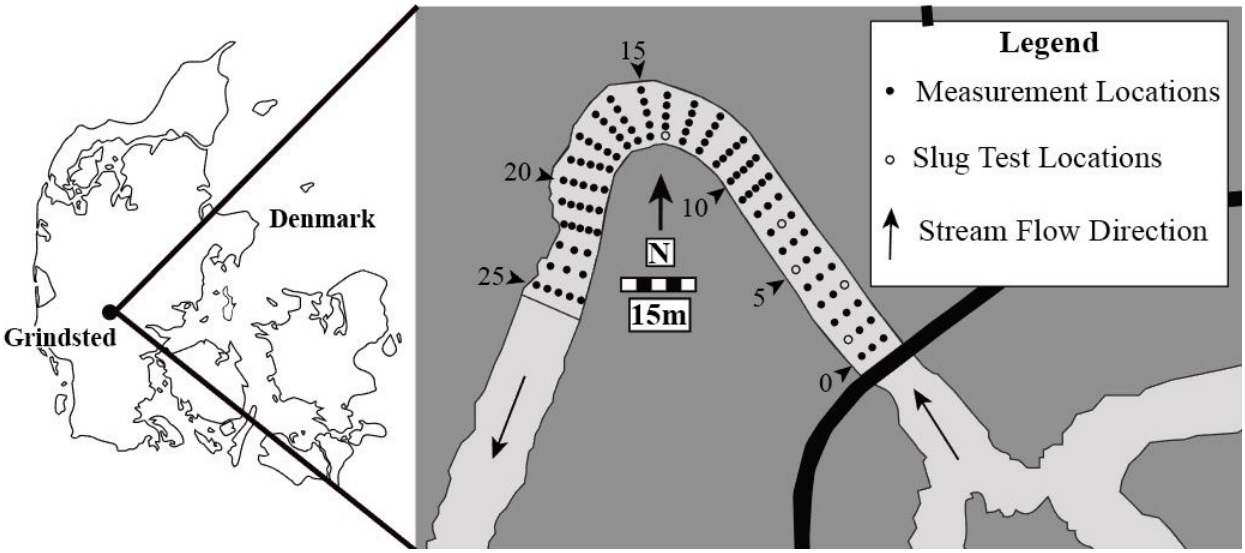

Figure 4.1: Grindsted is located centrally in Jutland, Denmark. The field site was a single meander of the *Grindsted Å*, a stream running through the town of Grindsted, was divided into 26 transects (numbered 0 to 25). Each transect comprised 3 or 5 equally spaced measurements taken along a line perpendicular to the flow direction. The black dots show each measurement location. Temperature gradient and SBPVP measurements were taken on transects 0 to 25, while hydraulic head measurements were limited to transects 0 to 21. Slug testing was conducted at the measurement locations shown as open dots.

4.3 Methods

4.3.1 Pore water sampling

Samples and replicates, for tetrachloroethene (PCE), trichloroethene (TCE), cis-dichloroethene (cDCE), and vinyl chloride (VC), were collected over several field campaigns from mini-piezometers, which were also used for hydraulic head measurements (Figure 4.2). Because the plume was previously characterized, and is considered to be in a near steady-state condition (Sonne et al., 2017; Rønde et al., 2017), it was assumed that the plume remained unchanged between sampling efforts. Therefore, this study uses concentration data from sampling campaigns conducted in Oct. 2014, May 2015, June 2016, and September 2016. All velocity data were collected concurrently with the June 2016 campaign. Each water sample was collected by first purging the mini-piezometer with three well volumes and then collecting the samples in 20 to 40 mL glass vials with Teflon lined lids, sealed without headspace. The samples were preserved with 4 M sulfuric acid, and stored at 10^{o} C until analysis. Full analysis was completed within four weeks of collection. Analyses were conducted at the Technical University of Denmark using an Agilent 7980 Gas Chromatograph with an Agilent 5675 C mass-selective detector (GC-MS), following the procedure presented in McKnight et al. (2012). The quantification limits for these analyses were 0.06 μg/L for PCE, 0.043 μg/L for TCE, 0.048 μg/L for cDCE, and 0.0500 μg/L for VC).

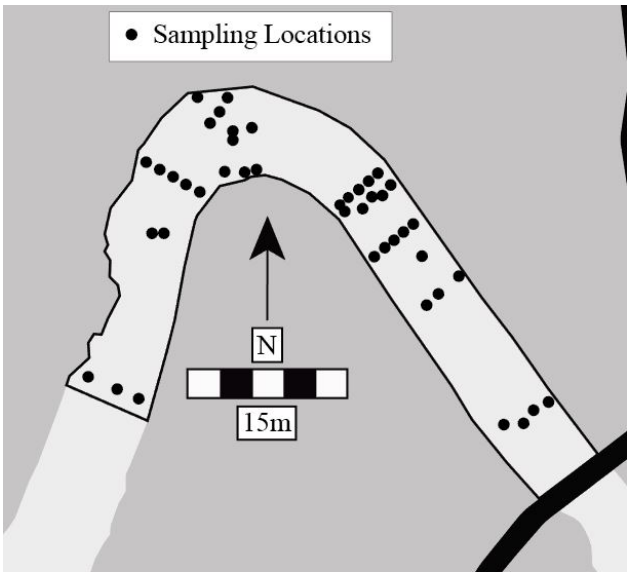

Figure 4.2: Pore water samples were collected from mini-piezometers at various locations in the stream and used to generate a map of contaminant concentrations near the interface of Grindsted stream. All samples were collected from depths between 40 cm and 70 cm, and analyzed for the presence of chlorinated ethenes.

4.3.2 Sediment characterization

To discern streambed heterogeneity, and reduce the errors associated with estimating K for Darcy calculations, the sediment at each measurement location was visually examined and documented. Slug tests were subsequently conducted in the *Grindsted Å* stream bottom across a representative sample of sediment types. Some recommendations were taken from Butler Jr (1997) (i.e. making sure screen wasn't clogged). One departure from Butler's recommendations is that only two tests, instead of three were completed at each location (locations shown in Figure 4.1). Only two tests were conducted because the results were so similar between replicates, a third test was not needed (see 3.1). K was measured in duplicate at 5 locations, for a total of 10 *in situ* tests (two measurement locations for silty sand, two locations for sand, and one location for gravelly sand, all at 40 cm depth). Sediment-type specific values for K were then applied to the location-specific discharge calculations, assuming locally isotropic conditions (discussed in the Results and Discussion section).

Slug tests were conducted using a drive-point piezometer with a 10 cm screen. A pressure transducer (programmed to gather data every 0.5 s) was placed in the piezometer and the system was left to equilibrate. After equilibration, water slugs of 1 m height were introduced to the piezometer. Data from the tests exhibited a straight line overdamped response. The data from these tests were processed in AQTESOLV (Inc., 2016), where K for each sediment type was calculated with the Hvorslev method (Hvorslev, 1951).

4.3.3 Temperature gradient measurements

Temperature surveys can offer a fast, inexpensive method of characterizing the GWSWI in detail. In the *Grindsted Å*, an Ebro TFN-520 Type K handheld thermometer was deployed using a steel spear to measure temperature gradients in 108 locations (Figure 4.1). In this study, the approach

of Schmidt et al. (2007) was adopted, using the following one-dimensional analytical solution:

$$q_z = -\frac{k_{fs}}{p_f c_f z} ln \frac{(T_Z - T_L)}{(T_0 - T_L)} \tag{4.1}$$

where q_z is Darcy flux in the vertical direction (ms^{-1}), k_{fs} is the thermal conductivity of the solid-fluid system ($Js^{-1}m^{-1}K^{-1}$), $p_f c_f$ is the volumetric heat capacity of the fluid ($Jm^{-3}K^{-1}$), z is the depth of measurement (m), T_z is the temperature at depth z (°C), T_L is the temperature of the groundwater which is fixed for all calculations (°C), and T_0 is the temperature at $z = 0$ (°C).

The assumptions of this solution, which are also described in Schmidt et al. (2007), are the following: (1) one-dimensional flow in the vertical direction, (2) ascending flow (meaning, the solution is not valid for downward flow (Turcotte and Schubert, 1982), (3) streambed temperatures are in quasi-steady state during the period of measurement, and (4) the properties of the sediment and fluid are assumed to be homogeneous over the entire temperature profile.

The known variables include z (depth of measurement), which was 40 cm (in this case), k_{fs} was assumed to be 2.2 $Js^{-1}m^{-1}K^{-1}$ (Hopmans et al., 2002) and $p_f c_f$ is 4.19 x 10^6 $Jm^{-3}K^{-1}$. This leaves only the three temperature values unaccounted for in equation 4.1. T_L, the temperature of groundwater, was determined to be 8.6 °C by averaging samples collected from streambank wells. T_0 is the temperature at the sediment-water interface. This value was measured along with a surface water measurement T_{sw} at every measurement location. T_z is the measurement of temperature at depth z, which was also taken at each measurement location by inserting the temperature spear into the sediment at 40 cm depth, the deepest a probe could be installed without damage (Figure 4.3). The 40 cm depth was selected in an effort to reach a zone beneath active horizontal hyporheic flow. The measurements were processed using the analytical solution presented above (Eq. 4.1) coded into an Excel sheet to determine q_z.

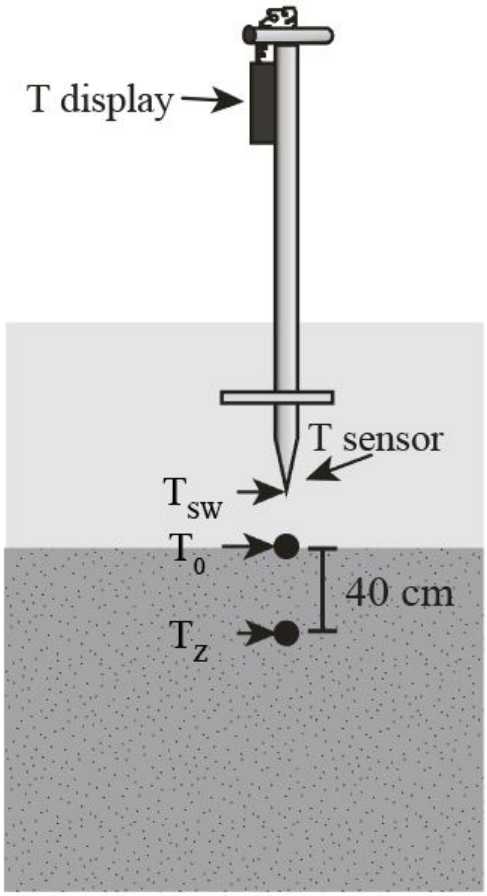

Figure 4.3: Temperature surveys require three measurements at each location, plus a measurement of the temperature of the groundwater (T_L) (not shown above): one in the surface water (T_{sw}), one at the sediment-water interface (T_0), and one below the interface (40 cm below, in this study) (T_Z). All measurements, except T_L, were taken over (or under) the same location on the streambed.

4.3.4 Darcy calculations

Darcy calculations are commonly applied to the estimation of water flux across the GWSWI (for example, Lee and Cherry (1979); Baxter et al. (2003); Rosenberry et al. (2008). To apply Darcy's Law to the *Grindsted Å* streambed, mini-piezometers were installed in 92 locations across 22 transects (Figure 4.1). The piezometers were constructed from clear polyvinyl chloride (PVC) pipes (open ended with approximately 2 cm inner diameter). Each mini-piezometer was installed with a drive-point to a depth of approximately 40 cm below the streambed, and the hydraulic gradient (i = ΔH/ΔL) was measured between that depth and the stream channel water (therefore, ΔL = 40 cm). The water levels in the piezometers were and allowed to equilibrate for 24 hours before measurements of hydraulic head ($H \pm 0.7$ cm) were collected. A Solinst Model 101 Water Level Meter was used to measure water levels inside the mini-piezometers and a stilling well was used to determine the water level of the stream channel water (Baxter and Hauer, 2000; Baxter et al., 2003) (Figure 4.4). In all measurement locations, the gradient either indicated upward flow or was not possible to quantify because ΔH was less than 0.7 cm, the uncertainty of a head measurement. The groundwater velocities from mini-piezometer data were calculated using the following modification of Darcy's law:

$$v = \frac{Ki}{n} \tag{4.2}$$

Based on previous studies of the site, a uniform effective porosity (n) of 0.3 was assumed (Rügge et al., 1999; Lønborg et al., 2006). Estimates of K were gathered from slug tests, as described above in the Sediment Characterization section.

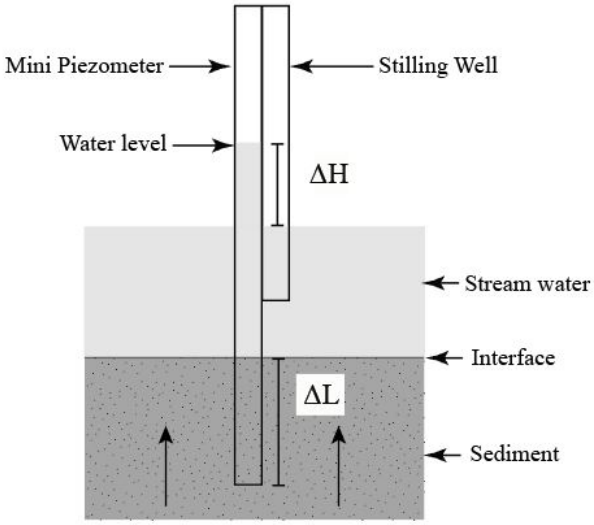

Figure 4.4: The mini-piezometer set-up used in the field. This example shows upward flow, as designated by the arrows and the difference in hydraulic head between the mini-piezometer and the stilling well.

4.3.5 Streambed point velocity probes

The streambed point velocity probe (SBPVP) was developed to provide high density datasets describing exchange across the GWSWI without reliance on gradient *i* or *K* information. The SBPVP estimates velocity by conducting a mini-tracer test on the surface of a 1-inch diameter drive point probe, which is inserted 7 to 10 centimeters into the streambed. The tracer is chosen on the basis of electrical conductivity contrast with the surrounding water. Further details can be obtained from Cremeans and Devlin (2017). The SBPVP was installed at 108 measurement locations (Figures 4.1, 4.5), at depths of about 7 to 10 cm beneath the sediment water interface Cremeans and Devlin (2017). To prevent horizontal hyporheic flow from influencing tests, a hyporheic shield (22 cm outer diameter and 61 cm height) was attached to the instrument (3.6 cm outer diameter and 4.5 cm height), isolating the vertical component of flow for measurement (Figure 4.5). All tests were conducted with tracer injection volumes ranging from 0.1 mL to 1 mL, as determined experimentally Cremeans and Devlin (2017) with tracer concentrations between 1 g/L NaCl and 2 g/L NaCl, as required. SBPVP tests lasted from 3 minutes to 3.5 hours. All data were processed in VelProbePE (Schillig, 2012).

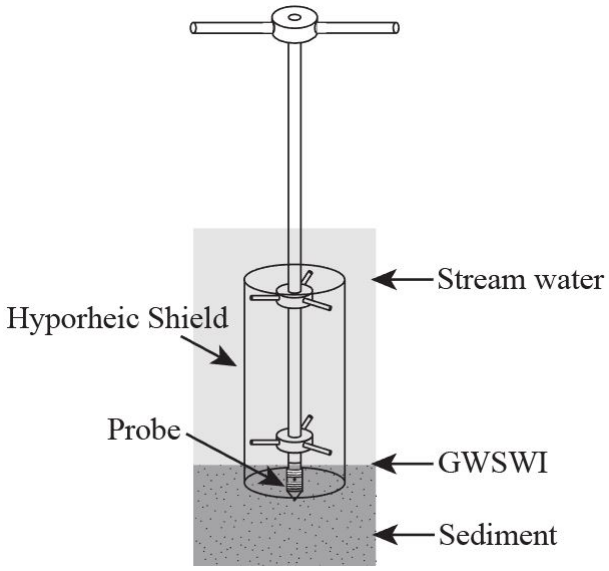

Figure 4.5: The SBPVP is installed 7 to 10 cm below the GWSWI, with a hyporheic shield to prevent the influence of non-vertical through-flow on measurements.

4.3.6 Contaminant mass discharge calculations

Visual representations of the in-stream chlorinated ethene mass discharge zones, sediment types, and measured velocity distributions were created with ArcGIS10 using the Inverse Distance Weighting (IDW) interpolation method. IDW is considered a "conservative" interpolator in this case, because low to moderate influence was assigned to empirical measurement points that were far from the interpolated points (a power of 3 with 2 neighbors, and a power of 2 with 12 neighbors, respectively). The application of IDW is described in full detail in the ArcGIS10 documentation (ESRI, 2017). The effect of these choices is that relatively sharp and localized boundaries are defined around the measured points that form localized extremes of the measurement range (high or low). Given the relative sparseness of the pollutant concentration dataset (compared to the SBPVP grid), the IDW scheme used here is expected to err on the side of underestimating pollutant masses, because unsampled areas of high pollutant concentration would be overlooked in the interpolation calculations. By comparison, the velocity data were collected on a denser grid than the water quality samples and, therefore, were less susceptible to interpolation-related errors. Velocity data (from SBPVP, piezometer, and temperature methods) and chemical concentration data were interpolated with IDW at the same cell size (0.171 m^2). These interpolated datasets, plus an assumed uniform porosity of 0.3, provide the necessary values to calculate a preliminary mass discharge:

$$J_{total} = n * \sum_{i=1}^{m} C_i * v_i * A_i \tag{4.3}$$

where J_{total} is the total mass discharge (kg/yr), C_i is the concentration in each cell (kg/m^3), v_i is the velocity in each cell (m/yr), n is the effective porosity (dimensionless) in each cell, and A_i is the area of each cell (m^2) (common cell size, given above), m is the number of cells in the IDW grid. Mass discharges of chlorinated ethenes into the stream are presented in PCE equivalents with units of kg/yr. Each compound was converted to a PCE equivalent using the following equation:

$$PCE\,Equivalent\,Mass = Compound\,Mass * \frac{PCE\,Molar\,Mass}{Compound\,Molar\,Mass} \tag{4.4}$$

Table 4.1: Summary of K values measured in the *Grindsted Å* streambed

Location	Test 1	Test 2
Transect 1 (gravelly sand)	$2.448x10^{-4}m/s$	$2.564x10^{-4}m/s$
Transect 3 (silty sand)	$5.421x10^{-5}m/s$	$4.938x10^{-5}m/s$
Transect 5 (sand)	$1.075x10^{-4}m/s$	$1.088x10^{-4}m/s$
Transect 7 (sand)	$1.043x10^{-4}m/s$	$9.821x10^{-5}m/s$
Transect 14 (silty sand)	$4.722x10^{-5}m/s$	$4.652x10^{-5}m/s$

Implicit in these calculations is the assumption that the pollutant concentrations and velocity measurements represent the same location near the GWSWI. Given that all measurements were conducted within the top 7 to 70 cm of the stream bottom, the assumption is consistent with obtaining a useful approximation of the discharge patterns. It must be acknowledged, however, that the possibility of horizontal pollutant transport away from the sampling points before discharging to the stream could have occurred in some locations. Also, the possibility of transformations occurring at some locations within the top 70 cm of sediments, cannot be ruled out.

4.4 Results and discussion

Concentration data describing the plume of chlorinated ethenes suggested they were present in the streambed throughout the study reach, but were most concentrated near the apex of the meander and near transect 10, immediately upstream of the apex (Figure 4.6A). The streambed consisted of three observable sediment types: silty sand, sand, and gravelly sand (Figure 4.6B). Slug tests conducted in each sediment type indicated that the silty-sand sediments were characterized, on average, by $K = 4.92 * 10^{-5}m/s$, the sandy sediments by $K = 1.05 * 10^{-4}m/s$, and the gravelly sand sediments by $K = 2.51 * 10^{-4}m/s$ (Table 4.1). The sediment types were mapped in detail, based on the grid shown in Figure 4.1, and the range of K was found to be quite narrow for each type. Therefore, the associated Darcy calculations depending on these data are thought to be quite representative of the site. Nevertheless, the number of slug tests performed was small and could contribute to uncertainty in the calculations in some cases.

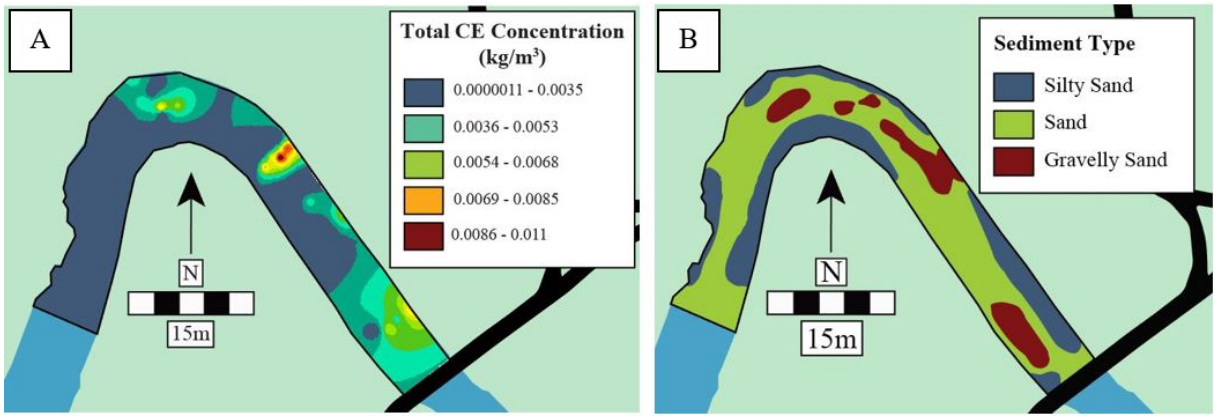

Figure 4.6: (A) Preliminary assessment of chlorinated ethene distributions in the shallow streambed sediments (40 to 70 cm depth, as PCE equivalents). (B) The stream bottom was also assessed for sediment type. Three main sediment types were established and a series of slug tests was conducted to determine *K* for each type (Table 4.1).

To begin the estimation of the groundwater-surface water exchange rate, the temperature gradient method was applied. The temperature-derived pattern of flow reveals relatively low discharges upstream of the meander, with localized regions of higher flow through the meander and slightly downstream (seepage velocities up to 129 m/yr) (Figure 4.7). The streambed was subsequently surveyed using mini-piezometers to obtain hydraulic gradient data (on the same sampling grid). Due to time constraints associated with installation and equilibration of the mini-piezometers, four fewer transects were examined by this method (Figure 4.8A). The estimated groundwater discharges from the mini-piezometer data (expressed here as velocities for consistency) suggested a pattern of heterogeneous flow that was spatially similar to the temperature data discussed above; the upstream region of the study reach was associated with relatively low discharges and the discharges at the meander apex and downgradient segment were characterized by localized regions of relatively high velocities (Figure 4.8A).

Comparison of the Darcy-derived velocities and the temperature-derived velocities showed major differences (on the order of a factor of 10) in velocity magnitudes (Figures 4.7, 4.8A). The velocities were calculated with values of K from slug tests performed in the streambed, which assumed locally isotropic conditions in the sediments. This assumption may have resulted in conservatively large estimates of v, since vertical anisotropy was ignored. However, because the sediments were generally sandy, and testing was conducted in a single sediment stratum at each location, factors of anisotropy can reasonably be expected to be low, between 1.3 and 1.6 (Burger and Belitz, 1997), justifying our approximation of isotropic conditions in the streambed. Regardless, anisotropy of the bed sediments does not seem to fully account for the differences in flow magnitudes between the Darcy calculations and the temperature gradient calculations.

The anomalously low flux estimates from the temperature gradient method are explainable by potentially significant horizontal flow in the *Grindsted Å* streambed, associated with the penetration of stream water into the bed to a depth of at least 40 cm, as discussed in the Introduction (Lautz,

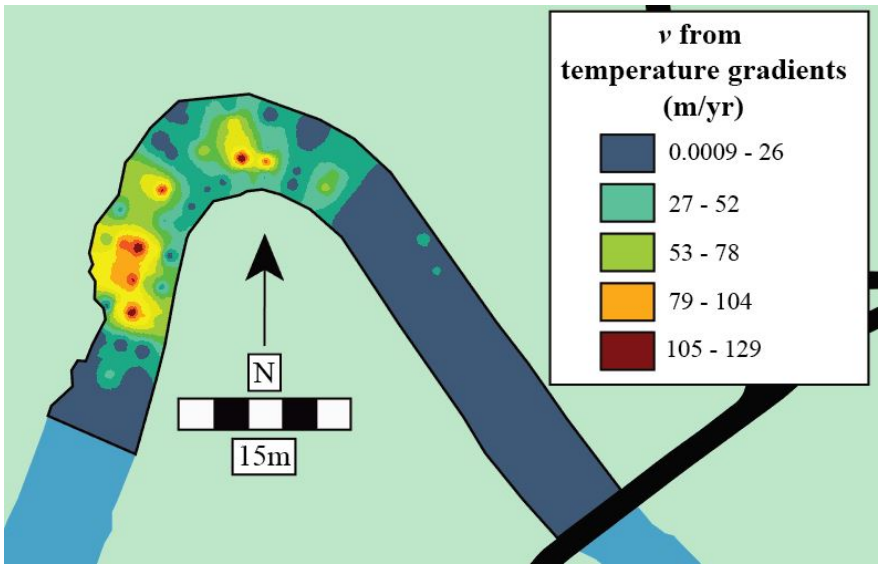

Figure 4.7: Temperature gradient measurements were the basis for a preliminary assessment of discharge patterns at the GWSW interface. The temperature measurements were made in the stream water column, at the sediment-water interface, and at 40 cm depth below the interface to support the calculations. Note that the scale of groundwater velocity from the temperature data is over an order of magnitude smaller than the scales determined by the other velocity estimation methods.

2010; Irvine et al., 2016; Munz et al., 2016). Assuming the Darcy-derived fluxes are representative of the actual vertical flows, this finding is illustrative of a potential limitation of temperature data to calculate groundwater fluxes in streambeds. Other limitations have been documented, such as the seasonal dependence of temperature gradients that limits the times of year when the method is applicable (Irvine et al., 2016). Despite the issues encountered in this work, it is noted that the temperature-based methods represent a fast and useful approach to streambed characterization, complimentary to the other methods used here, and they have been successfully applied in a variety of cases (Lautz, 2010; Lewandowski et al., 2011; Bhaskar et al., 2012; Lu et al., 2017).

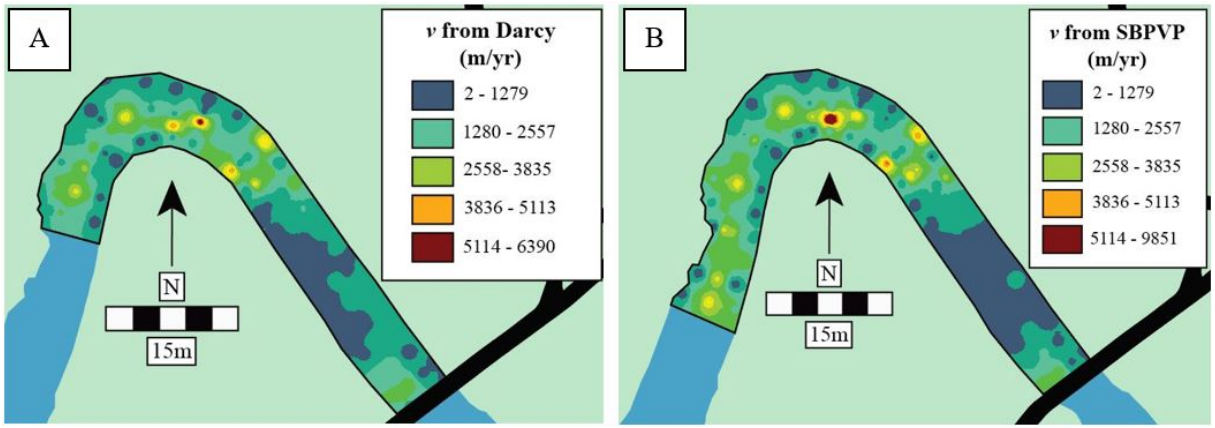

Figure 4.8: (A) Results of the Darcy method applied to measure exchange, using mini-piezometers. (B) Results of the SBPVP applied to the measurement of vertical streambed seepage velocities. Please note that upper limits are different for the two contour scales due to one measurement outlier (discussed in the text below).

The velocities measured using the SBPVP revealed very similar spatial patterns of flow compared to those found by the two preceding methods (Figure 4.8B). This result verifies the preliminary findings of Cremeans and Devlin (2017) with a more extensive dataset from the same site. Moreover, the velocity magnitudes suggested by the SBPVP data compared very well with those from the Darcy calculations. A linear correlation was found to exist between the two methods' estimated velocities; the values fell along a line with a slope of 1.08 with a 95% confidence envelope of $\pm$150 m/yr over a velocity range of 0 to approximately 500 m/yr, and $\pm$550 m/yr for velocities up to 5500 m/yr (Figure 4.9). The dataset contains one significant outlier which was not included in the 95% confidence interval calculations (shown in Figure 4.9 as an open circle). The anomalous point occurred at a location where the SBPVP measured a velocity of approximately 4,500 m/yr while the Darcy calculations led to an estimate of approximately 6,500 m/yr. In this case, it is thought that a change in the prevailing sediment type at 40 cm depth (noted during piezometer installation) led to the use of an unrepresentative hydraulic conductivity value in the Darcy calculation. This sediment change is local to this measurement location likely due to construction related to the installation of adjacent culverts, which may have disturbed the sediment at 40 cm depth.

The highest velocity value from the entire data set, measured by the SBPVP, is 9851 m/yr (27 m/day), which seems high but may result from a high convergence of streamlines from the bank to the streambed. The piezometer at this location behaved like a flowing artesian well, and the total hydraulic head there could not be measured. The corresponding point was omitted from Figure 4.9. The point was, however, included in the mass discharge calculations by using the measured SBPVP velocity value as measured, but assuming total hydraulic head there was at the elevation of the top of the piezometer casing. It is recognized that this approximation caused an underestimation of the Darcy-derived mass discharge at this point.

The Darcy-derived mass discharges were calculated to be within 435.2 to 438.2 kg/yr. Using the SBPVP data, the total chlorinated compound mass discharge (in PCE equivalents) was calcu-

lated to be between 437.9 and 444.1 kg/yr. In both cases, the lower estimate was calculated with a restrictive Inverse Distance Weighting (IDW in ArcGIS) interpolation of the concentration data (i.e., low influence was assigned to interpolated points far from the empirical points). In this interpolation, an exponent of 3 was assigned and the number of neighbors used was 2. The higher estimate was calculated with a more inclusive IDW interpolation of the chemical data (moderate influence assigned to interpolated points far from the empirical data points) (Figure 4.10). In this interpolation, the exponent was set at a value of 2 and the number of neighbors used was 12.

The streambed determinations of chlorinated mass discharge – from Darcy calculations and SBPVP measurements – compared well with similar estimations conducted using data from the northern streambank, as reported by Rønde et al. (2017). Based on Darcy calculations and PVP measurements along a control plane (defined as a plane "oriented perpendicular to the groundwater flow direction and that extends over the entire width and depth of the plume"), they estimated the total chlorinated compound discharge to be between 204 kg/yr and 372 kg/yr. The low value of this range was obtained using PVP data averaged over the control plane (Rønde et al. (2017), pg. 43), raising the possibility that some zones of coincident contamination and high flow rates were not sampled on the control plane. Note that the challenge of sampling the entire plume section is facilitated in the streambed, where flowlines converge. The highest estimate of mass discharge at the stream bank reported by Rønde et al. (2017) was associated with Darcy calculations, which used a geometric mean value of K (1.8 10^{-4} x m/s) from slug tests in streambank wells and a hydraulic gradient normal to the control plane from piezometers installed on the streambank and in the streambed (0.034).

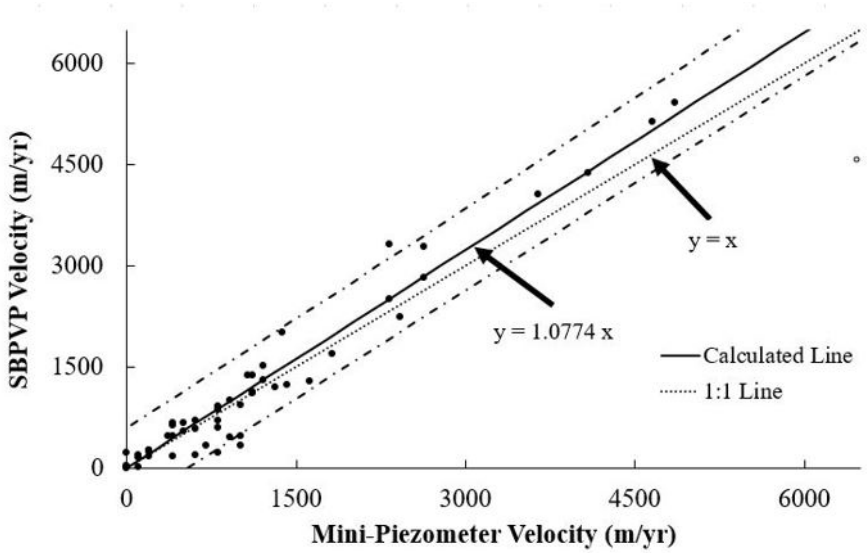

Figure 4.9: A plot of SBPVP velocities compared with Darcy-derived velocities from the *Grindsted Å*. A single outlier is shown as an open circle. The black dots represent the experimental data, the dot-dash lines represent the error envelope with 95% confidence, based on the measured velocity range of 0 to about 5000 m/yr.

As expected from the water flux calculations, the total contaminant mass discharge calculated with the temperature data yielded a much lower range of total chlorinated ethene discharge than both the Darcy and SBPVP datasets (4.7 kg/yr to 5.1 kg/yr). For reasons previously discussed, and because the mass discharges from the other methods substantially exceeded these values, the temperature-derived estimations are thought to be erroneously low.

With detailed knowledge of the distributions of water discharge and chlorinated ethene occurrence in the streambed, it is possible to calculate mass discharge rates using equations 4.3 and 4.4. Most importantly, the resulting pattern of total equivalent PCE mass discharges is not exactly represented by either the water velocity or pollutant concentration patterns in the streambed (compare Figures 4.6, 4.7, 4.8, and 4.10). This divergence could occur as a result of either physical or chemical/microbial processes. For example, where the highest flow zones do not coincide with the highest concentration zones, the less aggressively flushed sediments are able to retain the highest levels of contamination for a longer period of time. Alternatively, the divergence could be the result of differential transformation (or biotransformation) rates; sediments with slightly greater water resi-

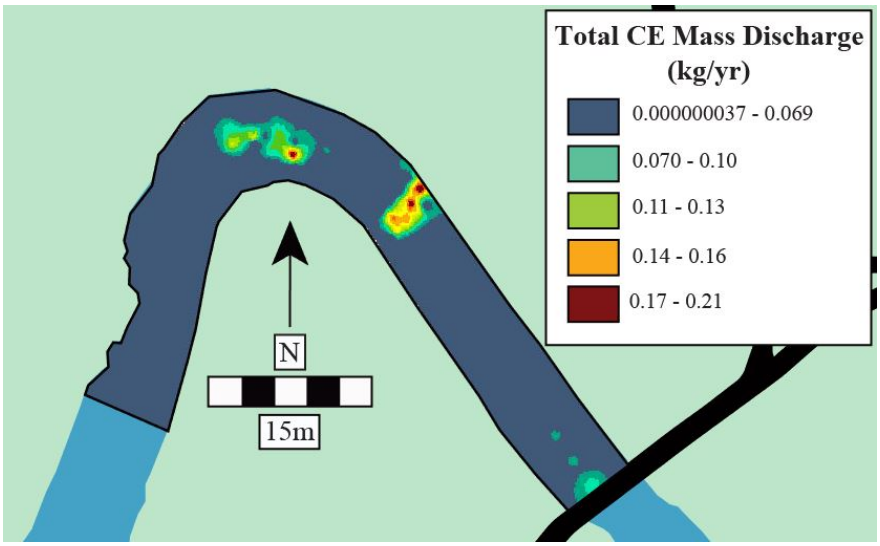

Figure 4.10: Contaminant mass discharge (J) was calculated using equation 4.3 based on concentrations from Figure 4.6A, and SBPVP data (v_i) shown in Figure 4.8B.

dence times may have maintained the redox conditions necessary for dechlorination reactions that produce cDCE and VC, hence these compounds – which make up the majority of the chlorinated ethene loading at the *Grindsted Å* – would be associated with the lower seepage velocity zones. Note also that the locations where transformations took place could have been some distance upgradient of the streambed. Regardless of the reasons for the divergence, this phenomenon implies that concentration distributions do on their own reflect the risk associated with mass discharges across the GWSWI. The same implication applies to flow measurements: high groundwater flux estimates do not necessarily correspond to high contaminant mass discharges. Therefore, the results of this study suggest that detailed characterization of both the flow and concentrations may be needed to properly assess risk. Moreover, knowledge of the locations of highest contaminant mass discharges can be used to identify zones of greatest concern and guide highly focused remediation plans, with associated cost and treatment efficiencies.

4.5 Conclusions

Field validation of the SBPVP suggests that it is a useful tool for high resolution monitoring and identification of localized regions of high flow. Spatial patterns of flow distribution (i.e., loca-

tion of high flow and low flow) tended to be similarly identified from temperature spears, mini-piezometers and the SBPVP suggesting that the patterns of flow are well-delineated by all methods. However, considering the magnitude of a previously reported total mass discharge (across a control plane on an adjoining bank of the stream, 204 to 372 kg/yr), only the SBPVP and mini-piezometer data reflect reasonable mass discharge values, 437.9 to 444.1 kg/yr and 435.2 to 438.2 kg/yr, respectively.

While the Darcy and SBPVP methods were similarly viable in determining mass discharge (and complementary in the type of data they provided), the SBPVP survey was conducted more quickly and with less manpower than the mini-piezometer survey. This outcome presents clear potential advantages for the use of the SBPVP in future investigations at the GWSWI of shallow streams. While the SBPVP can efficiently provide detailed spatial information about flow distribution and magnitude, the results from this work suggest that the temperature gradient method, which is fastest to implement, could be used to great advantage in combination with the SBPVP by identifying or verifying locations of the greatest water fluxes across the GSWSI.

4.6 Acknowledgements

The authors would like to extend thanks to the Madison and Lila Self Graduate Fellowship for support of Mackenzie Cremeans as well as the University of Kansas Doctoral Research Fund, Kansas Geological Foundation, and GEOCON (Innovation Fund Denmark, contract no. 1305-00004B) for supporting the work. From the Technical University of Denmark, Anne Th. Sonne, Nicola Balbarini, and Vinni Rønde are acknowledged for collaborative discussions. Bent Skov is acknowledged for assistance in the field, and Hanne Bøggild is acknowledged for her assistance with the chemical analysis.

Chapter 5

Evaluation of flow patterns in a vertical flow bioreactor in Commerce, Oklahoma

Prepared for submission to Groundwater Monitoring & Remediation

5.1 Abstract

In this study, the streambed point velocity probe (SBPVP) was used to characterize flow through the bed of a passive Vertical Flow Bioreactor (VFBR) pond at the Mayer Ranch passive treatment system (PTS) in Commerce, Oklahoma. The VFBR was constructed to remove metals from groundwater originating from the Tri-State Superfund site to the north, and discharging naturally from springs at the site. The velocity data were validated with a water balance and metals loading rates in the VFBR bed were estimated for comparison with a previously reported treatability test. The outflow calculated from SBPVP data came within 30% of the value suggested by measured inflow rates. Water flow rates through the reactive bed were found to be an order of magnitude greater than those employed in prior column testing. However, the resulting low residence times were offset by apparently rapid chemical reactions and observed loading rates (42 mg/m^3/d) considerably below the capacities demonstrated in the laboratory tests (80 to 90 mg/m^3/d). As a result, the treatment system achieves its design objectives.

Keywords: mine water, passive treatment, point velocity probe, tracer test

5.2 Introduction

The Tar Creek Superfund site is located on approximately 40 square miles of northeast Oklahoma in the abandoned Picher Mining Field. To treat metals-contaminated water from historic mining activities, a passive treatment system (PTS) was designed and constructed by the University of Oklahoma in Commerce, Oklahoma (Figure 5.1). The PTS design was motivated by the release of regulated chemical constituents in the mine water over a period of 25 years, and construction was completed in the 29th year of mine water discharge from springs in Commerce. Geochemical sampling has shown that when the contaminated mine water arrives at the surface, it contains notable concentrations of iron (192 mg/L), cadmium (0.015 mg/L), lead (0.067 mg/L), nickel (0.91 mg/L), arsenic (0.064 mg/L) and zinc (8.24 mg/L). Aluminum, cobalt and manganese are also present in trace amounts (Nairn et al., 2010).

Contaminated mine water reaches the PTS as artesian flow and, once in the PTS, water flows through a series of processing units. The initial unit (C1) is an oxidation pond, which drains through a branching outlet to two parallel series of ponds constructed as replicate treatment trains. The treatment process comprises the following: surface-flow aerobic wetlands/ponds (C2N and C2S), vertical flow bioreactors (C3N and C3S), reaeration ponds (C4N and C4S), and horizontal flow limestone beds (no surface flow in these units, C5N and C5S). The branched flow is then recombined into a final polishing pond (C6). The system has been in operation since 2008 and has regularly met its treatment objectives, based on chemical analysis of the PTS outflow (Nairn et al., 2011).

The purpose of this field study was to characterize the flow through one of the VFBR units, C3S, to assess possible heterogeneity of flow through the reactive bed material, and to estimate metal

removal rates for comparisons with the treatability work done during the design phase of the PTS project (LaBar and Nairn, 2016).

5.2.1 Treatment pond C3S

The VFBR C3S occupies area of 774 m^2. It was constructed with a 0.46 m thick layer of organic substrate (45% spent mushroom compost, 45% hardwood chips, and 10% manufactured limestone sand, hereafter referred to as SMS) underlain by a layer of limestone gravel containing perforated pipe networks to collect the treated water and deliver it to the next pond in the treatment system (Nairn et al., 2009). The gravel is underlain by a low permeability geotextile liner. The overall PTS was designed to accommodate flows of up to 1000 L/minute (Nairn et al., 2010), corresponding to a maximum flow capacity of 500 L/minute in C3S (with the remaining 500 L/minute passing through C3N). Prior to this study, the pond had been in operation about nine years and there were indications that the bed had become compacted. Permeability testing of the bed was subsequently undertaken and the hydraulic conductivity (K) was estimated with four methods: (1) field falling head tests (K = 29 cm/day), (2) slug testing using the Bower and Rice method (K = 17 cm/day), and (3) laboratory falling head tests on cores collected in the field (K = 43 cm/day) (Page, 2016). To address concerns regarding compaction and low K in the substrate, University of Oklahoma personnel conditioned the bed by draining the pond and physically loosening the bed material in 2016. After reconditioning, the bed was tested again for its permeability, this time by slug tests in selected locations (Dr. Bob Nairn, Pers. Comm.). The reconditioned bed was estimated to have a hydraulic conductivity (K) of approximately 259 cm/day (Dr. Bob Nairn, Pers. Comm.). Note that all velocity measurements described in this study occurred through the higher K reconditioned bed.

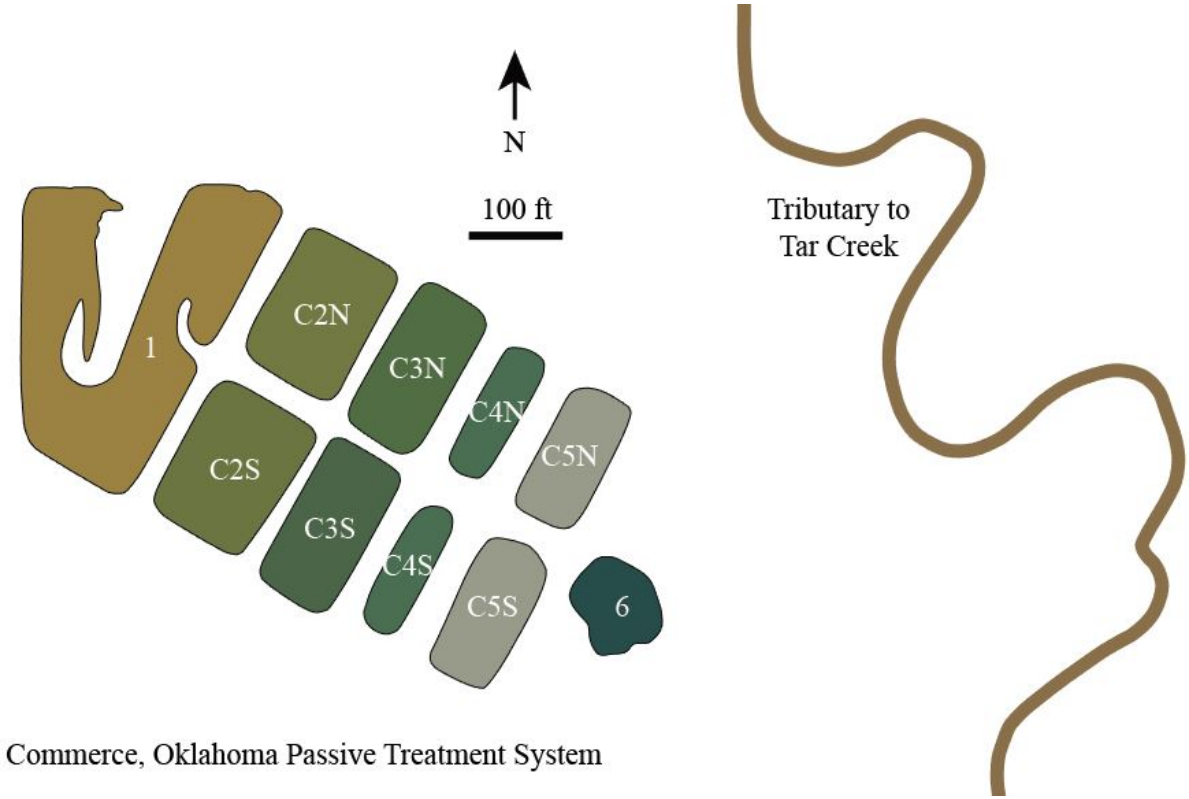

Figure 5.1: The passive treatment facility in Commerce, Oklahoma directs artesian seeps of mine wastewater through a set of processing units to remove harmful chemical constituents. Once the water has been treated by all 6 kinds of unit, it is released back into Tar Creek via a nearby tributary.

5.3 Methods

To determine patterns of flow through the bed of the VFBR, the streambed point velocity probe (SBPVP) was used to make nine measurements across three transects. The transects were spaced equally from the edges of the unit (Figure 5.2). Measurement locations along each transect were selected to provide as even a sampling of the pond bed as possible, with some consideration given to installation ease (in some locations the probe could not be satisfactorily advanced, possibly due to blockage by large wood chips) and limitations arising from the length of the SBPVP electrical cabling. No measurements were at the pond edges, where the bed was subhorizontal and the reactive bed medium pinched out to be replaced by low permeability geotextile. The area of the pond underlain by these sloped sides were omitted from the area estimated for the pond (774 m^2).

Because the site water has high total dissolved solids (TDS), a saline tracer provided insufficient electrical conductivity contrast to support SBPVP testing. To overcome this problem, deionized water was used in all tests. The tracer was manually introduced in 1-mL injections performed over 27 s to 36 s. Tracer breakthrough curves were analyzed with VelprobePE (Schillig, 2012), modified to include analysis by the method of moments (!!!!!Devlin, 2017), which was used in all cases. The probe was seated between 5 and 8 cm beneath the SMS surface. The probe was installed with a horizontal hyporheic shield, as previously described (Cremeans and Devlin, 2017), modified with saw teeth to facilitate cutting through the plant mats found growing on the SMS bed. Eight installations were performed accessing the measurement site by wading into the pond, and one additional location was instrumented from a canoe, due to low bed competence. The SBPVP was further modified with the addition of a piece of sponge in the injection port, to prevent the fine material in SMS from invading the line and causing a clog.

The inflow rate to the pond was measured in triplicate with a calibrated collection container and a stopwatch on the day the SBPVP measurements were completed. The outflow rate could not be directly measured because the drainage pipes to the next pond were below surface. Since the pond

was not noticeably filling or draining, the outflow rate was assumed to equal the inflow rate in the following calculations. To calculate a pond-wide retention time in the VFBR bed (equation 5.1), the volume of pore water in the compost layer was estimated with equation 5.2. The bed was assumed to be fully saturated.

$$t_r = \frac{V_{pw}}{Q_{ss}} \tag{5.1}$$

$$V_{pw} = n * V_{SMStot} = n * A_{SMStot} * d \tag{5.2}$$

where, t_r is the retention time of water in the SMS bed material (T), V_{pw} is the volume of pore water in the saturated SMS material, (L^3), Q_{ss} is the steady state flow rate through the pond (L^3T^{-1}), n is porosity (dimensionless), d is the thickness of the SMS bed (L), V_{SMStot} is the saturated volume of the SMS bed material (L^3), and ASMStot is the area of the pond underlain by SMS (L^2). Here units are presented in generalized form, with L equal to length, and T equal to time.

An estimate of Q_{ss} derived from the SBPVP measurements, Q_{SBPVP}, assuming a uniform bed porosity, n,

$$Q_{ss} \cong Q_{SBPVP} = n \sum_i v_i A_i \tag{5.3}$$

where n is porosity, and A_i is the area of pond represented by the SBPVP measurement at location i. Combining equations 1, 2, and 3, and assuming the SBPVP measurements areas (A_i) are equal it can be shown that

$$t_r = \frac{md}{\sum_i v_i} \tag{5.4}$$

where m is the number of measurement areas. This shows that residence time can be determined without reference to the porosity or the specific size of the measurement areas (as long as the assumptions of area and porosity equalities are reasonable). This is a useful result, since porosity can be a parameter with notable uncertainty attached to it, as discussed in the Water Balance section, below.

The values of Q_{SBPVP} can be used to estimate metal loadings to the SMS (Watzlaf et al., 2004),

$$M_{Lij} = \sum_i C_i Q_{SBPVP} \tag{5.5}$$

where M_{Lij} is the mass loading of contaminant j at location i (M T^{-1}) and M is the generalized unit for mass. For consistency with previously reported laboratory values and for the purposes of this report, mass loadings are reported on a per volume of SMS basis, for which equation 5 can modified as follows,

$$M_{Lij} = \sum_i \frac{C_i Q_{SBPVPi}}{V_{SMSi}} \tag{5.6}$$

where M_{LVij} is the volume-based mass loading and V_{SMSi} is the volume of saturated SMS associated with sampling location i.

5.4 Results

The SBPVP velocity survey revealed a fairly uniform pattern of infiltration rates through the SMS in pond C3S. Measured velocities ranged from 106 cm/day to 186 cm/day, except near the inlet pipe (P3 in Figure 5.2) where a value of 54 cm/day was determined. Darcy calculations, using the post-reconditioning K value of $3.00 * 10^{-5}$ m/s, a total flow rate of $2.79 * 10^{-3} m^3/s$ (Table 5.1), and assuming n = 0.33, led to estimated seepage velocities in the bed of 0.94 m/day, within the range of the measured values. The anomalously low seepage velocity at P3 is hypothesized to be the result of selective degradation of the substrate near the inlet, resulting in relatively rapid accumulation of muck. The inlet area was also the location where SBPVP deployment from a canoe was necessary, due to the softness of the bed, which is consistent with the hypothesis. The variability in sediment texture, between the inlet area and the rest of the pond, was noted during the re-conditioning of the pond bed, indicating that seepage velocities were probably low at that location before the re-conditioning took place in 2016 (Dr. R. Nairn, pers. comm).

5.4.1 Water balance

To assess the accuracy of the SBPVP velocity estimations, a water balance calculation was performed. Measurements of the inflow rates to C3S (Q_{ss}) were in the range of $2.70 * 10^{-3} m^3/s$ to $2.80 * 10^{-3} m^3/s$ on the day of testing (Table 5.1). If this was also the flow through the pond bed, then the seepage velocity can be estimated from

$$v = \frac{Q_{ss}}{An} \tag{5.7}$$

where A is the total area of the pond. Assuming $Q_{ss} = 2.79 * 10^{-3} m^3/s$, n = 0.33, and A = 774 m^2, this calculation leads to v = 0.94 m/day, in agreement with the previous Darcy calculation.

Each of the SBPVP measured velocities may be assumed to represent an equal area of the VFBR (about 86 m^2). When these values are used in Eq 5.3, and the porosity is again assumed to be homogeneously 0.33, the total SBPVP-derived flow rate overestimates the average measured inflow rate by about 30%, with a value of $3.59x10^{-3} m^3/s$ (Table 5.2). This level of agreement is considered quite good and is probably attributable to the limited range of seepage velocities found to exist in the bed. The consistency of flow rates from the Darcy calculation and the independent water balance calculations provide strong corroborative evidence that the SBPVP measurements are representative of seepage velocities in the pond bed.

The 30% discrepancy in the water balance is easily accounted for in the assumed porosity term; for example, if the porosity is assumed 0.26 instead of 0.33, the water balance produces nearly exact agreement between the measured inflow rate and Q_{SBPVP}. However, the porosity of SMS was reported to be in the range of 0.42 to 0.87 in laboratory experiments LaBar and Nairn (2016) and further work by Page (2016) suggests a range of 0.487 to 0.888, so the empirically derived value of 0.26 appears to be low. Nevertheless, compaction of the pond bed could have contributed to a porosity below that observed in laboratory testing, and 0.26 is within the range of effective

porosities in field studies involving porous media (Freeze and Cherry, 1979; Wiedemeier, 1999), so a lower than expected porosity cannot be entirely ruled out.

Applying these results to equation 5.4, and again assuming d = 0.46 m, the retention time for water in the SMS bed is calculated to be 3.27 x 10^3 s, or 9.08 hours (ranging from about 7 hours to about 11 hours for specific measurement areas, and about 20 hrs near the inlet pipe (P3 in Figure 5.1). Therefore, the residence time in the pond bed is considerably shorter than that reported for the treatability columns (72 hours) (LaBar and Nairn, 2016). However, given concentration data from the pond outflow, the smaller residence time doesn't appear to be a problem for the water treatment processes.

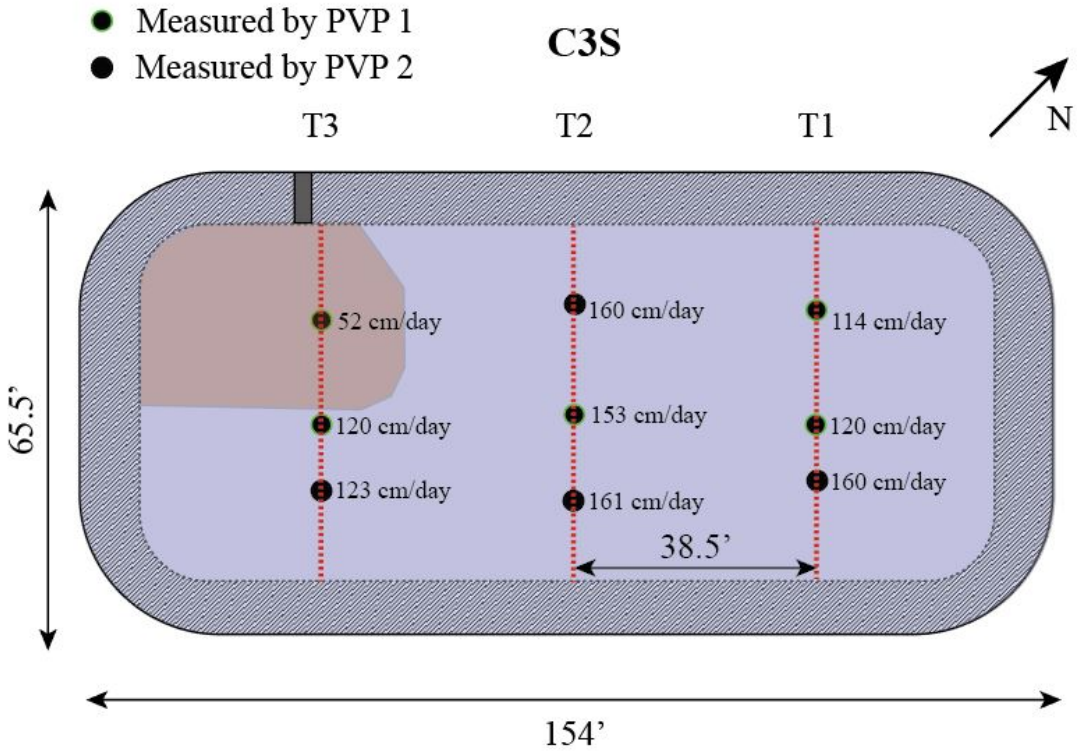

Figure 5.2: Aerial map view of the C3S pond, with SBPVP sampling locations shown. The first number displayed by the sampling locations is the velocity estimated by Method of Moments calculations. The second number is an optimized velocity estimated by fitting a 1-D solution to the advection dispersion equation to the tracer breakthrough curves.

Time(s)	Volume (L)	Rate of water entering (m^3/s)
3.89	11	0.002828
4.21	11.5	0.002732
4.08	11.5	0.002819

Table 5.1: Inflow Measurements (5/16/2017)

SBPVP (cm/day)	SBPVP (m/s)	Area of Cell (m^2)	n	Q_i (m^3/s)	n	Q_i (m^3/s)
54.0	6.25E-06	86.0	0.33	1.77E-04	0.26	1.38E-04
160.0	1.85E-05	86.0	0.33	5.26E-04	0.26	4.09E-04
106.0	1.23E-05	86.0	0.33	3.48E-04	0.26	2.71E-04
116.0	1.34E-05	86.0	0.33	3.81E-04	0.26	2.96E-04
148.0	1.71E-05	86.0	0.33	4.86E-04	0.26	3.78E-04
101.0	1.17E-05	86.0	0.33	3.32E-04	0.26	2.58E-04
110.0	1.27E-05	86.0	0.33	3.61E-04	0.26	2.81E-04
161.0	1.86E-05	86.0	0.33	5.29E-04	0.26	4.11E-04
138.0	1.60E-05	86.03	0.33	4.53E-04	0.26	3.52E-04
Totals:		773.9		3.59E-03		2.79E-03

Table 5.2: Water balance assuming equal areas around sampling points and two porosities.

In addition to porosity uncertainty, another possible source of error in the water balance arises from the assumption of equal representative areas for each measurement. A positive bias in the total Q_{SBPVP} could arise if the anomalous area surrounding the inflow pipe is larger than assumed in Table 5.2. To investigate the sensitivity of the calculations to this possibility, additional calculations were performed in which the areas proximal to the inlet were adjusted to allow the inlet sampling area to grow in size. Four inlet area scenarios were considered: 86.0 m^2, 129.0 m^2, 172.0 m^2, and 193.5 m^2 (Figure 5.3). In each case, Eq. 5.3 was re-evaluated to obtain the associated value of Q_{SBPVPi}. The largest possible value for the inlet area was estimated to be 193.5 m^2, if the boundaries of the inlet area were not to cross a neighboring sampling location. Inspection of Figure 5.3 shows that uncertainty in the size of the low velocity zone of near the inlet cannot fully account for the difference between Q_{SBPVP} and Q_{ss}.

A third explanation for the discrepancy between Q_{ss} and Q_{SBPVP} could arise from the assumption of steady state flow. While pond height did not look noticeably different, during the testing

period, it was observed that the inflow varied between days with rain events occurring overnight. It is possible that C3S was undergoing a net draining of water during the testing period, accounting for flows out of the pond, through the bed material, exceeding flows into the pond.

Finally, the SBPVP sampling density was relatively sparse. Sampling density may not be a severe problem in this case, given the observed similarity of infiltration rates across the pond, and the insensitivity to moderate variations to that distribution shown in Figure 5.3. Nevertheless, sparse sampling density by its very nature can miss local incidences of heterogeneity that may affect overall flow rates in an important way. For example, Schillig et al. (2016) demonstrated the effect of a thin, high permeability stratum on the rate of nitrate mass discharge toward municipal wells in Ontario, Canada. The stratum was missed by early characterization work with relatively low well density. Béland-Pelletier et al. (2011) showed that chemical monitoring point density was the likely primary source of error in estimating contaminant mass fluxes through a fence of multilevel monitors in the CFB Borden aquifer, Ontario, Canada, which is generally regarded as nearly homogeneous (Mackay et al., 1986). In the current case, a higher sampling density would be useful along the boundaries of the VFBR, and in the vicinities of the largest observed velocity variations (particularly in the inlet area of C3S) to better determine the presence of preferential flow paths or zones of excessive compaction and clogging.

5.4.2 Metals removal rates

LaBar and Nairn (2016), conducted laboratory column experiments in which simulated groundwater containing 0.5 mg/L of each of (partial list) Cd, Ni, Pb, and Zn was passed through a SMS medium consisting of a 2:1 by volume mixture of the SMS and river rock. The volume of reactive medium was 19.3 L and the flow rate was maintained at 3 L/day, resulting in an expected residence time in the medium of about 72 hrs, assuming a porosity of 0.5. The effluent concentrations of each of the metals was on the order of 0.05 mg/L, leading to estimated removal rates of each metal (Zn, Cd, Ni, Pb) being in the range of 85 to 93 mg/m^3/d (LaBar and Nairn (2016) Table 3).

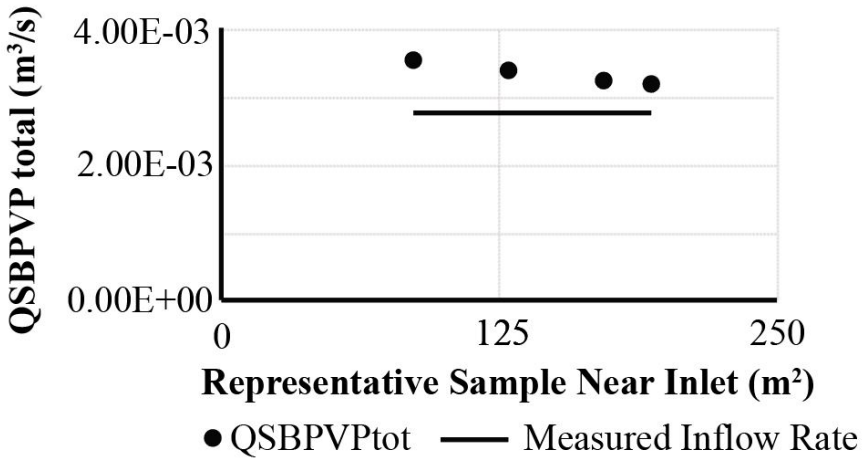

Figure 5.3: The effect of enlarging the inlet sampling area in the water balance. The inlet area has the lowest infiltration rate of the bed. Increasing the size of this area decreases the total infiltration rate of the pond. As shown, the decrease of total infiltration is never sufficient to achieve a balance with the influent.

The data from the laboratory investigation above can be used in conjunction with the C3S pond investigation. As discussed in the Water Balance section, the measured velocities of water moving through the SMS bed material correspond to residence times in the bed between about 7 and 11 hours everywhere except near the inlet pipe, where residence times approached 20 hours. These times are 5 to 10 times less than those established in the treatability columns, raising concerns over the long-term viability of the SMS treatment bed. Note that this comparison applies only to times in the pond bed material, not to the overall residence time in the pond, which would be greater and could affect metals removal from the water. Also, the treatability testing focused on the reactive material capacity to remove metals from the water, not the kinetics of removal. LaBar and Nairn (2016) showed that the majority of Zn, Cd, Pb, and Ni mass was removed from the synthetic water by the processes of adsorption to organics substrate material and precipitation as sulfides. Since both metals sorption by organic material, and the processes of sulfate reduction to sulfide, and subsequent precipitation, are known to occur over the timeframe of minutes to hours (Richards and Pallud, 2016; Arshadi et al., 2014), it is likely that in this case the low residence times in the C3S pond bed pose no immediate threat to the system performance (Table 5.3). This is supported by

the low metals concentrations in the effluent of C3S, as reported by LaBar and Nairn (2018).

The order of magnitude larger seepage velocity in the pond bed, compared to the treatability columns, potentially contributed to relatively large loading rates in the field case. To gain insight into the magnitude of the metals loading to C3S, data reported by LaBar and Nairn (2018) were used in equations 5.5 and 5.6 (Table 5.3). These data, which were collected prior to the reconditioning of the SMS, represent field conditions at a time when the seepage velocity in the pond bed may have been relatively low. Therefore, the calculations that follow should be considered speculative.

As before, assuming equal areas represented by each water velocity measurement, and assuming a bed porosity of 0.33, the total loading of all metals (Zn, Cd, Ni, Pb) to C3S was calculated to be 4.16 x 10^4 mg/m^3/d (Table 5.3), approaching three orders of magnitude greater than the column loadings. Nevertheless, data collected from the pond effluent showed that metals effectively removed from the influent water (80 to 90% removal for Zn and Ni, which had influent concentrations of 0.5 mg/L or greater) (LaBar and Nairn, 2018). Thus, the shorter residence times and greater loadings did not appear to compromise the VFBR performance. This result demonstrates that the VFBR system is very robust.

Sampling Area No.	**Q_{SBPVPi}**	**V_{SMSi}**	**Cd_R**	**Zn_R**	**Pb_R**	**Ni_R**	**Cd_{ML}**	**Zn_{ML}**	**Pb_{ML}**	**Ni_{ML}**
Unitless	m^3/s	m^3	mg/L	mg/L	mg/L	mg/L	$mg/m^3/d$	$mg/m^3/d$	$mg/m^3/d$	$mg/m^3/d$
1	1.77E-04	3.96E+01	1.00E-03	4.81	0	4.83E-01	3.87E-01	1863.74	0	1.87E+02
2	5.26E-04	3.96E+01	1.00E-03	4.81	0	4.83E-01	1.15E+00	5522.19	0	5.54E+02
3	3.48E-04	3.96E+01	1.00E-03	4.81	0	4.83E-01	7.60E-01	3658.45	0	3.67E+02
4	3.81E-04	3.96E+01	1.00E-03	4.81	0	4.83E-01	8.32E-01	4003.59	0	4.02E+02
5	4.86E-04	3.96E+01	1.00E-03	4.81	0	4.83E-01	1.06E+00	5108.03	0	5.13E+02
6	3.32E-04	3.96E+01	1.00E-03	4.81	0	4.83E-01	7.25E-01	3485.88	0	3.50E+02
7	3.61E-04	3.96E+01	1.00E-03	4.81	0	4.83E-01	7.89E-01	3796.51	0	3.81E+02
8	5.29E-04	3.96E+01	1.00E-03	4.81	0	4.83E-01	1.16E+00	5556.71	0	5.58E+02
9	4.53E-04	3.96E+01	1.00E-03	4.81	0	4.83E-01	9.90E-01	4762.89	0	4.78E+02
Totals	3.59E-03	3.56E+02					7.85E+00	3.78E+04	0	3.79E+03
T_{MR}:	4.16E+04	($mg/m^3/d$)								

Table 5.3: Summary of calculation of mass loading to C3S

[Summary of calculation of mass loading to C3S, using velocity data measured in 2017, and metals concentration data published in LaBar and Nairn (2018). Cd_R, Zn_R, Pb_R, and Ni_R are the removals of the constituents noted (in mg/L). Cd_{ML}, Zn_{ML}, Pb_{ML}, amd Ni_{ML} are the calculated mass loadings of the noted constituents. T_{MR} is the total mass removal.]

5.5 Conclusions

Three independent methods were used to quantify seepage velocities in the C3S VFBR pond in Commerce, Oklahoma: a water balance, a Darcy's Law calculation, and direct velocity measurements with a SBPVP. In all three cases the seepage velocity was found to be on the order of 1 m/d, on average. The SBPVP also permitted an assessment of the variability of flow in the pond bed, which was found to be within a factor of 1.6 everywhere except near the inlet to the pond, where the substrate material may have degraded most quickly and accumulated a fine-grained, low-permeability sediment layer.

A water balance performed on C3S yielded inflows and SBPVP-derived outflows agreeing to within 30%, using the generic assumptions of a 33% porosity and equal areas represented by each velocity measurement. The discrepancy could be explained by uncertainty in the effective porosity value (n = 0.26 produces a perfect balance), a velocity sampling grid that was insufficiently dense, or that flow through the pond was not at steady state on the day the velocity measurements were made.

The hydraulic data collected in this work indicated that the residence time of water in the reactive SMS bed material was as much as an order of magnitude less than that in the pre-design treatability testing. This potential problem appears to have been offset in part by fast mechanisms of removal – further kinetic studies are required to verify this conclusion. Overall, the metals loading rates and removal rates in C3S were almost three orders of magnitude higher than those established in the treatability testing columns, suggesting that the system is highly robust.

5.6 Acknowledgements

The authors would like to extend thanks to the Madison and Lila Self Graduate Fellowship for support of Mackenzie Cremeans. Trevor Osorno (University of Kansas) and Bryan Page (University

of Oklahoma) are acknowledged for their assistance in the field.

Chapter 6

Conclusions and recommendations

6.1 Statement of technical and scientific contributions

The objectives of this study, as stated in the Introduction, are the following: 1) to develop and laboratory validate a new device capable of generating high-density datasets at the groundwater-surface water interface in a time-efficient and cost-effective way, while also minimizing potential sources of error; 2) to apply the fully developed and laboratory validated SBPVP to the *Grindsted Å* field site, to determine if the device worked in field settings; 3) to fully evaluate the SBPVP against established tools for measuring flow across the GWSWI; and 4) to apply the high-density datasets to field problems to gain further insight into patterns of groundwater-surface water exchange and their influence on contaminant mass discharges. In general, this study accomplishes these objectives by expanding the knowledge of water exchange across the GWSWI using high-density datasets (from measurements in the GWSWI itself) to evaluate these flows. This study focuses, in part, on characterizing a contaminated field site where natural groundwater-surface water exchange involves measurable levels of contaminants. To broaden the settings examined, a geo-engineered system is also included.

This study focuses on water exchange, and associated processes, at the groundwater-surface water interface (GWSWI). The primary technical outcomes of this research are: 1) the design, and

testing of a new tool, the streambed PVP (SBPVP), for quantifying flow across the GWSWI (objective 1); 2) a demonstration and field assessment of the tool in a side-by-side assessment of four of the currently and commonly used methods of measuring flow across the GWSWI (objectives 2, 3); 3) the introduction and validation of a new approach for quantifying contaminant mass flux into a stream, based on the SBPVP (objective 4) and 4) a demonstration that the new approach can provide uncommonly detailed flux distribution data of great value to risk assessment efforts (objective 4) 5) the application of this method to the characterization and performance assessment of a passive vertical flow bioreactor (VFBR) that was serving as part of a remediation system for removing heavy metals from discharging spring water (objective 4). Detailed conclusions associated with these technical contributions are given below in the Conclusions section.

The primary scientific outcomes of this research are: 1) the mapping of a stream reach showing the separate contributions to contaminant mass flux from water flow and contaminant concentrations. This separation has been well known in a conceptual sense, but its demonstration with field data at the sub-meter scale is novel (objectives 2 and 4); 2) this research has shown, with field measurements using multiple methods, that the variability of flow across the GWSWI is large compared to the reproducibility of flow measurements commonly used. This suggests the importance of mapping discharge zones in the greatest detail possible to ensure that all important points of discharge are found (objective 3); 3) through field-based mass loading calculations, made possible by SBPVP measurements, the attenuation capacity of an engineered woodchip and compost substrate was greater than design specifications by about three orders of magnitude (objective 4).

6.2 Conclusions

The dissertation aimed to develop and validate the SBPVP, and apply the tool to specific field problems. To this end, the SBPVP was tested in the laboratory, and then in the field. It was concluded that the SBPVP could be installed in sandy sediments up to 11 cm deep without bias and a measurement range of 50 cm/day to 450 cm/day was established. In the field, the SBPVP produced

results comparable to mini-piezometer data and Darcy calculations. Further, use of a hyporheic shield was found to be an effective way to isolate the vertical component of flow in the streambed and measurements were made from 18 cm/day to 2700 cm/day. A full measurement range was not determined. The SBPVP was successfully deployed on foot and from a boat, in depths up to 3 m.

A more thorough comparison of methods revealed that SBPVP and mini-piezometer data (supported with slug testing) provided similar estimates of vertical seepage velocity, though the variance of the mini-piezometers was higher (likely due to the challenges of assigning accurate location-specific values of the Darcy parameters K, and i). Seepage meters produced velocity estimations that were comparable to mini-piezometer derived velocities, but had a consistent negative bias. The reasons for this bias are not known for certain but could be related to the relatively large footprint of the seepage meter compared to the other methods, and/or unknown issues related to the construction or deployment of the devices. Temperature gradient data led to large underestimations of vertical seepage velocities, likely because of horizontal hyporheic flow. All methods tested were consistent in their ability to detect a qualitative increase in seepage velocities from the south end of the test transect to the north end.

Detailed mapping of the discharge through the *Grindsted Å* streambed using the SBPVP, and mini-piezometers, led to contaminant mass discharge estimates that were in good agreement with independently estimated mass loadings determined across a transect on the north streambank. This finding increases confidence in the reliability of the SBPVP method. Temperature gradient data correctly identified the major discharge zones faster than the SBPVP and mini-piezometer methods. However, the magnitudes of discharge estimated from temperature gradients were much smaller than those estimated from any other method. Even so, rapid delineation of discharge zones could be useful and, at sites where this bias doesn't occur, the temperature gradient method is the fastest way to determine discharge. The second fastest method was the SBPVP, which could be rapidly deployed and then take subsequent measurements in times typically less than one to two

hours (as opposed to 24+ hours with the mini-piezometers). This speed of execution, coupled with the value of knowing both the location and the magnitude of discharge, suggests that the SBPVP method is very competitive from the perspective of time, and associated cost, requirements. When coupled with contaminant concentration data from the streambed, SBPVP estimates of seepage velocity can be used to calculate contaminant mass discharges. This work showed that the locations of such discharge zones did not exactly correspond to either the locations of highest discharge or contaminant concentrations. Since site characterization programs may typically focus on either discharge zone mapping or plume mapping, they may miss details related to the true source of risk, the contaminant mass discharge zones.

The SBPVP was also applied to the assessment of a manmade vertical flow bioreactor (VFBR) in Commerce, Oklahoma. Overall, SBPVP measurements of flow through the VFBR compared well with water balance calculations and Darcy calculations for the system, providing confidence in the accuracy of the measurements. Flow through the VFBR was found to be relatively uniform, except for a limited zone near the inlet, where substrate degradation rates may have been accelerated and flow was much slower. Throughout the VFBR, mass loadings of metals to the sediments were nearly three orders of magnitude greater than those considered in treatability tests. Yet, outflow concentration measurements suggest the system performs satisfactorily despite the high loadings, establishing the robustness of this remediation approach. The quantification of the actual mass loadings to the VFBR advances the technology by providing a means of identifying possible sources of future failures or for the purposes of updating lifetime estimates for the VFBR bottom substrate.

6.3 Recommendations

Throughout the development and application of the SBPVP, a few design upgrades were made including the addition of teeth to the hyporheic shield, removable brackets, and an updated injection port. However, to increase the applicability of the SBPVP, there are a few additional modifica-

tions that could be useful. For example, modifications allowing the measurement of horizontal hyporheic flow rates and the addition of a sampling port (to gather co-located shallow streambed water samples) would be useful. Additionally, future work should be done to develop the use of variograms to define the variability of seepage velocities in duplicate measurements. The tests reported here were based on a minimal number of separate tests (4) and future testing should look at the same procedure applied to 10 to 20 points distributed on the same scale (5 m), assuming conditions similar to those encountered at the Grindsted site. Further studies should be conducted on the capacity of VFBR substrate mixture to better establish porosity, hydraulic conductivity, reaction kinetics and maximum loading capacity. With these data more fully established, an SBPVP survey would provide an accurate barometer on the current state of health of the VFBR, and its remaining lifetime.

Appendix A

Streambed point velocity probe schematics

A.1 Original design

The streambed point velocity probe schematics were created as a collaborative effort between Allen Hase, and Mackenzie Cremeans. These schematics are the initial design and, therefore, do not include design upgrades added after the initial build. Figures A.1 and A.2 show the metal pieces of the probe, which were fabricated from stainless steel. Figure A.3 shows the plastic pieces, which were 3D printed on a UPrint by Dimensions with acrylonitrile butadiene styrene (ABS) plastic. Figure A.4 is a schematic of the assembled SBPVP, showing the probe on the left and the full assemblage (with pipe lengths and hyporheic shield) on the right. Due to the variability in metal fabrication and 3D printing, all of which was conducted in-house, each device has its own set of measurements that may or may not line up perfectly with these schematics. Therefore, when you are conducting your measurements, be sure to use the measurements from your specific device to calculate velocities.

A.2 Design updates

Design updates include making a threaded center bracket to improve the ease of removal and reattachment of the hyporheic shield, cutting a new slot in the side of the top pipe of the probe

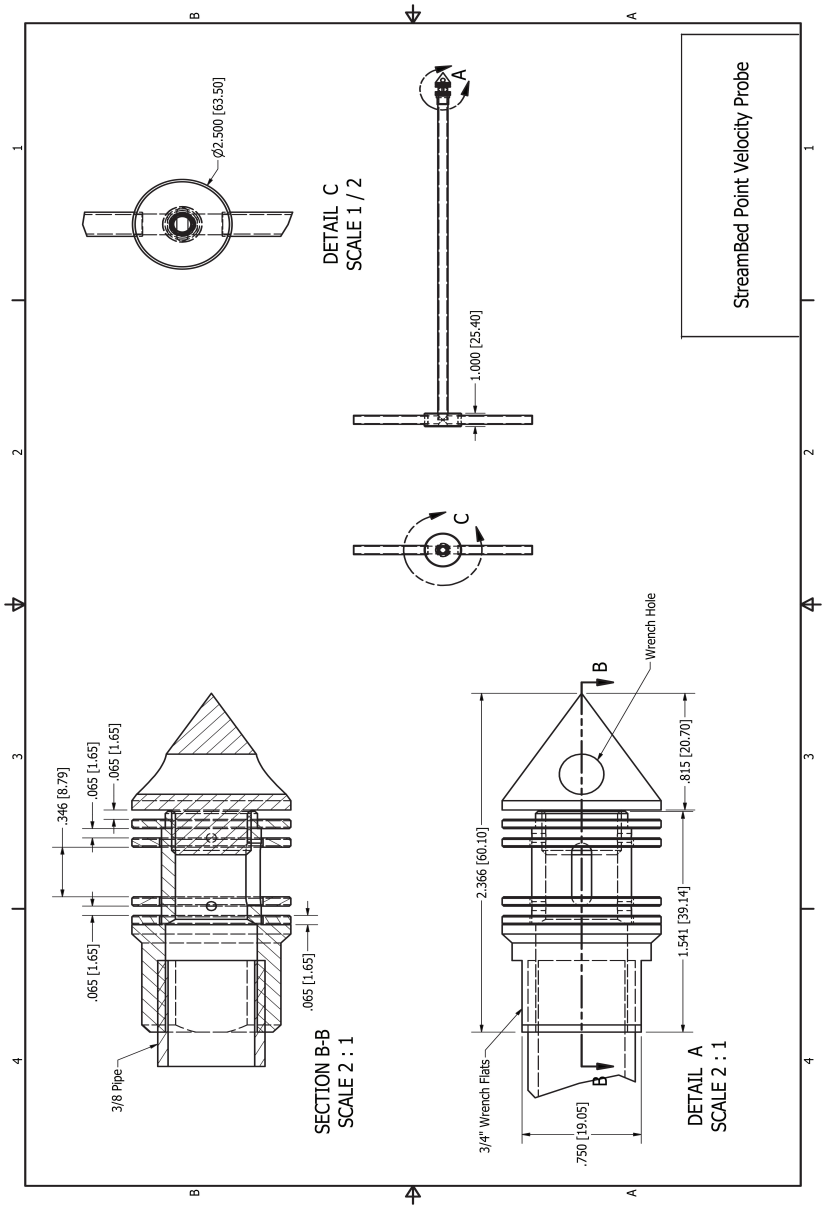

Figure A.1: SBPVP schematics, page 1

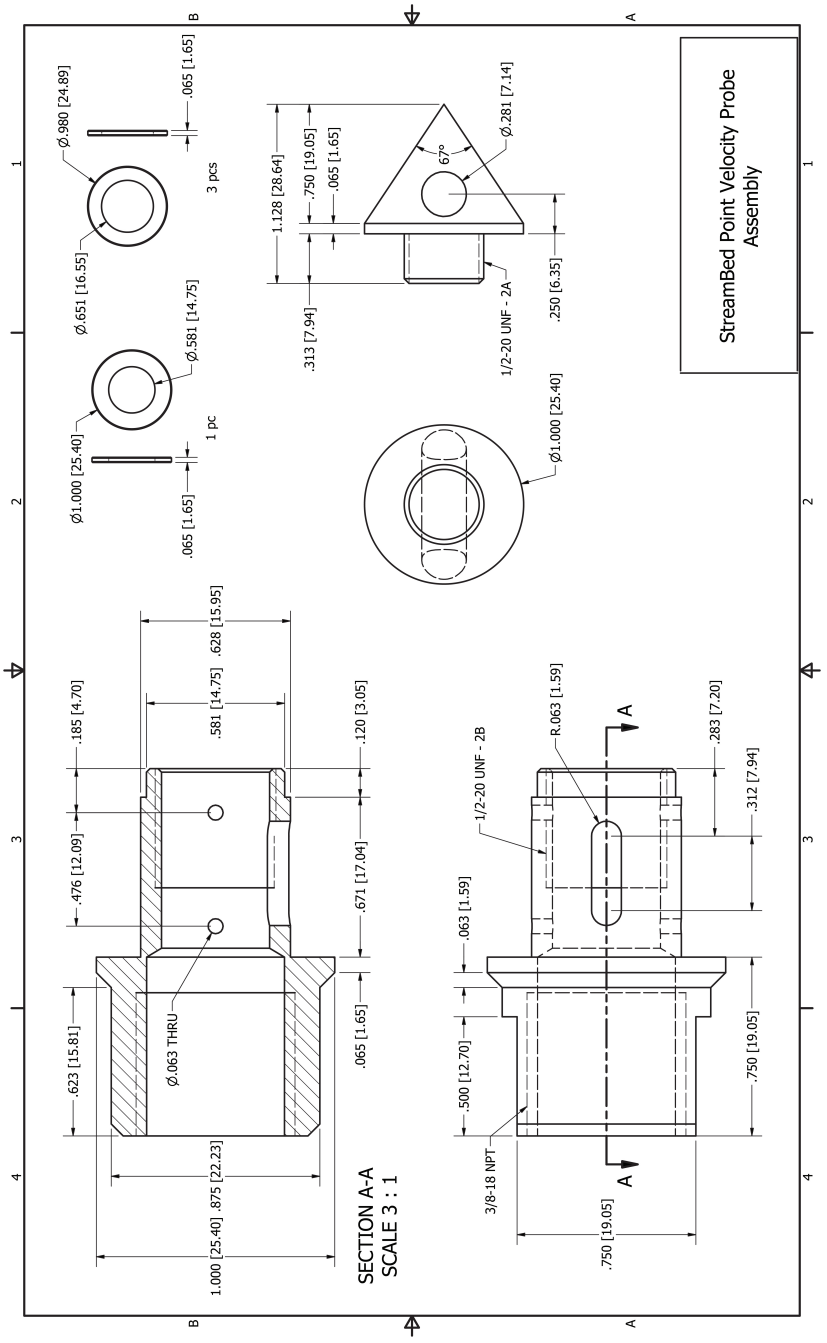

Figure A.2: SBPVP schematics, page 2

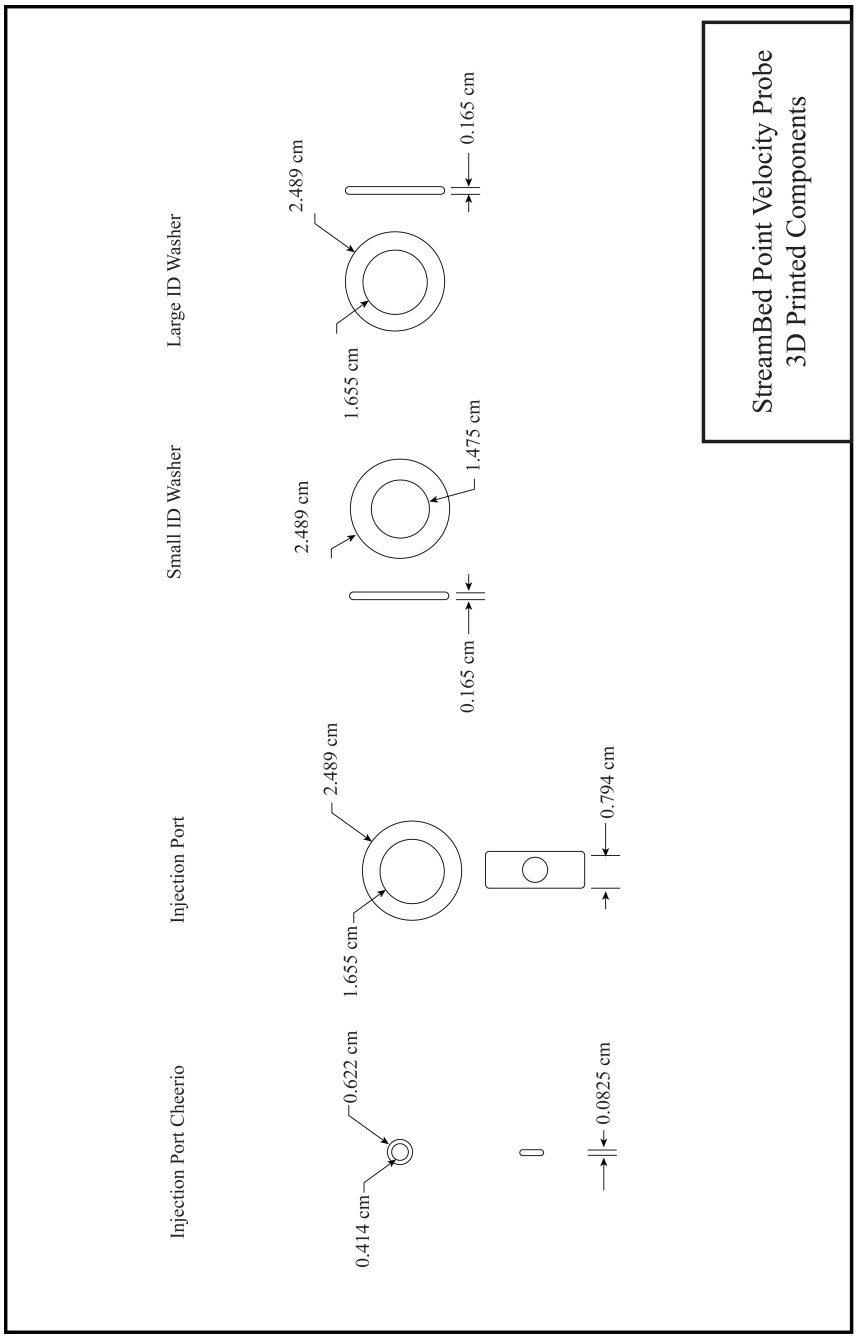

Figure A.3: SBPVP schematics, page 3

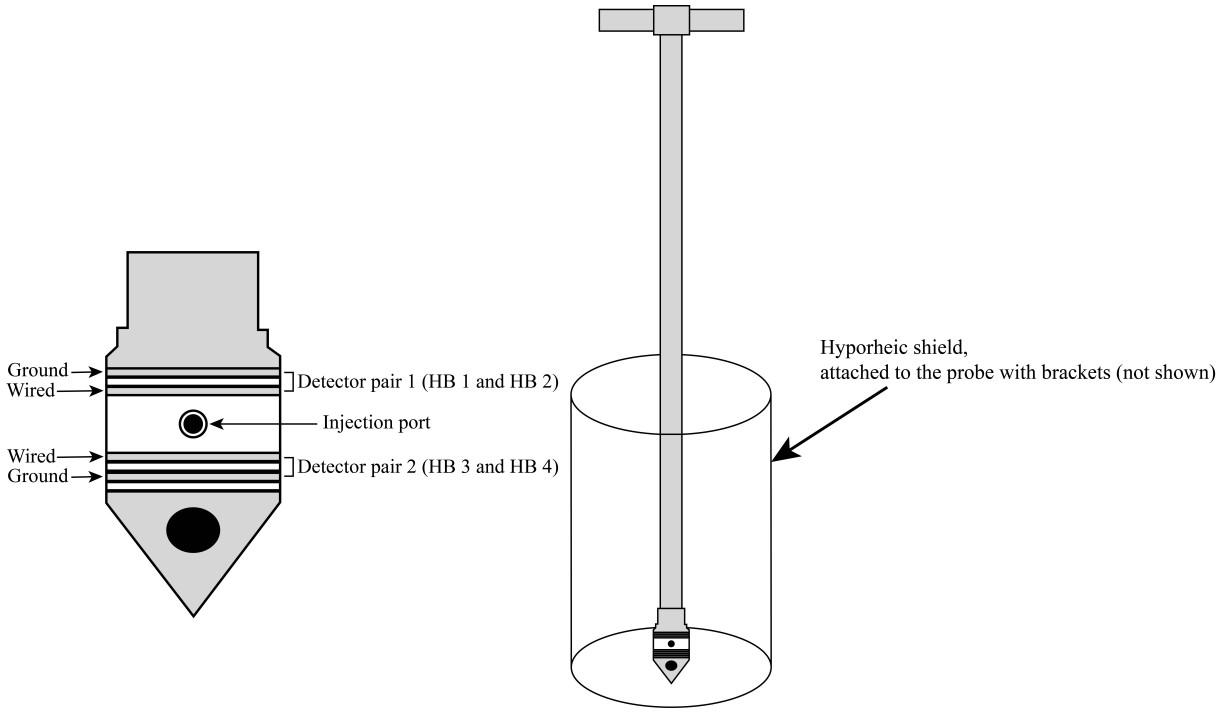

Figure A.4: The SBPVP probe assembled (left), plus the lengths of pipe and hyporheic shield (right).

(to allow for a more forceful direct-push installation into harder substrates), adding teeth to the hyporheic shield (to allow for installation through plant mats), and an improved injection port, for use in fine-grained materials (Figure A.5). Further design plans were made, but not executed. These include creating an SBPVP with an adjustable probe angle as well as a multi-level SBPVP, to measure exchange at multiple depths simultaneously.

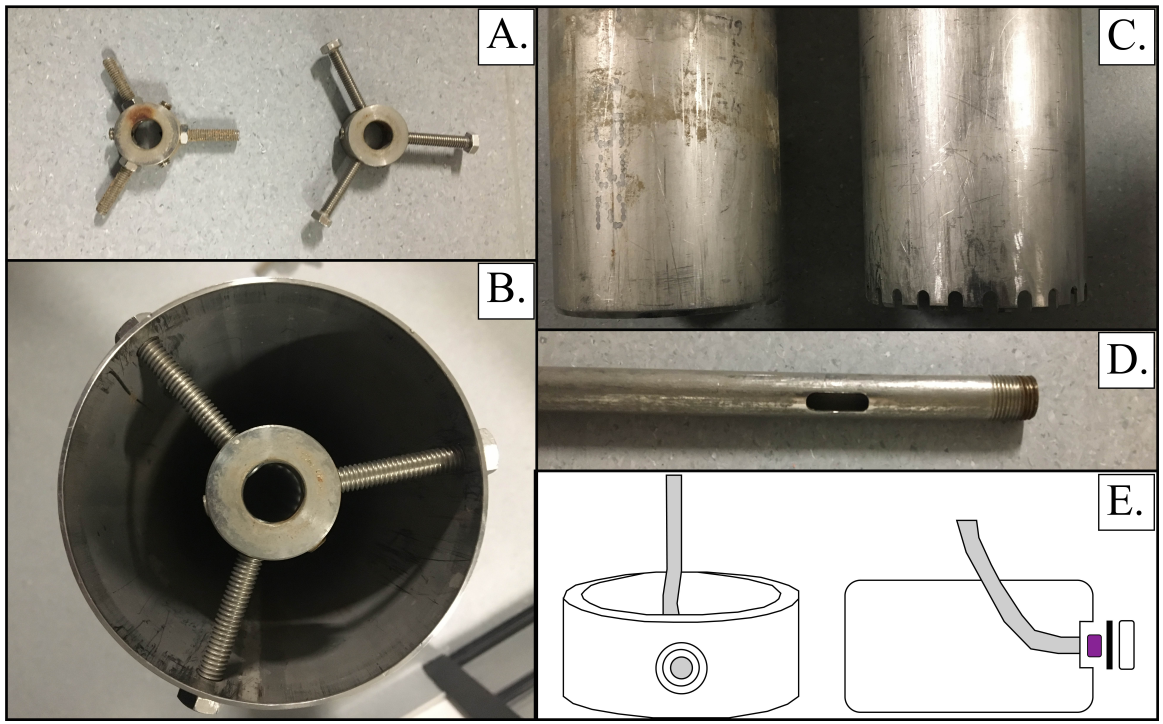

Figure A.5: SBPVP design updates, since 2014. (A) Threaded removeable centralizing brackets replaced welded brackets, to improve ease of removing SBPVP from the shield for repairs and cleaning (B) Threaded removable brackets as they fit into the shield (C) Addition of another kind of hyporheic shield. On the left, the original, with a single sharp edge along the bottom to ease installation at the groundwater-surface water interface. On the right, a toothed shield designed to help cut through plant mats (and other debris) on top of the groundwater-surface water interface. The latter was particularly helpful at the Commerce, Oklahoma site (Chapter 5) (D) A slot cut into the top of the piping, below the handle, allows for installation by hammering (useful for the Raadvad preliminary study discussed in Appendix M) (E) An updated tracer port, with a sponge (purple) behind the nytex screen (black rectangle), held in the tracer port piece by a plastic cheerio (small white rounded rectangle). The purpose of this update was to prevent the tracer line from clogging with fine grained materials.

Appendix B

Streambed point velocity probe build and wiring

B.1 Building a streambed point velocity probe

The streambed point velocity probe, itself, is made of 11 pieces, not including the wires and injection line. The stainless steel probe shank and drive point make up the base of the probe (B.1). There are four stainless steel washers that act as the detector pairs on this probe, with 3 ABS plastic washers and one ABS plastic port (plus a tracer port cheerio) to separate the detector pairs. The drive point is threaded to screw into the shank, holding the remaining pieces onto the shank compressed together (Figure B.2). To fully assemble the probe for field work, the wiring and tracer line must be installed during probe assembly and run through an appropriate length of pipe for the depth of water. Then, the handle, centralizing brackets, and the hyporheic shield must be attached (Figure B.3). For the probe depicted, all metal pieces were fabricated in the University of Kansas Physics Shop, and all plastic pieces were 3D printed on uPrint by Dimensions 3D printer. Each component was designed in Google SketchUp and dimensions are detailed in Appendix A.

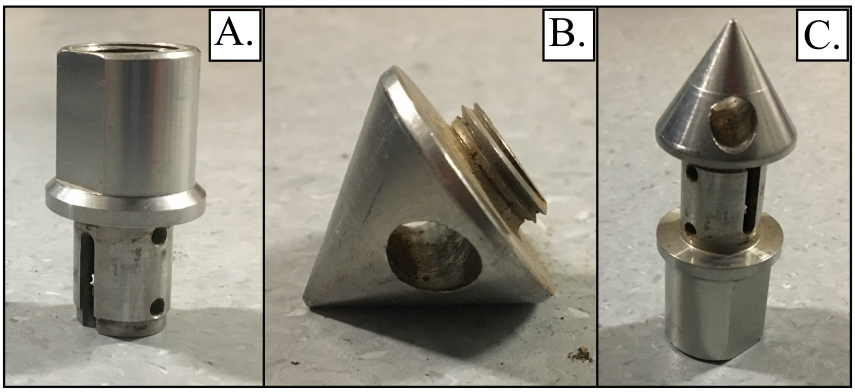

Figure B.1: Main body of the SBPVP (A) Probe shank, including wiring holes and a slot for the tracer line, is inside threaded on both ends to be attached to pipe (on the top) and to the probe tip (on the bottom). (B) Probe tip, with a hole included to allow for tightening with tools. This piece is pointed to allow for easier installation at the groundwater-surface water interface. (C) The two pieces, as they fit together.

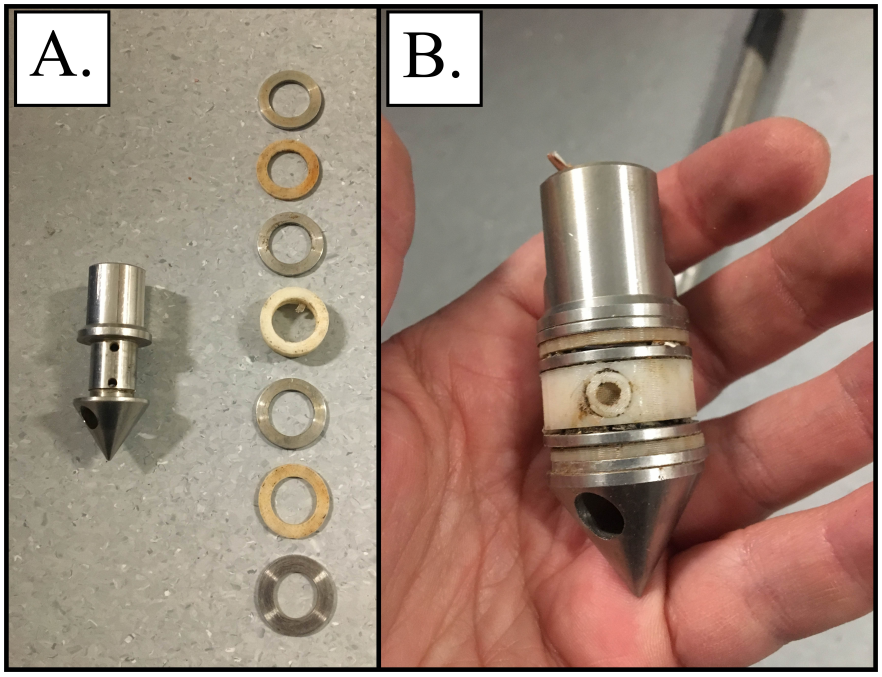

Figure B.2: (A.) All the plastic and metal pieces, in order, which make up the rest of the probe (with the main body shown on the left) (B.) An assembled probe (wiring and tracer line not included).

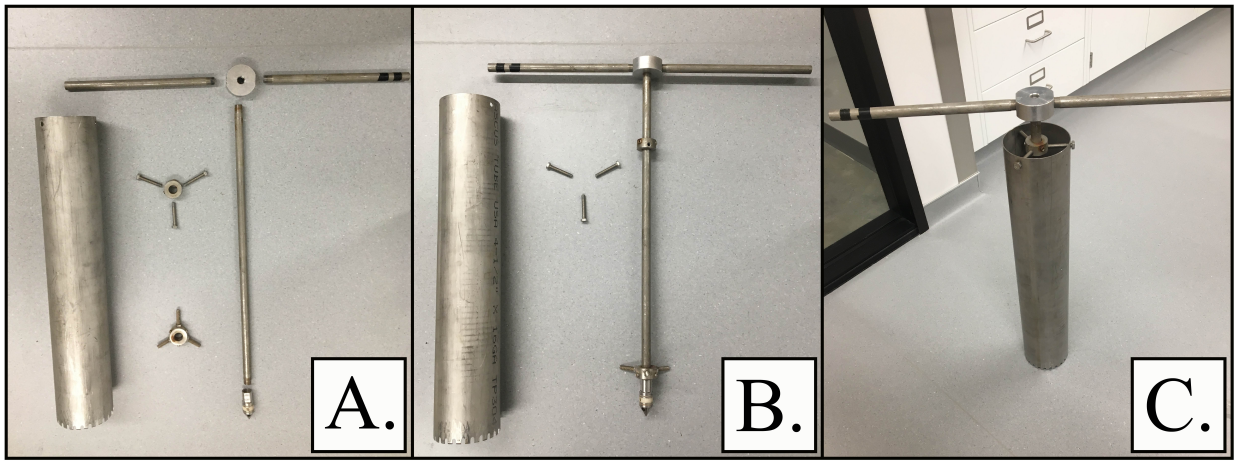

Figure B.3: To finish probe assembly, (A.) lay out the probe (Figure B.2B) and remaining pieces (probe handle pieces, centralizing brackets, hyporheic shield, and lengths of pipe) (B.) Place centralizing brackets on the pipe (threaded bracket nearest to the handle side). Put handle together and attach to pipe. Screw the probe onto the pipe. (C.) Attach the piece described in (B.) to the hyporheic shield using the threaded centralizing bracket (which should be on top).

B.2 Wiring a streambed point velocity probe

The streambed point velocity probe (SBPVP) operates on the same electrical principles as the original point velocity probe, just with fewer halfbridges. As shown in the diagrams below, the SBPVP only has four halfbridges. Halfbridges 1 (up) and 3 (down) are duplicated by halfbridges 2 (up) and 4 (down), respectively. The duplication is merely a safeguard, should one set of wiring short circuit, break, or otherwise have bad contact with its detector pair mid-testing. Additionally, to have a fully functioning probe, there must be a ground wire (attached to the pipe above the probe and to a ground slot in the datalogger) and a spider (connected to the four halfbridge slots and the excitation slot on the datalogger). Visual explanations of the SBPVP wiring are presented in Figures B.4.

In order to collect data, the datalogger must be attached to a battery and have a program downloaded onto it. An example of a datalogger program (specifically, the one used most often throughout this study) can be found below in Appendix C. To view the data, the datalogger must be attached to a computer with LoggerNet downloaded on it, via an RS-232 cable. Data can be viewed during collection or afterward. The data are processed in VelProbePE fitting either with the Advection-Dispersion Equation (ADE) or method of moments. These are described more thoroughly in the preceding chapters.

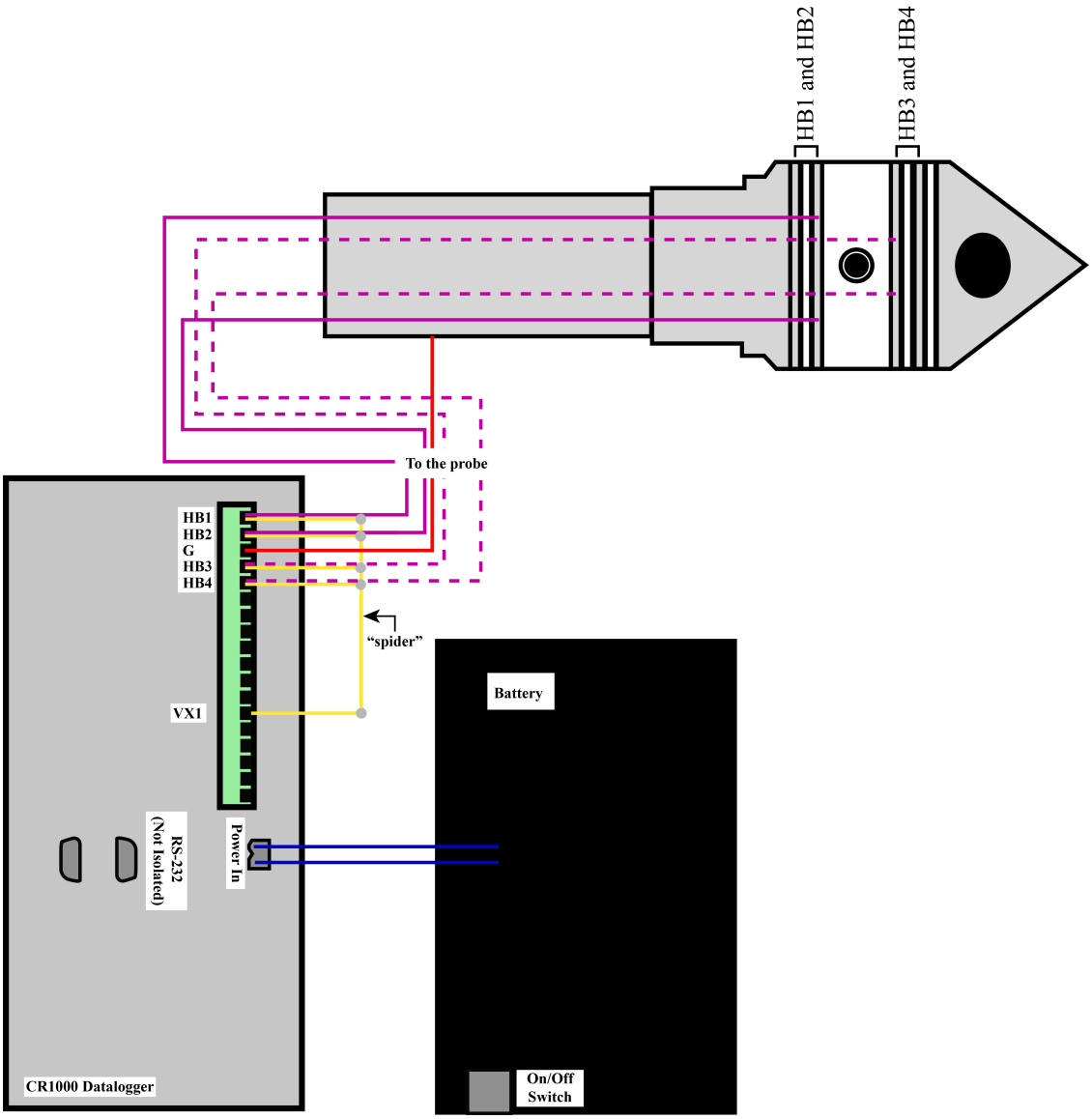

Figure B.4: SBPVP wiring diagram, depicting the battery to datalogger to SBPVP connections, and indicating which plug is the correct one for a laptop connection.

Appendix C

Example datalogger program

This is an example of a datalogger program written in Cr Basic for use on CR1000 dataloggers to collect SBPVP data. It instructs the datalogger how to collect data through the SBPVP halfbridges by measuring electrical resistivity on a series of halfbridges.

```
    'CR1000
'Created by SCWIN (2.3)
'Declare Variables and Units
Public Batt_Volt
Public HalfBR(16)
Units Batt_Volt=Volts
Units HalfBR=mV
'Define Data Tables
DataTable(Devlin,True,-1)
DataInterval(0,1,sec,10)
Minimum(1,Batt_Volt,FP2,False,False)
Sample(1,HalfBR(1),IEEE4)
Sample(1,HalfBR(2),IEEE4)
Sample(1,HalfBR(3),IEEE4)
```

```
Sample(1,HalfBR(4),IEEE4)
Sample(1,HalfBR(5),IEEE4)
Sample(1,HalfBR(6),IEEE4)
Sample(1,HalfBR(7),IEEE4)
Sample(1,HalfBR(8),IEEE4)
'Sample(1,HalfBR(9),IEEE4)
'Sample(1,HalfBR(10),IEEE4)
'Sample(1,HalfBR(11),IEEE4)
'Sample(1,HalfBR(12),IEEE4)
'Sample(1,HalfBR(13),IEEE4)
'Sample(1,HalfBR(14),IEEE4)
'Sample(1,HalfBR(15),IEEE4)
'Sample(1,HalfBR(16),IEEE4)
EndTable
'Main Program
BeginProg
Scan(1,Sec,25,0)
'Default Datalogger Battery Voltage measurement Batt_Volt:
Battery(Batt_Volt)
'Generic Half Bridge measurements HalfBR(1):
BrHalf(HalfBR(1),1,mV2500,1,1,1,2500,True,0,_60Hz,1.0,0.0)
BrHalf(HalfBR(2),1,mV2500,2,1,1,2500,True,0,_60Hz,1.0,0.0)
BrHalf(HalfBR(3),1,mV2500,3,1,1,2500,True,0,_60Hz,1.0,0.0)
BrHalf(HalfBR(4),1,mV2500,4,1,1,2500,True,0,_60Hz,1.0,0.0)
BrHalf(HalfBR(5),1,mV2500,5,1,1,2500,True,0,_60Hz,1.0,0.0)
BrHalf(HalfBR(6),1,mV2500,6,1,1,2500,True,0,_60Hz,1.0,0.0)
BrHalf(HalfBR(7),1,mV2500,7,1,1,2500,True,0,_60Hz,1.0,0.0)
```

BrHalf(HalfBR(8),1,mV2500,8,1,1,2500,True,0,_60Hz,1.0,0.0)

’BrHalf(HalfBR(9),1,mV2500,9,2,1,2500,True,0,_60Hz,1.0,0.0)

’BrHalf(HalfBR(10),1,mV2500,10,2,1,2500,True,0,_60Hz,1.0,0.0)

’BrHalf(HalfBR(11),1,mV2500,11,2,1,2500,True,0,_60Hz,1.0,0.0)

’BrHalf(HalfBR(12),1,mV2500,12,2,1,2500,True,0,_60Hz,1.0,0.0)

’BrHalf(HalfBR(13),1,mV2500,13,2,1,2500,True,0,_60Hz,1.0,0.0)

’BrHalf(HalfBR(14),1,mV2500,14,2,1,2500,True,0,_60Hz,1.0,0.0)

’BrHalf(HalfBR(15),1,mV2500,15,2,1,2500,True,0,_60Hz,1.0,0.0)

’BrHalf(HalfBR(16),1,mV2500,16,2,1,2500,True,0,_60Hz,1.0,0.0)

CallTable(Devlin)

NextScan

EndProg

Appendix D

Vertical flow NeST floor schematics

The Vertical Flow NeST was developed as an offshoot from the work in Bowen et al. (2012). The NeST developed by Bowen et al. (2012) simulates horizontal flow, the magnitude of which is controlled by pumping velocity. In order to test a device made to quantify groundwater-surface water exchange, a NeST that simulates vertical flow had to be constructed. The nested tank design remained very similar, with the exception of higher walled tanks and no holes in the tanks. To create upward or downward flow, a floor was designed in Trimble SketchUp, and 3D printed with a UPrint by Dimensions with acrylonitrile butadiene styrene (ABS) plastic. Due to limitations of the 3D printer stage (which can print to a maximum of 17 cm by 14.5 cm), the floor was printed into 16 interlocking pieces. The 8 pieces that comprised the top of the floor had 560 perforations, which were filled with synthetic sponge to prevent sand from filling the box. Water velocity is controlled by pumping rate, and thus, theoretical seepage velocity can be calculated.

Above the floor, medium sand is hand packed into the tank to a depth of 40 cm. Above the sand, there was open water, which was pumped back into the high head tank to maintain the head gradient. An "expected velocity" can be calculated with the following:

$$v = \frac{Q}{A * n} \tag{D.1}$$

where v is the expected velocity (L/T), Q is the discharge from the pump (L^3/T) (usually measured with a graduated cylinder and a stopwatch), A is the area of the NeST floor where flow can be directed upward (L^2), and n is the porosity of the sediment in the tank (unitless). More details about testing in the NeST can be found in Chapter 2 of this dissertation.

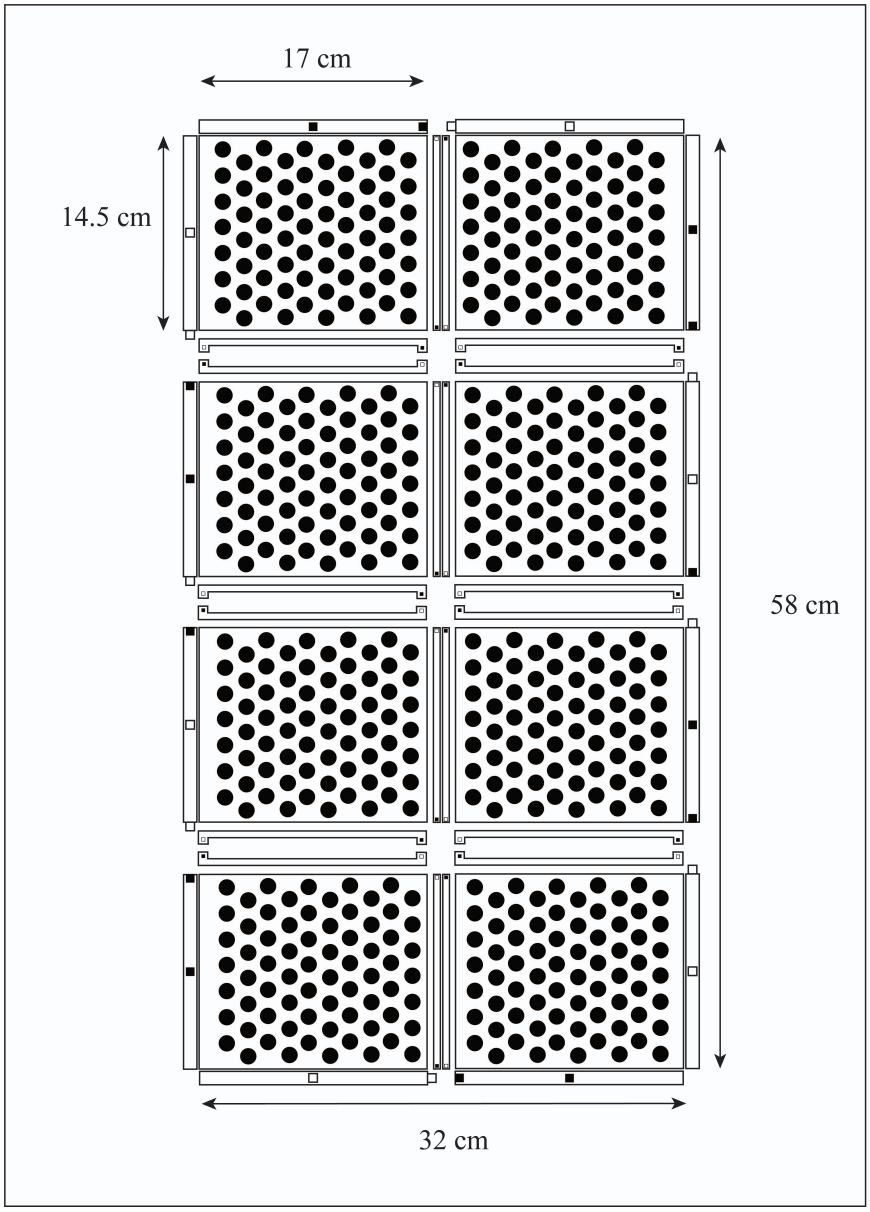

Figure D.1: Vertical flow NeST, schematic of the top

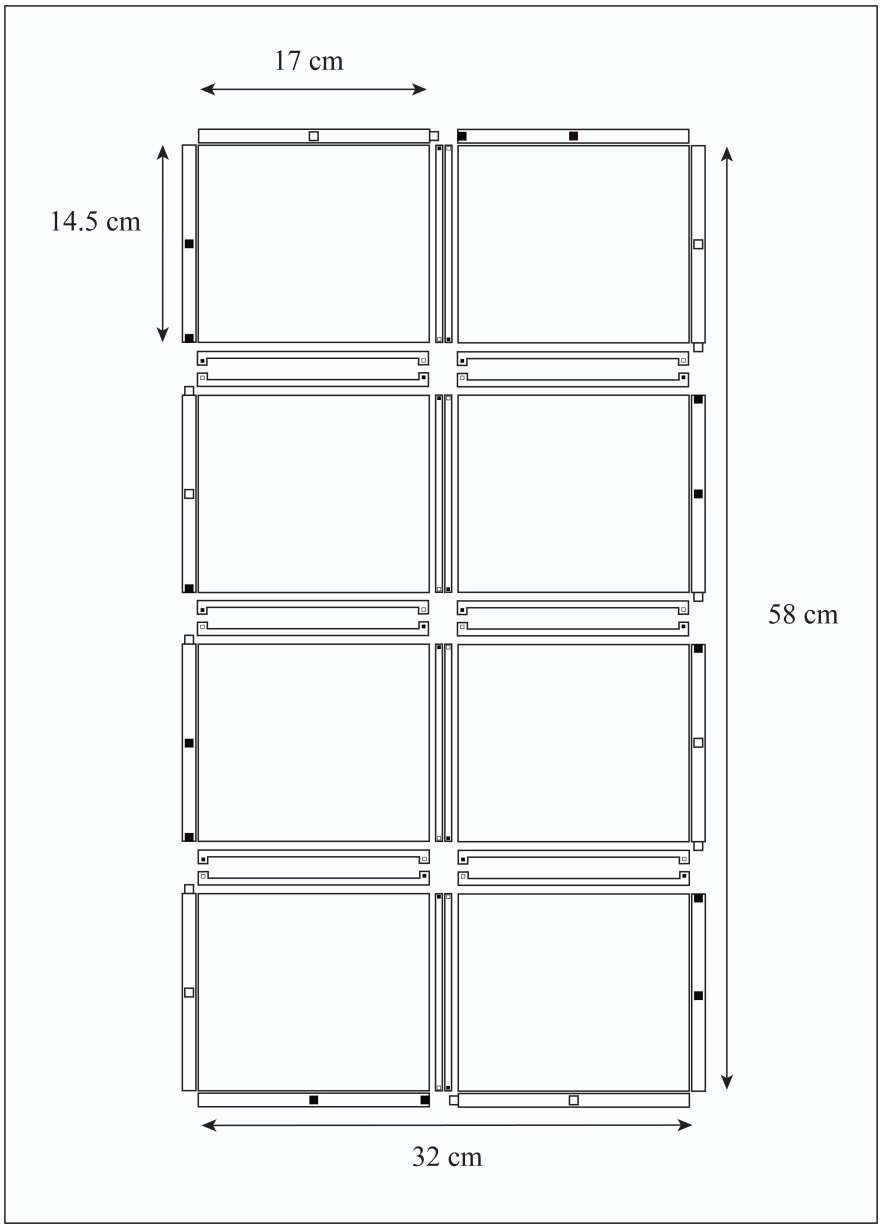

Figure D.2: Vertical flow NeST, schematic of the bottom

Appendix E

A simple model of the NeST

As discussed in Chapter 2, the simplicity of the NeST experimental set-up lent itself well to a very simple modeling approach to predict outcomes. The model results are presented briefly in Figure 2.3 and the building of the model is further clarified here. The extent of non-uniformities in the NeST were assessed with a two-dimensional (2D) steady-state flow model executed in Excel. As stated in Chapter 2, and repeated here for convenience, the model domain had no-flow boundaries on the left and right sides, a constant head boundary on the top, and a repeating series of constant flux nodes separated by no flow nodes along the bottom, to represent the alternating inflow perforations and 'dead' zones of the floor panel. Homogeneous, isotropic, steady state conditions were assumed throughout the sand, leading to the following finite difference equation to describe flow:

$$\frac{\Delta\frac{\Delta h}{\Delta x}}{\Delta x} + \frac{\Delta\frac{\Delta h}{\Delta y}}{\Delta y} = 0 \tag{E.1}$$

where $h_{i,j}$ is the head at node (i,j) and Δx, Δy are the distances between nodes as represented in the model. The model was prepared in Excel with Δx = Δy which permitted Equation E.1 to be simplified to:

$$h_{i,j} = \frac{h_{i+1,j} + h_{i-1,j} + h_{i,j+1} + h_{i,j-1}}{4} \tag{E.2}$$

with the head at each node in the model calculated, the vertical hydraulic gradient ($grad_{vertical}$) between each node could be determined from:

$$grad_{vertical} = \frac{h_{i,j} - h_{i,j+1}}{\Delta y} \tag{E.3}$$

The model grid was 21 nodes vertically by 36 nodes horizontally, representing Δx = Δy = 1 cm. Information regarding the accompanying laboratory testing can be found in Chapter 2.

Appendix F

Injection Testing

F.1 Injection length and style tests

To determine the effect of hand injections on measurements, a comparison between hand injections (conducted by M. Cremeans) and mechanized injections (using a KD Scientific Multi-Syringe Infusion Pump, Model 220) was made at three different injection speeds and two different pumping speeds (Figure F.1, F.2). A comparison of the three injection speeds, with the mechanized method, at the same pumping speed is also made in Figure D.3. As shown by these results, injection style and speed have very little effect on curve shape, from the start of the curve over the peak. The tails of each curve varied, but this had little effect on the velocity calculations, as shown in tables D.1 and D.2. The variety in velocity values suits the variability inherent to peristaltic pumps, which is reflected in the range given by the theoretical velocity calculations for these tests. The results of this laboratory study suggest that the bulk movement of tracer is negligibly affected by the noise introduced in hand injections (as compared with perfectly even mechanized injections) and by injection speed over a range of 5-20 s.

Mechanized injections were completed over a larger range of injection times (5s – 60s). The results (summarized in Figure F.4, F.5, and Tables F.3 and F.4) suggest that very long injection times affect the velocity calculation by biasing the peak to arrive slower than expected (based on

theoretical velocities). Injection lengths up to 30 s provided reasonable measurements at the fast pumping speed (approximately 1550 cm/day) (Figure F.4). All injection lengths provided reasonable measurements at the slow pumping speed (approximately 215 cm/day) (Figure F.5). This suggests that if your injection speed is not markedly slower than the speed the water is moving, your breakthrough curve can be reliably used to calculate a velocity. Additionally, the variability in velocity values is much higher at high velocities, suggesting that the device becomes less reliable when the water is moving quickly. However, this is unlikely to affect measurements in the field because groundwater velocities tend to be slow (100 - 200 cm/day, on average).

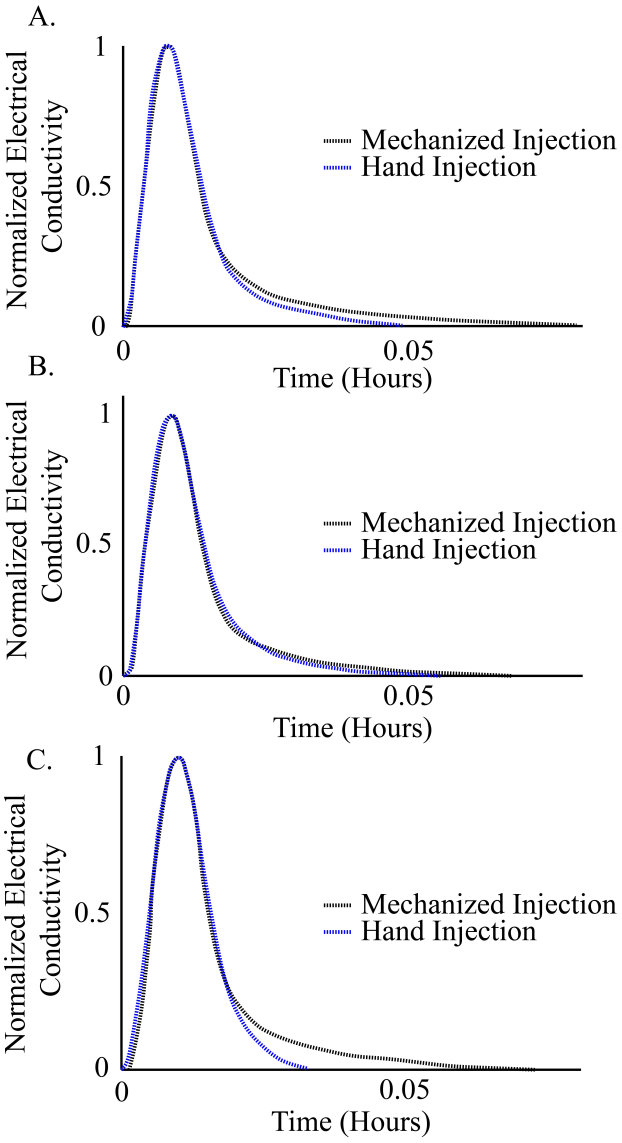

Figure F.1: The above graphs show a comparison of injections conducted by a machine and injections conducted by hand at three different injection speeds at a fast rate of flow. Graph A is a comparison of 5 s injections. Graph B is a comparison of 10 s injections. Graph C is a comparison of 20 s injections. All curves have been normalized in the y-direction to allow analysis of curve shape. In each graph, the black dots are the mechanized injection and the black x's are the hand injections. Overall, the fit is good in all three until the tail of the curve begins. In the graphs summarizing the 5 and 10 s curves, the observed curve shapes remain nearly identical throughout. In the graph of 20 s tests, the tails diverge after the majority of the mass of tracer has passed by the detectors.

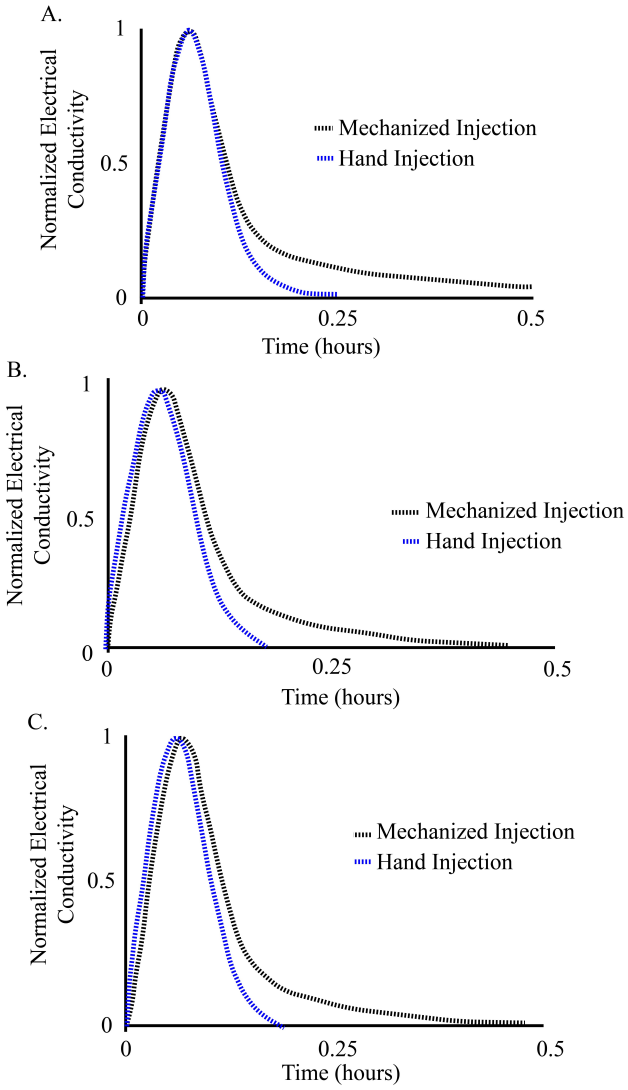

Figure F.2: The above graphs show a comparison of injections conducted by a machine and injections conducted by hand at three different injection speeds at a slow rate of flow. Graph A is a comparison of 5 s injections. Graph B is a comparison of 10 s injections. Graph C is a comparison of 20 s injections. All curves have been normalized in the y-direction to allow analysis of curve shape. In each graph, the black dots are the mechanized injection and the black x's are the hand injections. Overall, the fit is good in all three until the tail of the curve begins. In the 5 s and 10 s curves, the observed curve shape remains nearly identical throughout. In the 20 s graph, the tails diverge after the majority of the mass of tracer has passed by the detectors.

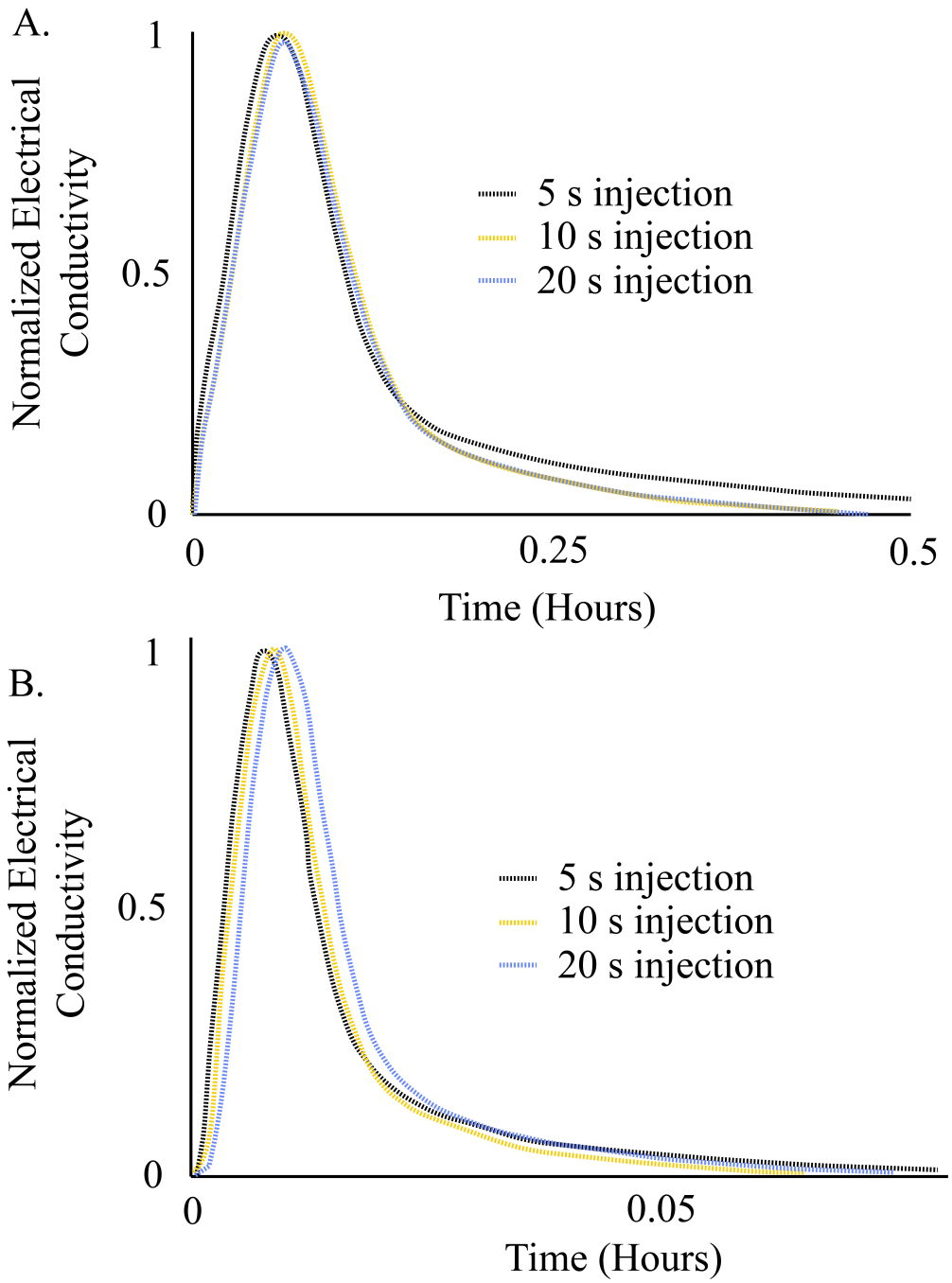

Figure F.3: (A) A comparison of three injection speeds (as conducted by the syringe pump) at the slow pump speed. (B) A comparison of the three injection speeds (as conducted by the syringe pump) at the fast pump speed.

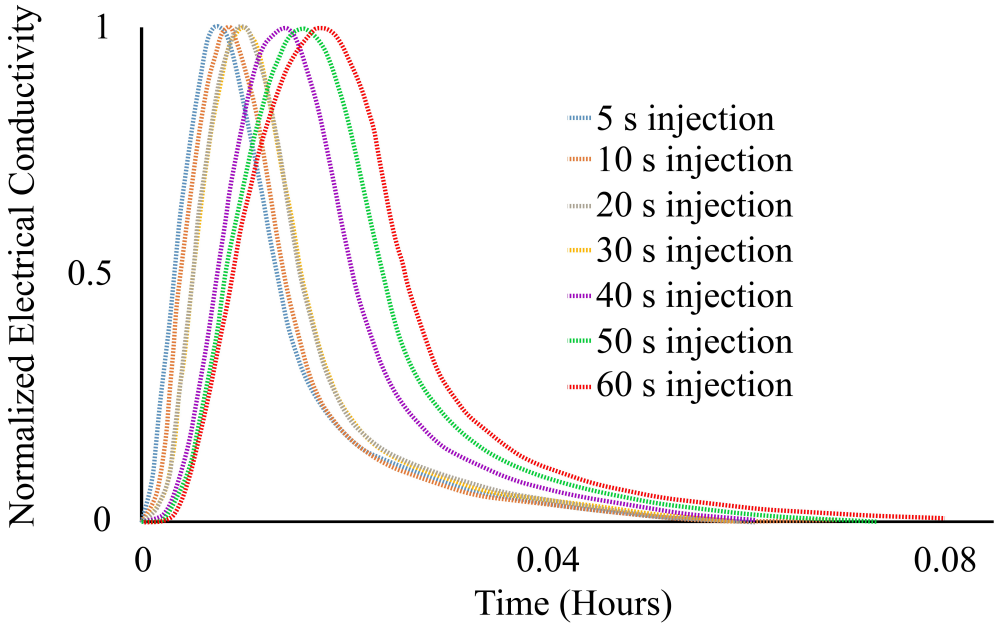

Figure F.4: An expanded view of injection speeds, as conducted by a syringe pump, from 5s to 60s injections at the fast pumping rate

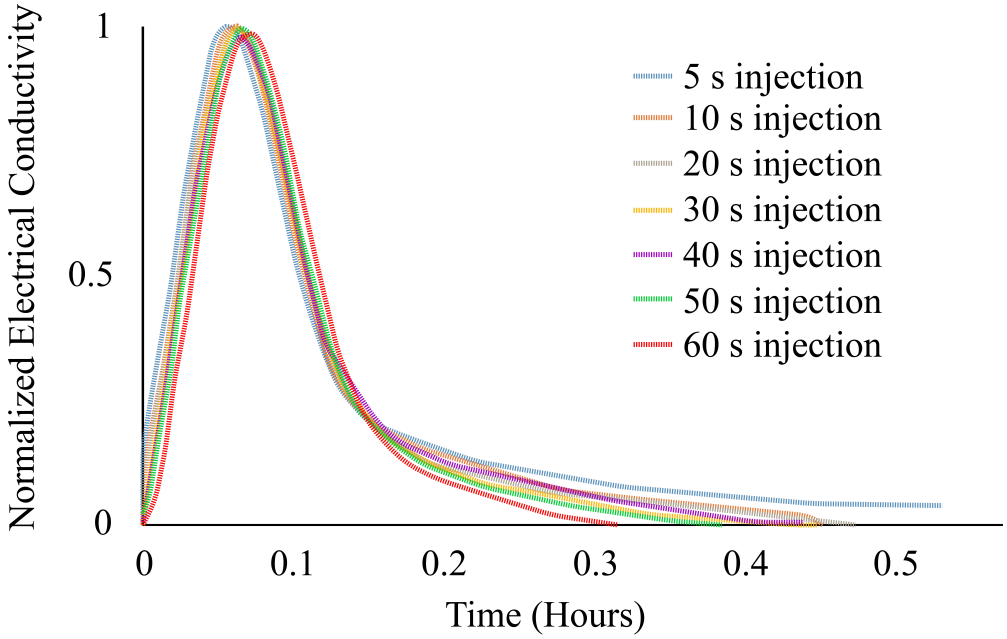

Figure F.5: An expanded view of injection speeds, as conducted by a syringe pump, from 5s to 60s injections at the slow pumping rate

F.2 Injection volume, length, and rate

Injection volume is an important consideration when conducting tests in the field. Therefore, a laboratory study was designed to determine the effect of injection volume on signal strength to suggest a field protocol. To determine best practice, injection volumes were varied during the slow pumping speed from the study of injection style (approximately 215 cm/day). All injections were completed by a syringe pump to remove any inconsistencies associated with hand injections.

To look at volume and injection rate, tests were completed at two injection lengths, 20 seconds and 30 seconds, to add to the commentary of Appendix D. In the 30 s injection series, volumes were varied from 0.1 mL to 1.0 mL in 0.1 mL intervals. In the 20 second injection series, due to limitations of the syringe pump, volumes were varied from 0.1 mL to 0.6 mL in 0.1 mL intervals. Injection rate ranged from 18 mL/hr to 120 mL/hr. In the 20 second injection length tests,

Test Number	**Velocity (cm/day)**	**Dispersivity**	**Pulse Width**	**Injection Speed (s)**
Test 21	196.4	0.17	0.0041	5
Test 22	200.4	0.13	0.0040	10
Test 23	198.1	0.12	0.0042	20
Test 28	233.5	0.12	0.0043	5
Test 29	230.0	0.07	0.0032	10
Test 30	230.0	0.07	0.0033	20

Table F.1: Slow pump speed tests – Method of Moments results

Test Number	Velocity (cm/day)	Dispersivity	Pulse Width	Injection Speed (s)
Test 1	1631.5	0.13	0.0037	5
Test 4	1580.4	0.10	0.0039	10
Test 5	1405.0	0.08	0.0036	20
Test 16	1686.2	0.13	0.0050	5
Test 17	1575.4	0.11	0.0045	10
Test 19	1487.5	0.08	0.0040	20

Table F.2: Fast pump speed tests – Method of Moments results

Test Number	Velocity (cm/day)	Dispersivity	Pulse Width	Injection Speed (s)
Test 21	196.4	0.17	0.0041	5
Test 22	200.4	0.13	0.0040	10
Test 23	198.1	0.12	0.0042	20
Test 24	197.2	0.12	0.0036	30
Test 25	192.1	0.12	0.0037	40
Test 26	195.8	0.10	0.0035	50
Test 27	194.2	0.09	0.0035	60

Table F.3: Injection length comparison – slow pump speed

Test Number	Velocity (cm/day)	Dispersivity	Pulse Width	Injection Speed (s)
Test 1	1631.5	0.13	0.0037	5
Test 4	1580.4	0.10	0.0039	10
Test 5	1405.0	0.08	0.0036	20
Test 7	1395.8	0.08	0.0036	30
Test 10	1047.8	0.07	0.0032	40
Test 12	920.2	0.07	0.0024	50
Test 13	846.1	0.07	0.0027	60

Table F.4: Injection length comparison – fast pump speed

the 0.1 mL, 0.2 mL, and 0.3 mL tests resulted in ideal curves which are easily fit in VelProbePE (Figure F.6 A, B, C). The 0.4 mL, 0.5 mL, and 0.6 mL tests are increasingly less ideal (Figure F.6 D, E, F). Analysis of the curves suggests that tracer is pushed onto the detector pairs by the speed of the injection (not the pumped water flow), which is the initial spike (first visible in the 0.3 mL test, and progressively more pronounced with greater volumes injected over the same time interval). The 0.4 mL and 0.5 mL tests feature a second "hump" which is likely the tracer pushed onto the bottom detector pair being carried over the top detector pair (effectively acting as a second "pulse"). Notably, the second pulse is absent from the 0.6 mL test, likely, this is due to tracer being pushed off the surface of the probe, making it unable to pass over the bottom detector pair and then the top detector pair (Figure F.6 F). The 30 s tests display similar curve types, with ideality extending to 0.4 mL, likely due to the slower rate of injection (Figure F.6 A, B, C, D, E, F).

A comparison of the 20 second and 30 second injection tests, from 0.1 mL to 0.6 mL suggests that the rate of injection, with larger volumes of tracer, causes non-ideal curve shapes. While the shape is not the typical breakthrough curve, the bulk movement of the tracer still represents a close match to the theoretical velocity when interpreted with the Method of Moments technique.

F.3 Injection concentration

When designing a field test, injection concentration should be considered as well. To conduct a useful test, the contrast in electrical conductivity between the tracer and the surrounding aquifer water should be high enough to produce a noticeable, clear signal. In a general sense, a deionized water tracer should be used in aquifers with high conductivities, such as those with high salt concentrations, to provide enough contrast. Conversely, in aquifers that have low conductivities (that is, freshwater aquifers with low salt concentrations) a saline tracer should be used. In practice, it can sometimes be difficult to tell which tracer to use. To discern the effect of tracer concentrations, a laboratory study was designed around the use of three different tracer concentrations: 0.25 g/L NaCl, 0.5 g/L NaCl, and 1 g/L NaCl (Figure F.7). All tracers were tested in tap water from the

Kansas Geological Survey with a background electrical conductivity of 0.5 to 0.6 mV.

As expected, it was found that the higher concentrations of NaCl tracer solutions produced more notable signals in the freshwater laboratory system (Figure F.7). Interestingly, the 0.25 g/L NaCl solution is less conductive that the water in the laboratory apparatus, and therefore, displays a curve in the opposite direction (Figure F.7). As a result, this curve, when interpreted in VelProbe, does not need to be inverted but can be interpreted "as is."

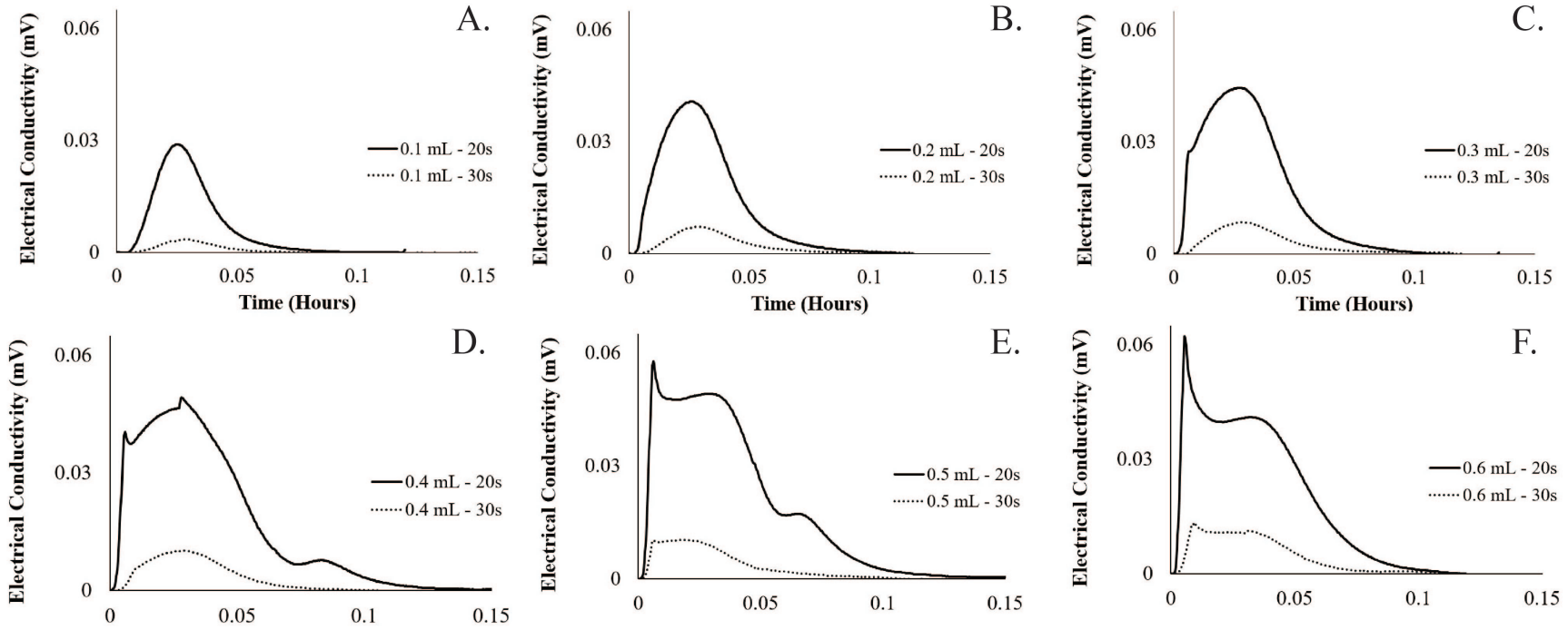

Figure F.6: At the slow pumping speed, injection volume appears to have an effect on curve shape. Smaller volumes have a more ideal curve shape, while larger volumes have a less ideal curve shape. Longer injection times seem to produce ideal curves over a slightly longer range. These longer (30s) injection times produced curves with significantly lower amplitudes due to a change in injection concentration. 20s injections used a 1 g/L NaCl tracer solution, while 30s injections used a 0.5 g/L NaCl tracer solution.

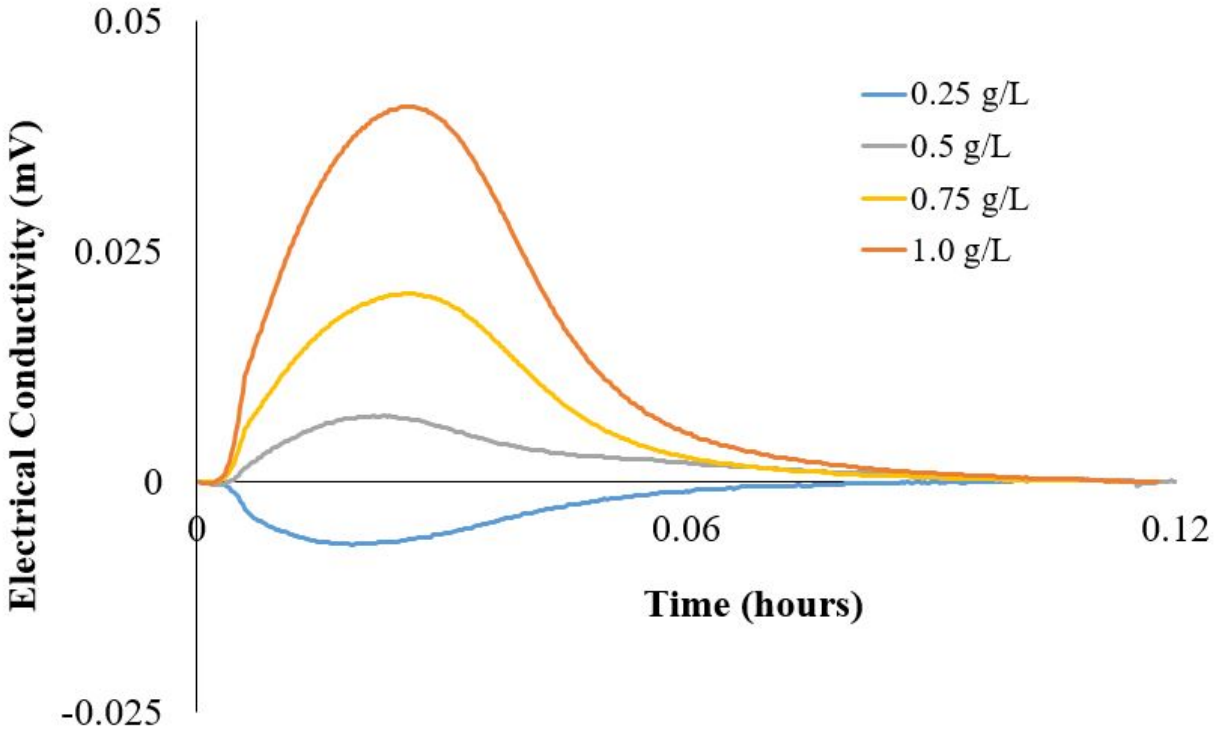

Figure F.7: In the four tests shown above, pumping velocity, injection length, and injection rate were held constant while tracer concentration was changed. As expected, tracers with higher contrasts resulted in BTCs with more notable signals. The test with 0.25 g/L solution shows the result of using a tracer with less conductivity than the surrounding aquifer.

Appendix G

Laboratory depth test data

The tables in this appendix detail the data collected during the laboratory depth testing sequence described in Chapter 2. The table includes the depth of installation, the expected velocity, the measured velocity, and the ratio of measured to expected velocity.

Install Depth (cm)	Expected v (cm/day)	Measured v (cm/day)	Measured/Expected
7	452.7	446	0.99
7	452.7	449	0.99
7	452.7	440	0.97
7	452.7	450	0.99
7	452.7	445	0.98
7	452.7	444	0.98
7	452.7	448	0.99
7	452.7	451	0.996
7	452.7	452	0.998
7	452.7	450	0.99
9	430.8	430	0.998
9	430.8	432	1.00
9	430.8	429	0.995
9	430.8	434	1.01
9	430.8	423	0.98
9	430.8	428	0.99
9	430.8	431	1.00
9	430.8	433	1.01
9	430.8	430	0.998
9	430.8	427	0.99
11	445.4	530	1.19
11	445.4	499	1.12
11	445.4	500	1.12
11	445.4	495	1.11
11	445.4	501	1.12
11	445.4	496	1.11
11	445.4	385	0.86
11	445.4	430	0.97
11	445.4	450	1.01
11	445.4	430	0.97
13	423.5	325	0.77
13	423.5	330	0.78
13	423.5	331	0.78
13	423.5	369	0.87
13	423.5	340	0.80
13	423.5	332	0.78
13	423.5	365	0.86
13	423.5	330	0.78
13	423.5	341	0.81
13	423.5	360	0.85
13	420.1	302	0.72
13	420.1	286	0.68
13	420.1	284	0.68

Table G.1: Laboratory SBPVP depth test summary, page 1

Install Depth (cm)	**Expected *v* (cm/day)**	**Measured *v* (cm/day)**	**Measured/Expected**
17	411.6	362	0.88
17	411.6	344	0.84
17	411.6	325	0.79
19	415.3	273	0.66
19	415.3	331	0.80
19	415.3	311	0.75

Table G.2: Laboratory SBPVP depth test summary, page 2

Appendix H

Grindsted Å 2015 data summary

A preliminary study of the main field site, Grindsted, was conducted in the summer of 2015 with the SBPVP and temperature gradient methods, as well as a single location of seepage meter measurements (Figures H.1 and H.2). Fourteen transects with five measurement locations apiece, 70 measurement locations total, were completed with the temperature spear. Due to time constraints, only 10 locations were measured with the SBPVP. However, this preliminary study suggested that the streambed of the *Grindsted Å* was highly heterogeneous, with hot spots of high flow near the meander and comparatively lower flow near the bridge. This result prompted the further, more detailed study of this site in the summer of 2016.

Additionally, this field campaign highlighted the "order of magnitude" differences between the velocities suggested by the temperature spear data and the other methods. Due to this difference in measurements, the experimental design for 2016 was adapted to include an additional conventional method and to explore potential causes for the difference in measurements. All data collected are listed in Tables I.1, I.2, I.3, I.4, I.5, I.6, I.7, I.8, I.9, and I.10.

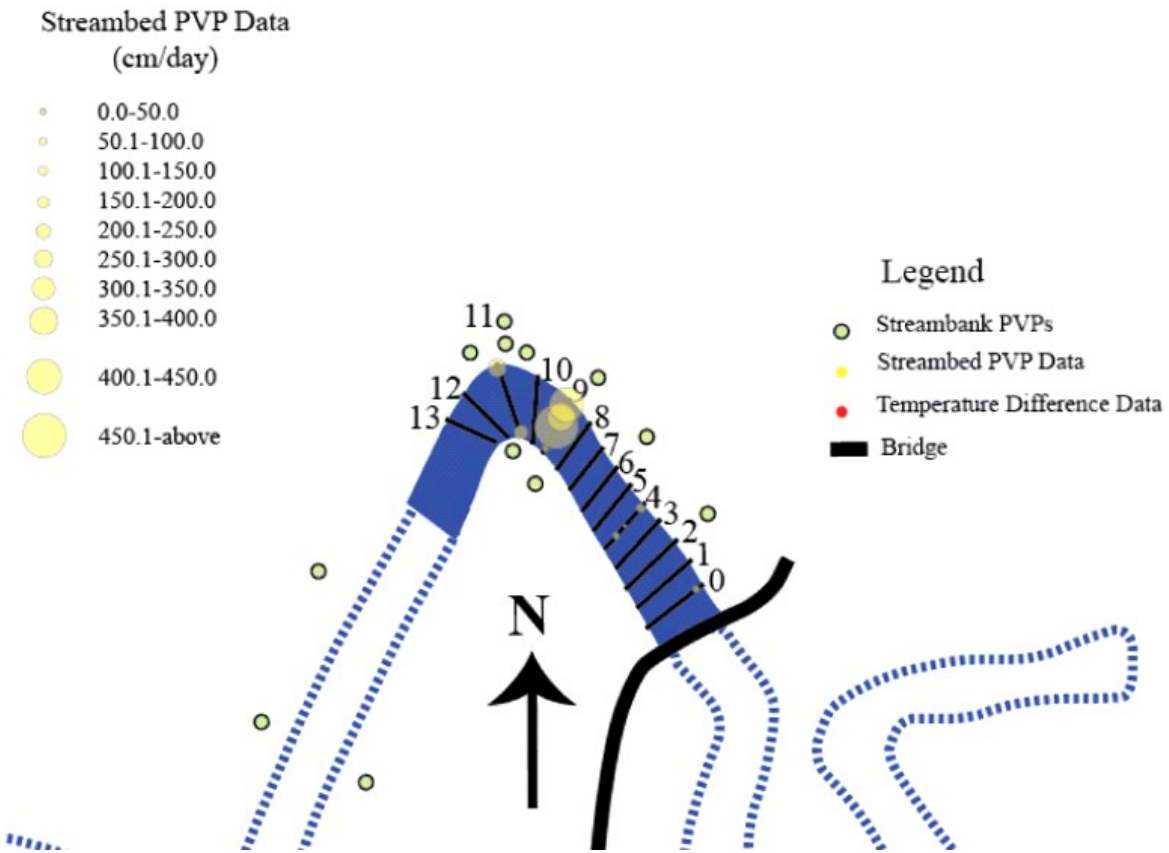

Figure H.1: SBPVP data from Grindsted, 2015

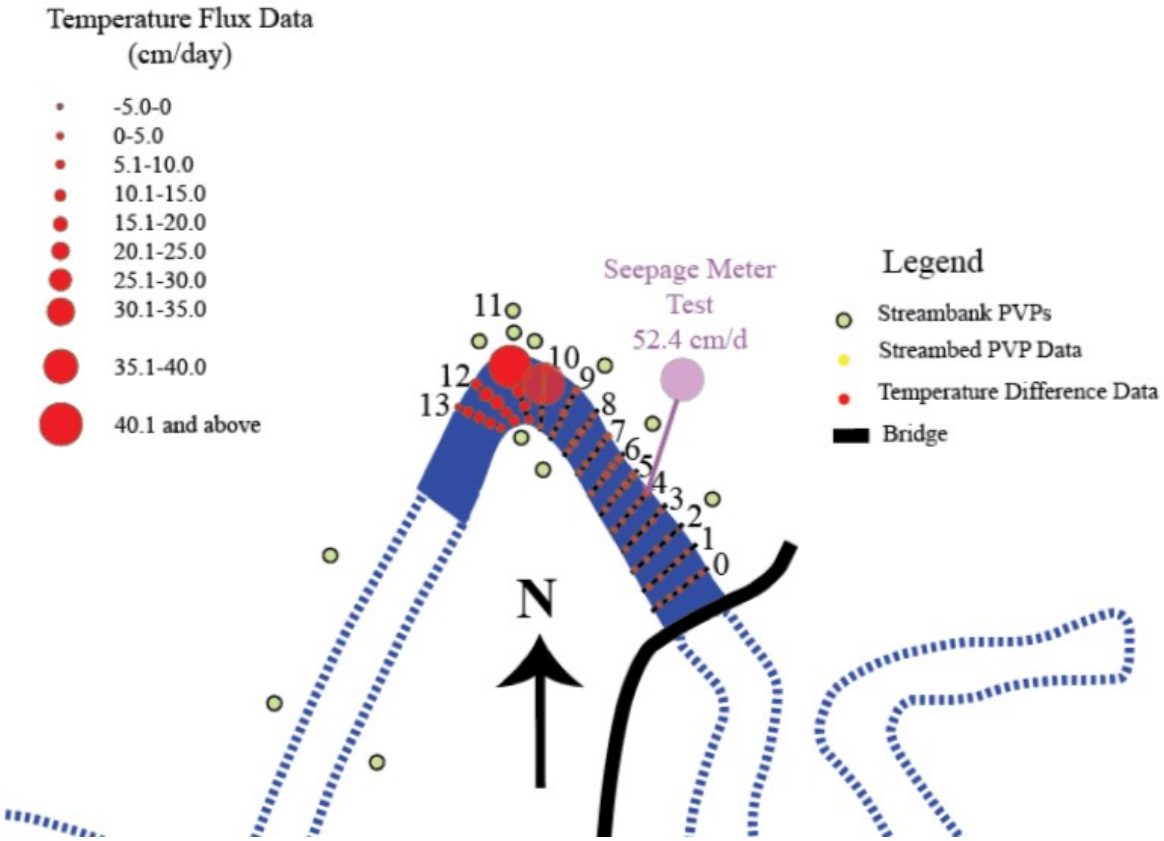

Figure H.2: Temperature data – Grindsted, 2015

Appendix I

Grindsted Å 2016 data summary

The data detailed below are those used to generate the figures presented in Chapter 3 of this dissertation. There are three velocity datasets (SBPVP, mini-piezometer, and temperature gradient). This campaign also included the collection of seepage meter data (presented in Chapter 3) and streambed morphology data. These datasets are also included for completeness.

I.1 SBPVP data – Grindsted, summer 2016

Below is the summary of the SBPVP field data discussed in Chapters 3 and 4 of this dissertation. All these data are used in Chapter 4, while only a small subset are used Chapter 3.

UTMx	UTMy	SBPVP Velocity (m/yr)
494600.6208	6179157.676	0.0
494593.7525	6179167.118	11.0
494600.8832	6179164.082	14.6
494614.439	6179134.648	20.1
494597.248	6179165.769	25.6
494589.2053	6179158.511	35.6
494585.664	6179151.501	69.4
494587.1083	6179164.575	109.5
494580.5865	6179150.438	116.8
494615.9315	6179131.987	127.8
494592.3123	6179160.312	149.7
494610.1698	6179142.575	166.1
494612.9415	6179137.242	171.6
494611.5963	6179139.915	182.5
494614.8828	6179142.018	189.8
494605.5565	6179150.249	215.4
494577.9383	6179145.102	215.4
494614.745	6179138.382	222.7
494616.237	6179135.777	244.6
494611.8475	6179143.639	244.6
494582.2088	6179143.273	244.6
494594.1055	6179160.592	251.9
494600.2973	6179162.903	255.5
494586.743	6179154.264	292.0
494575.7017	6179142.813	292.0
494618.035	6179136.905	328.5
494613.5253	6179144.704	328.5
494619.5065	6179134.17	438.0
494620.9005	6179131.535	456.3
494613.2395	6179140.967	456.3

Table I.1: SBPVP data – Grindsted, 2016 – page 1

UTMx	UTMy	SBPVP Velocity (m/yr)
494604.1442	6179161.934	473.8
494608.2568	6179155.664	474.5
494622.361	6179128.935	511.0
494607.4543	6179147.92	547.5
494588.0037	6179159.378	565.8
494603.2633	6179160.869	584.0
494603.765	6179156.253	598.6
494588.0467	6179163.389	616.9
494608.953	6179145.313	631.5
494610.472	6179146.301	657.0
494606.581	6179150.924	660.7
494611.991	6179147.288	693.5
494604.3122	6179152.996	693.5
494587.9755	6179156.958	784.8
494608.63	6179152.272	850.5
494586.679	6179157.443	850.5
494604.8005	6179156.948	912.5
494584.9045	6179148.611	923.5
494609.0405	6179148.956	927.1
494580.7	6179153.423	949.0
494598.5398	6179159.368	1003.8
494616.5485	6179139.521	1010.6
494584.3987	6179161.98	1043.9
494594.1055	6179163.855	1113.3
494593.929	6179165.487	1113.5
494617.719	6179133.078	1149.8
494617.4475	6179129.416	1168.0
494610.6268	6179149.992	1186.3
494589.4497	6179166.378	1186.3
494602.3825	6179159.805	1222.8
494585.6003	6179161.113	1259.3
494605.836	6179157.642	1277.5
494582.7895	6179158.899	1277.5
494607.6055	6179151.598	1295.8
494596.172	6179160.314	1368.8
494596.71	6179163.042	1368.8
494619.174	6179130.476	1387.0
494584.423	6179151.982	1405.3
494596.979	6179164.405	1507.5

Table I.2: SBPVP data – Grindsted, 2016 – page 2

UTMx	UTMy	SBPVP Velocity (m/yr)
494590.8617	6179159.833	1587.8
494601.5017	6179158.74	1694.7
494583.825	6179149.068	1719.2
494583.182	6179152.462	1825.0
494581.335	6179156.312	1861.5
494581.6443	6179140.243	1861.5
494579.5565	6179147.58	1934.5
494589.9233	6179161.019	1971.0
494599.1257	6179160.547	2007.5
494590.1653	6179164.861	2080.5
494584.086	6179158.414	2109.7
494581.431	6179146.805	2171.8
494581.941	6179152.942	2190.0
494585.391	6179154.776	2233.8
494577.1873	6179142.17	2233.8
494607.2707	6179154.997	2241.1
494619.035	6179126.867	2281.3
494583.3055	6179146.029	2281.3
494620.698	6179127.901	2336.0
494585.3825	6179157.929	2416.3
494588.985	6179162.204	2420.0
494591.5967	6179161.829	2493.0
494582.687	6179155.8	2591.5
494580.1587	6179140.885	2591.5
494586.802	6179160.246	2774.0
494609.6545	6179152.947	2810.5
494582.7455	6179149.525	2912.7
494594.282	6179162.223	3285.0
494606.2845	6179154.33	3321.5
494580.0735	6179144.188	3376.3
494581.666	6179149.981	3478.5
494584.039	6179155.288	3985.8
494578.673	6179141.528	3985.8
494605.2983	6179153.663	4062.5
494590.881	6179163.345	4380.0
494599.7115	6179161.725	4562.5
494606.8715	6179158.336	5131.9
494602.7295	6179155.559	5420.3
494596.441	6179161.678	9876.9

Table I.3: SBPVP data – Grindsted, 2016, page 3

I.2 Mini-piezometer data – Grindsted, 2016

Below is the summary of the mini-piezometer field data discussed in Chapters 3 and 4 of this dissertation. All these data are used in Chapter 4, while only a small subset are used Chapter 3.

UTMx	UTMy	Piezo-derived velocities (cm/day)
494622.361	6179128.935	111.0
494620.698	6179127.901	665.0
494619.035	6179126.867	609.0
494620.9005	6179131.535	55.4
494619.174	6179130.476	443.0
494617.4475	6179129.416	443.0
494619.5065	6179134.17	249.2
494617.719	6179133.078	359.9
494615.9315	6179131.987	110.8
494618.035	6179136.905	276.9
494616.237	6179135.777	83.1
494614.439	6179134.648	0.0
494616.5485	6179139.521	0.3
494614.745	6179138.382	221.5
494612.9415	6179137.242	110.8
494614.8828	6179142.018	166.1
494613.2395	6179140.967	249.2
494611.5963	6179139.915	27.7
494613.5253	6179144.704	193.8
494611.8475	6179143.639	55.4
494610.1698	6179142.575	55.4
494611.991	6179147.288	221.5
494610.472	6179146.301	138.4
494608.953	6179145.313	110.8
494610.6268	6179149.992	359.9
494609.0405	6179148.956	276.9
494607.4543	6179147.92	138.4
494609.6545	6179152.947	719.9
494608.63	6179152.272	221.5
494607.6055	6179151.598	332.3
494606.581	6179150.924	110.8
494605.5565	6179150.249	0.0
494608.2568	6179155.664	110.8
494607.2707	6179154.997	664.5
494606.2845	6179154.33	636.8
494605.2983	6179153.663	996.8

Table I.4: Piezometer – Grindsted, 2016 – page 1

UTMx	UTMy	Piezo-derived velocities (cm/day)
494604.3122	6179152.996	166.1
494606.8715	6179158.336	1273.6
494605.836	6179157.642	443.0
494604.8005	6179156.948	221.5
494603.765	6179156.253	221.5
494602.7295	6179155.559	1329.0
494604.1442	6179161.934	99.7
494603.2633	6179160.869	166.1
494602.3825	6179159.805	387.6
494601.5017	6179158.74	498.4
494600.6208	6179157.676	664.5
494600.8832	6179164.082	0.0
494600.2973	6179162.903	55.4
494599.7115	6179161.725	1772.0
494599.1257	6179160.547	376.6
494598.5398	6179159.368	249.2
494597.248	6179165.769	0.0
494596.979	6179164.405	332.3
494596.71	6179163.042	304.6
494596.441	6179161.678	1495.1
494596.172	6179160.314	293.5
494593.7525	6179167.118	27.0
494593.929	6179165.487	305.0
494594.1055	6179163.855	305.0
494594.282	6179162.223	720.0
494594.1055	6179160.592	55.0
494589.4497	6179166.378	304.0
494590.1653	6179164.861	554.0
494590.881	6179163.345	1119.0
494591.5967	6179161.829	637.0
494592.3123	6179160.312	27.0
494590.8617	6179159.833	415.0
494589.9233	6179161.019	526.0
494588.985	6179162.204	609.0
494588.0467	6179163.389	122.0
494587.1083	6179164.575	28.0
494584.3987	6179161.98	221.0
494585.6003	6179161.113	332.0
494586.802	6179160.246	720.0
494588.0037	6179159.378	138.0
494589.2053	6179158.511	0.0
494582.7895	6179158.899	304.6

Table I.5: Piezometer data – Grindsted, 2016 – page 2

UTMx	UTMy	Piezo-derived velocities (cm/day)
494584.086	6179158.414	526.1
494585.3825	6179157.929	775.3
494586.679	6179157.443	193.8
494587.9755	6179156.958	166.1
494581.335	6179156.312	498.0
494582.687	6179155.8	692.0
494584.039	6179155.288	941.0
494585.391	6179154.776	609.0
494586.743	6179154.264	83.0
494580.7	6179153.423	235.4
494581.941	6179152.942	545.1
494583.182	6179152.462	520.4
494584.423	6179151.982	396.5
494585.664	6179151.501	24.8
494584.9045	6179148.611	ND
494583.825	6179149.068	ND
494582.7455	6179149.525	ND
494581.666	6179149.981	ND
494580.5865	6179150.438	ND
494579.5565	6179147.58	ND
494581.431	6179146.805	ND
494583.3055	6179146.029	ND
494577.9383	6179145.102	ND
494580.0735	6179144.188	ND
494582.2088	6179143.273	ND
494575.7017	6179142.813	ND
494577.1873	6179142.17	ND
494578.673	6179141.528	ND
494580.1587	6179140.885	ND
494581.6443	6179140.243	ND

Table I.6: Piezometer data – Grindsted, 2016 – page 3

I.3 Temperature data – Grindsted, summer 2016

Below is the summary of the temperature field data discussed in Chapters 3 and 4 of this dissertation. All these data are used in Chapter 4, while only a small subset are used Chapter 3.

UTMx	UTMy	Temp-derived velocities (cm/day)
494622.361	6179128.935	0.15
494620.698	6179127.901	0.94
494619.035	6179126.867	1.04
494620.9005	6179131.535	0.50
494619.174	6179130.476	1.63
494617.4475	6179129.416	1.01
494619.5065	6179134.17	0.41
494617.719	6179133.078	0.92
494615.9315	6179131.987	0.16
494618.035	6179136.905	0.69
494616.237	6179135.777	0.67
494614.439	6179134.648	0.09
494616.5485	6179139.521	0.00
494614.745	6179138.382	0.15
494612.9415	6179137.242	0.08
494614.8828	6179142.018	0.32
494613.2395	6179140.967	1.22
494611.5963	6179139.915	0.46
494613.5253	6179144.704	1.63
494611.8475	6179143.639	0.52
494610.1698	6179142.575	0.53
494611.991	6179147.288	0.67
494610.472	6179146.301	0.69
494608.953	6179145.313	0.48
494610.6268	6179149.992	3.80
494609.0405	6179148.956	2.24
494607.4543	6179147.92	1.58
494609.6545	6179152.947	4.37
494608.63	6179152.272	1.80
494607.6055	6179151.598	2.00
494606.581	6179150.924	0.58
494605.5565	6179150.249	0.10
494608.2568	6179155.664	0.34
494607.2707	6179154.997	1.65
494606.2845	6179154.33	2.60
494605.2983	6179153.663	3.25

Table I.7: Temperature data – Grindsted, 2016 – page 1

This page is intentionally left blank

UTMx	UTMy	Temp-derived velocities (cm/day)
494604.3122	6179152.996	0.79
494606.8715	6179158.336	1.97
494605.836	6179157.642	0.63
494604.8005	6179156.948	0.69
494603.765	6179156.253	0.56
494602.7295	6179155.559	2.69
494604.1442	6179161.934	5.08
494603.2633	6179160.869	4.65
494602.3825	6179159.805	12.78
494601.5017	6179158.74	16.17
494600.6208	6179157.676	7.55
494600.8832	6179164.082	0.17
494600.2973	6179162.903	0.79
494599.7115	6179161.725	5.35
494599.1257	6179160.547	2.63
494598.5398	6179159.368	1.82
494597.248	6179165.769	0.00
494596.979	6179164.405	8.06
494596.71	6179163.042	6.93
494596.441	6179161.678	30.25
494596.172	6179160.314	6.93
494593.7525	6179167.118	5.16
494593.929	6179165.487	20.40
494594.1055	6179163.855	21.22
494594.282	6179162.223	35.52
494594.1055	6179160.592	6.93
494589.4497	6179166.378	2.90
494590.1653	6179164.861	5.90
494590.881	6179163.345	16.60
494591.5967	6179161.829	10.00
494592.3123	6179160.312	2.50
494590.8617	6179159.833	2.96
494589.9233	6179161.019	4.29
494588.985	6179162.204	4.85
494588.0467	6179163.389	1.09
494587.1083	6179164.575	0.61
494584.3987	6179161.98	16.93
494585.6003	6179161.113	19.86
494586.802	6179160.246	32.79
494588.0037	6179159.378	11.54
494589.2053	6179158.511	2.37
494582.7895	6179158.899	6.29

Table I.8: Temperature data – Grindsted, 2016 – page 2

UTMx	UTMy	Temp-derived velocities (cm/day)
494584.086	6179158.414	16.93
494585.3825	6179157.929	14.21
494586.679	6179157.443	6.78
494587.9755	6179156.958	4.84
494581.335	6179156.312	15.50
494582.687	6179155.8	30.20
494584.039	6179155.288	35.50
494585.391	6179154.776	24.20
494586.743	6179154.264	2.10
494580.7	6179153.423	24.19
494581.941	6179152.942	26.78
494583.182	6179152.462	32.55
494584.423	6179151.982	14.54
494585.664	6179151.501	5.97
494584.9045	6179148.611	17.00
494583.825	6179149.068	25.00
494582.7455	6179149.525	35.50
494581.666	6179149.981	24.20
494580.5865	6179150.438	2.10
494579.5565	6179147.58	1.11
494581.431	6179146.805	1.07
494583.3055	6179146.029	0.97
494577.9383	6179145.102	0.55
494580.0735	6179144.188	8.09
494582.2088	6179143.273	0.17
494575.7017	6179142.813	0.73
494577.1873	6179142.17	1.66
494578.673	6179141.528	3.48
494580.1587	6179140.885	2.00
494581.6443	6179140.243	0.92

Table I.9: Temperature data – Grindsted, 2016 – page 3

I.4 Seepage meter data – Grindsted, summer 2016

Below is the summary of the seepage meter field data discussed in Chapter 3 of this dissertation.

UTMx	UTMy	Seepage meter velocities (cm/day)
494614.439	6179134.648	12.85
494612.9415	6179137.242	25.10
494611.5963	6179139.915	19.26
494610.1698	6179142.575	26.33
494608.953	6179145.313	55.79
494607.4543	6179147.92	61.82

Table I.10: Seepage meter data – Grindsted, 2016

I.5 Stream bottom profiles – Grindsted, 2016

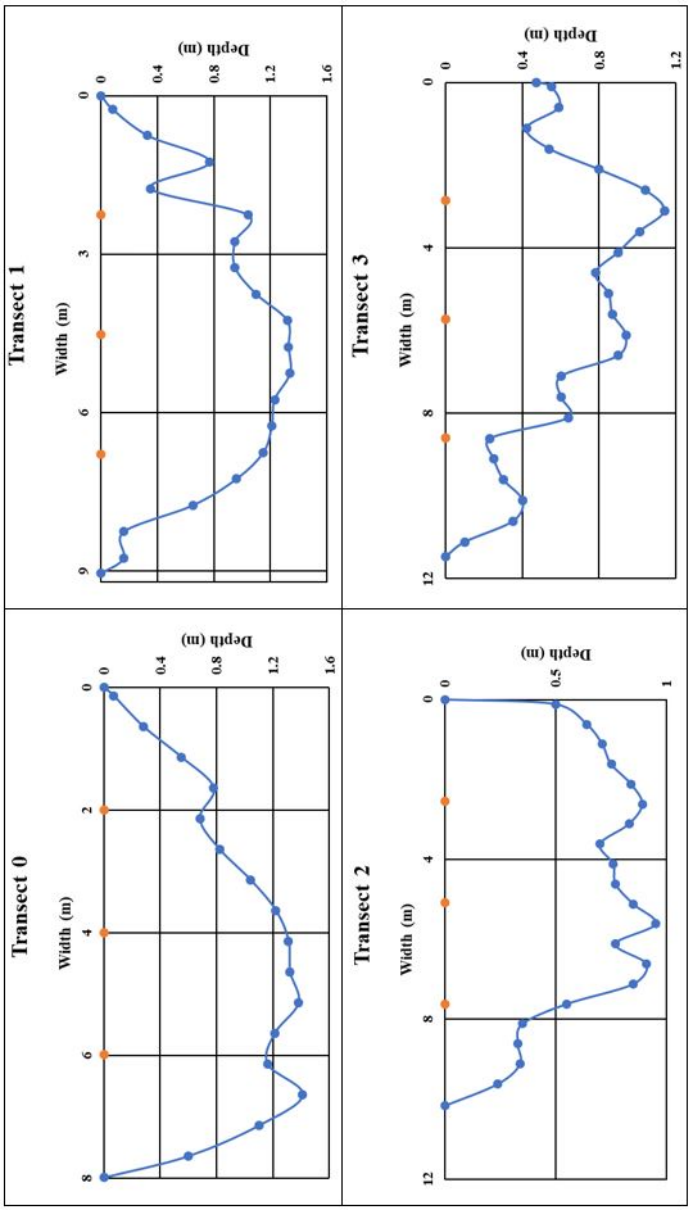

Figure I.1: Streambottom profiles, transects 0-3

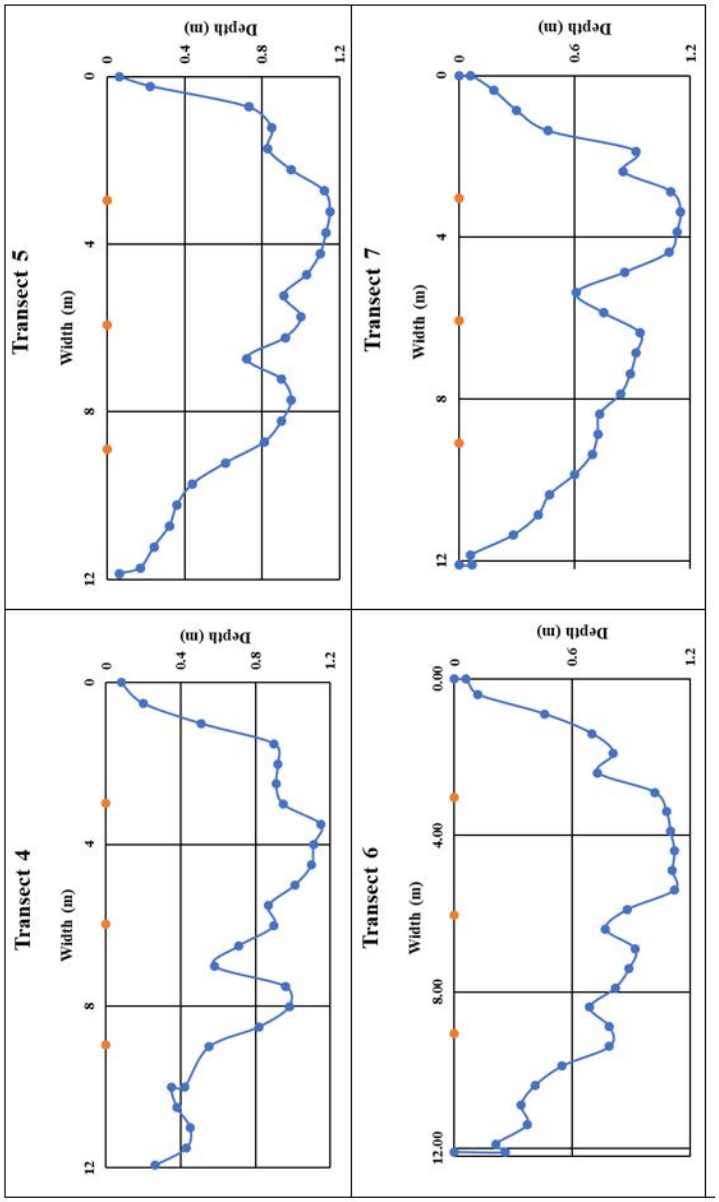

Figure I.2: Streambottom profiles, transects 4-7

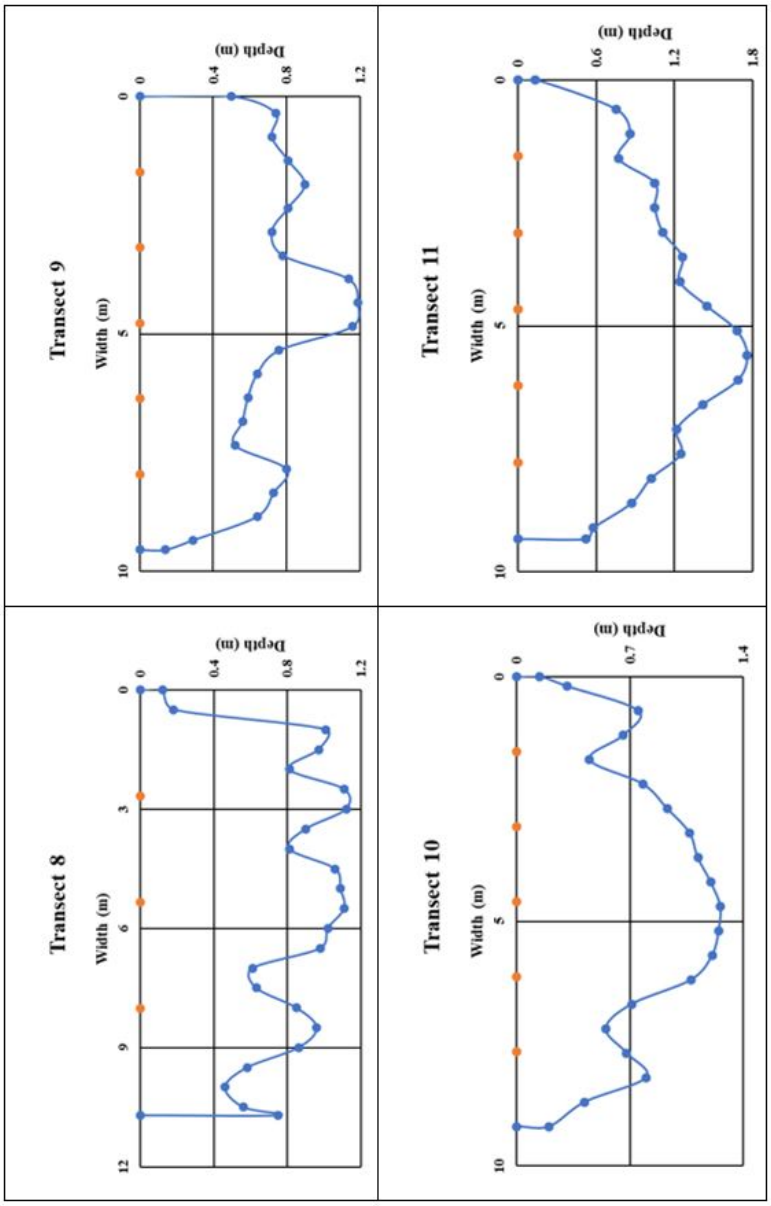

Figure I.3: Streambottom profiles, transects 8-11

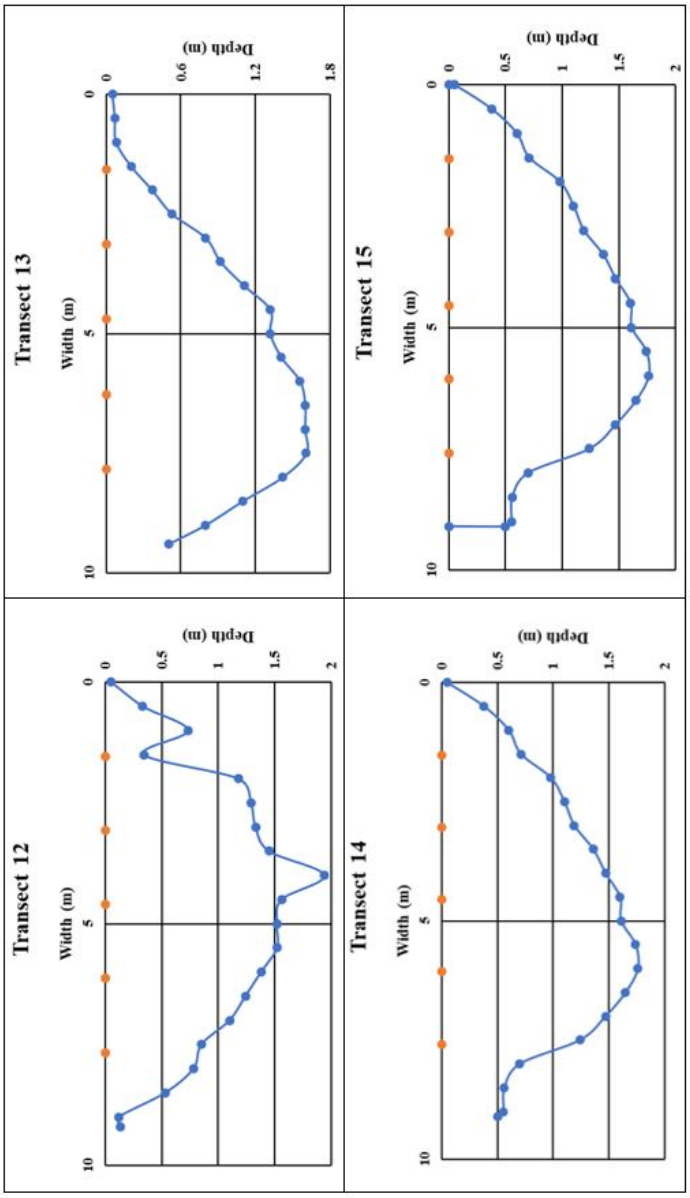

Figure I.4: Streambottom profiles, transects 12-15

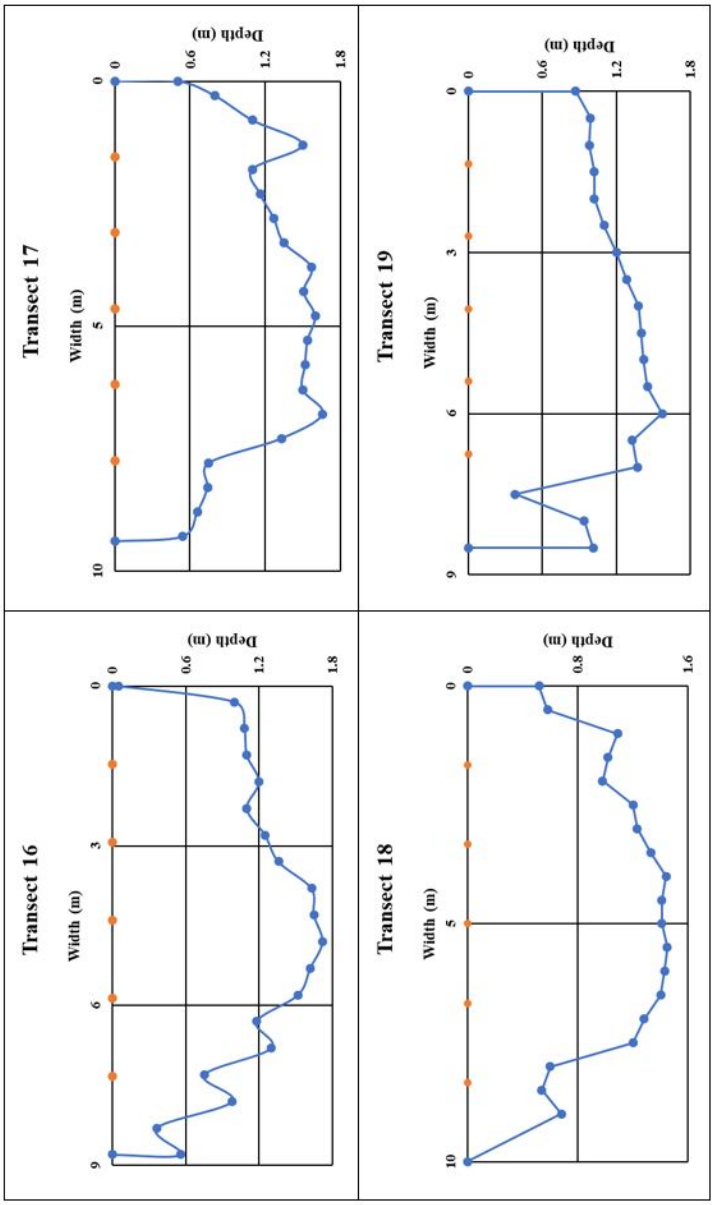

Figure I.5: Streambottom profiles, transects 16-19

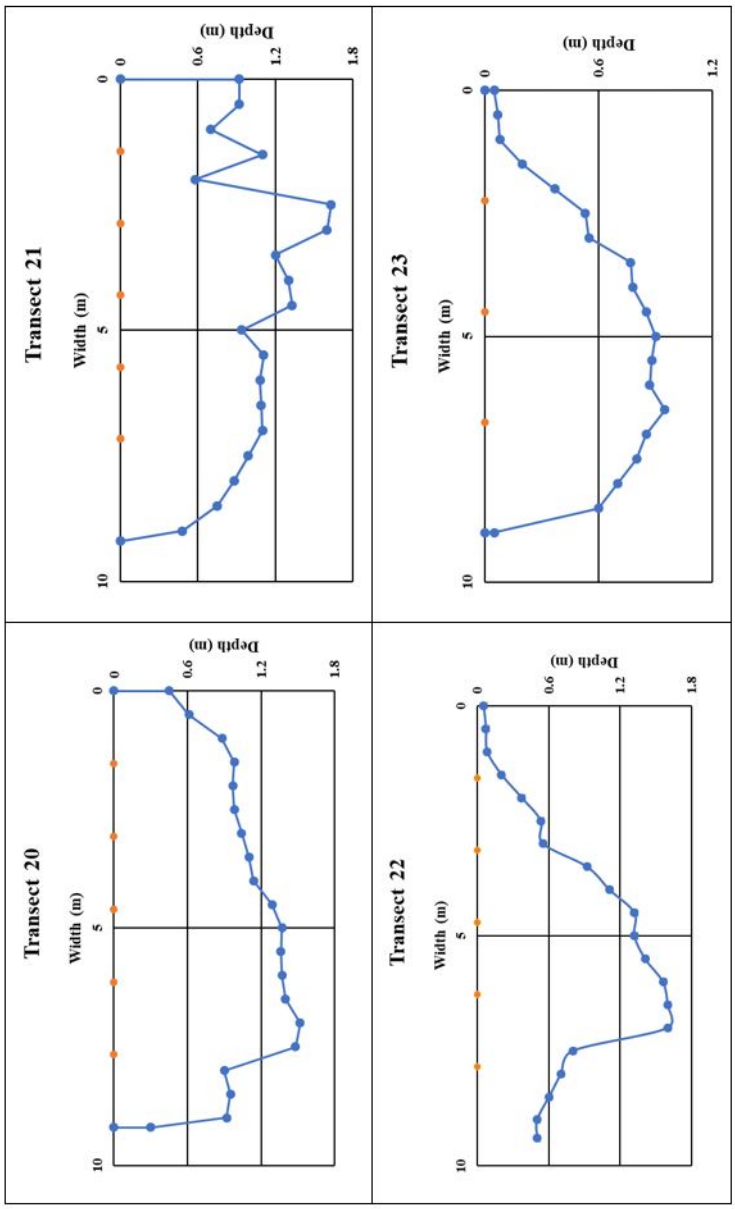

Figure I.6: Streambottom profiles, transects 20-23

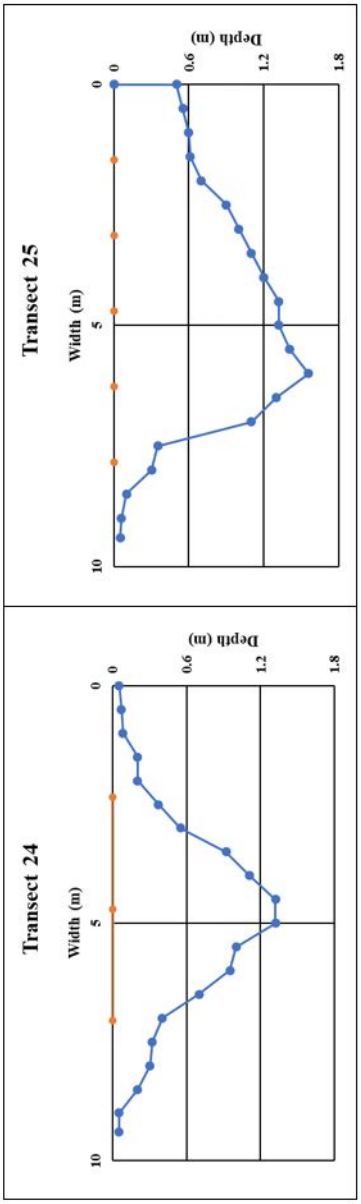

Figure I.7: Streambottom profiles, transects 24-25

Appendix J

A report on interpolation methods

J.1 Introduction

Over the last sixty-five years, the field of geostatistics has developed many useful tools and methods for spatial modeling and interpolation (Krige, 1951; Matheron, 1971, 1973). A well-known, and often used, geostatistical interpolation technique is kriging. Despite its popularity, it has been shown that kriging tends to produce overly smooth results and therefore, sometimes fails to accurately represent non-smooth processes (Goovaerts, 1997; Journel, 1974). Like all interpolation methods, kriging averages data points to interpolate the spaces between them. This causes kriging (and all exact interpolation methods) to (almost always) place local extremes at data locations. This can result in the underestimation of high values and the overestimation of low values, which makes representation of highly structured phenomena difficult (Mahmud et al., 2014). Stochastic simulation, by design, is more able to reproduce spatial patterns and roughness (as found in a variogram), but stochastic simulations are often more computationally expensive and require extensive knowledge of the site to ensure accuracy.

For the purpose of this report, we will compare results from various kinds of kriging with the inverse distance weighting method. Kriging is a stochastic method which can provide prediction, prediction standard error, probability, and quantile surface outputs. If measurement error is as-

sumed, kriging is an inexact interpolator, and if no measurement error is assumed it is an exact interpolator, like Inverse Distance Weighting. The advantages of this method include flexibility, an allowance for the assessment of spatial autocorrelation, the ability to obtain prediction standard errors, and the ability to decide the values of most parameters. The main disadvantages are that you have to make many decisions about transformations, trends, models, parameters, and neighborhood (which can be time and labor intensive), and that kriging has a tendency to over-smooth data surfaces, particularly when values in close proximity have large differences. The assumptions inherent in this method include that data comes from a stationary stochastic process and, some methods require that the data have a normal distribution (it's important to note that, in general, all interpolation schemes perform better under this condition).

Inverse Distance Weighting (IDW) is a deterministic, exact interpolation method that produces prediction output surfaces. The advantages of this method are that it is a fast computing method, with few parameter decisions, and no assumptions about the data. The disadvantages include that there is no assessment of prediction errors and that it produces distinctive "bullseyes" around data locations.

J.2 Data exploration

Prior to attempting to krige, the univariate distribution of the data was explored to determine the best kriging methods to try. For example, it might be important to know the distribution of the data because some kriging methods require a normal Gaussian distribution of data (Ordinary, Simple, and Universal kriging). While other methods do not require normal distribution of data, interpolation methods perform better (in general) when data is normally distributed, therefore, transforms are often applied to datasets to gain a normal distribution. For a histogram, this means the mean and median will be similar, the skewness will be near zero, and the kurtosis will be near 3. In the Normal QQ plot, the data is normally distributed if the points fall close to the 45 degree reference line. In the case of our data, the untransformed distribution is not normal and therefore,

transforming the data could be useful (Figure J.1). To attempt to organize the data in a normal

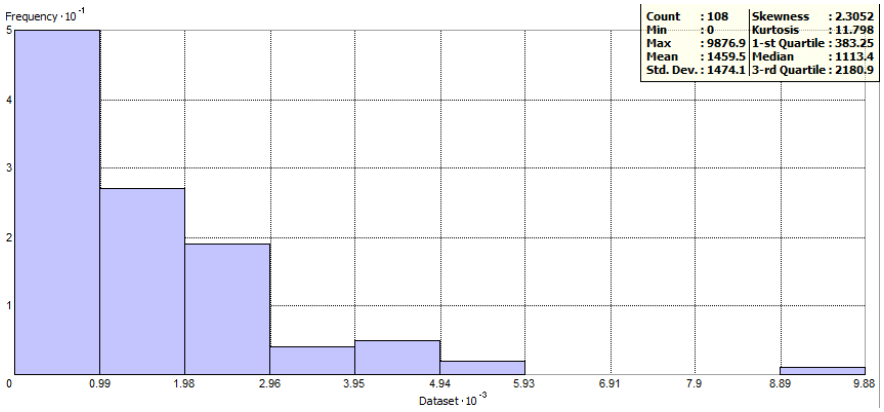

Figure J.1: Untransformed Data -– Preliminary exploration of distribution

distribution, several transform options are available (either by hand or within ArcMap), including: Log, Box-Cox, and Arc-Sin transforms. Log transforming our dataset brings it closer to normal distribution, where skewness should be near zero (goes from 2.3052 to -1.0633), kurtosis should be near three (11.798 to 4.19), and mean and median should be similar (1459.5 and 1113.4 to 2.9129 and 3.0467, respectively) (Figures J.1 and J.2). As noted before, the Normal QQ plot is another way to check if the data is normally distributed. Figure J.3 shows a comparison of the non-transformed data with the log transformed data. The log transformed data falls closer to the line, but has significant tailing on the low and high ends. Non-normal distribution is expected for field data sets. The spatial distribution of the points in the high and low tails is shown in Figure J.4 (highlighted in aqua on the QQ plot and on the map of data points). As described earlier, these points tend to be the highest and lowest in the dataset and, upon the inspection below, are also surrounded by points that suggest much higher or much lower velocities. Therefore, in this case, a normal score transform is advised to “force” the dataset to be normally distributed for kriging (Figure J.5).

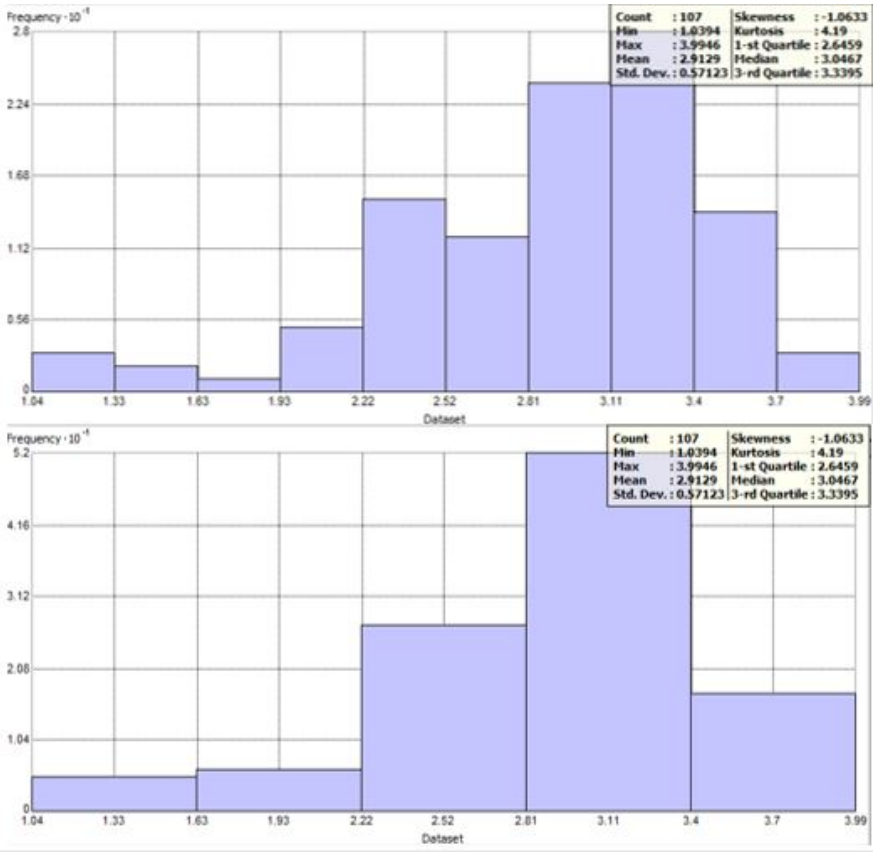

Figure J.2: A log transform of the data, which makes it almost normally distributed.

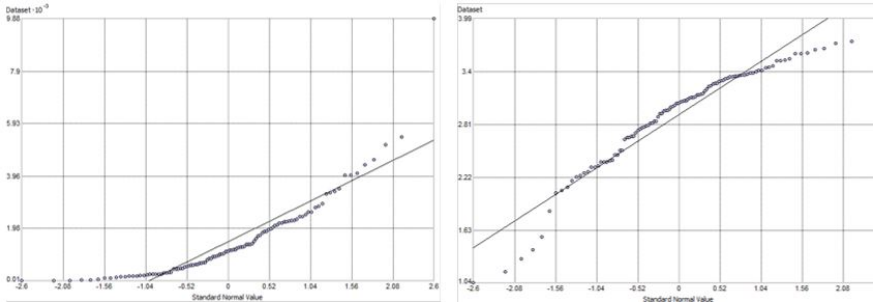

Figure J.3: On the left, a normal QQ plot of the untransformed data. On the right, a normal QQ plot of the log transformed data.

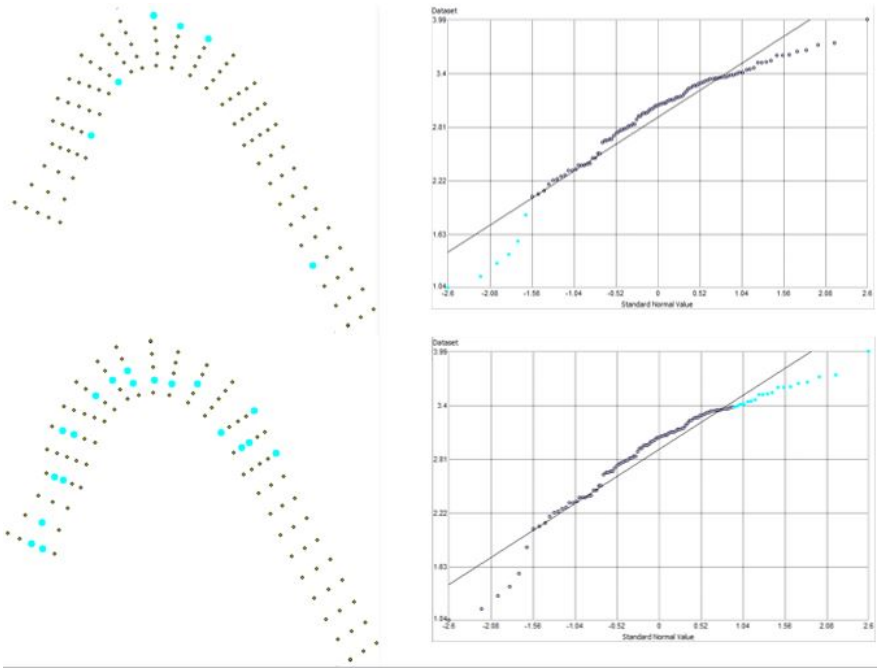

Figure J.4: An exploration of which points fall most off the normal distribution line. The points highlighted in aqua on each left image of the river meander points correspond to the points highlighted in aqua on the QQ plot directly to the right.

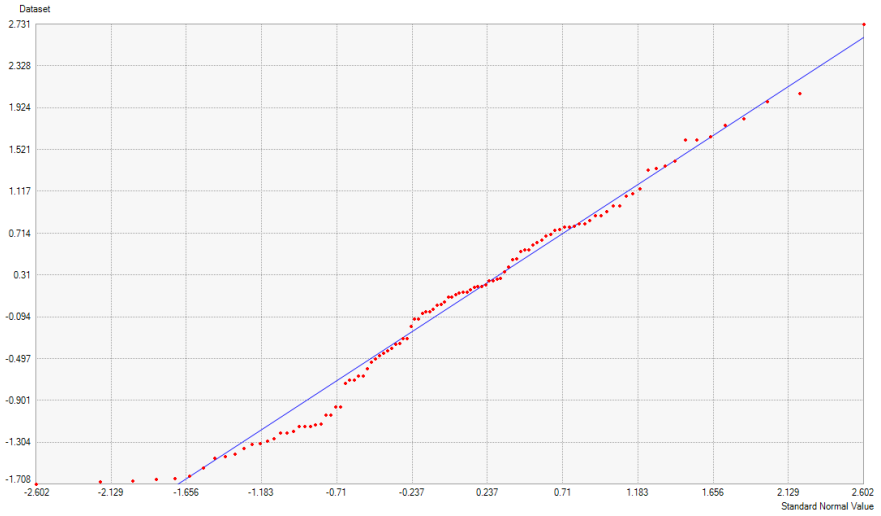

Figure J.5: In general, the normal score transform helps with the tails, but a slight low tail still exists, and the data still has some irregularities.

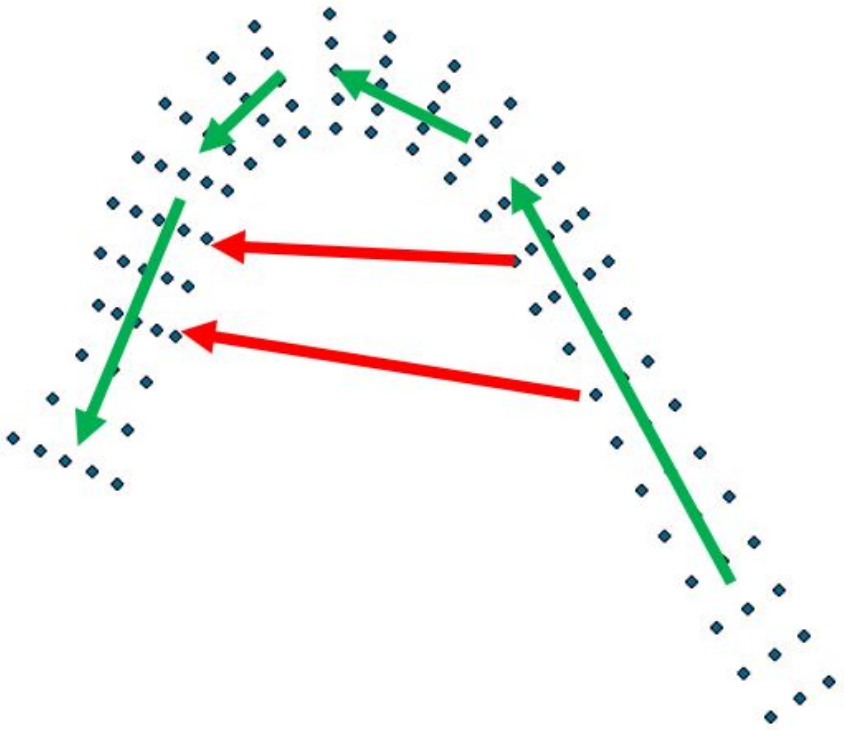

Figure J.6: Meanders are a non-ideal shape to krige because not all straightline distances are relevant to the process. Red arrows show the non-relevant paths (across the ground) ArcMap includes in the semi-variogram. Distances across ground surface are not relevant to semi-variogram analysis, only distances within the stream polygon (not shown explicitly). Therefore, paths (like those shown as green arrows) are the only distances that should be included in analysis.

J.3 Semi-variogram analysis

The next step in the kriging process is to examine the semi-variogram. The first attempt was made with the original form of the river. However, this introduces non-relevant distances to the semi-variogram, because the area cannot be restricted to the non-rectangular polygon of the meander (Figure J.6). Therefore, in order to more effectively examine the semi-variogram (and potentially reduce the error of the kriging), the river meander was "straightened" (maintaining the correct distances between points and river width) (Figure J.7).

Figure J.7: The data points, after transformation into a roughly rectangular polygon (while maintaining appropriate distances between data points).

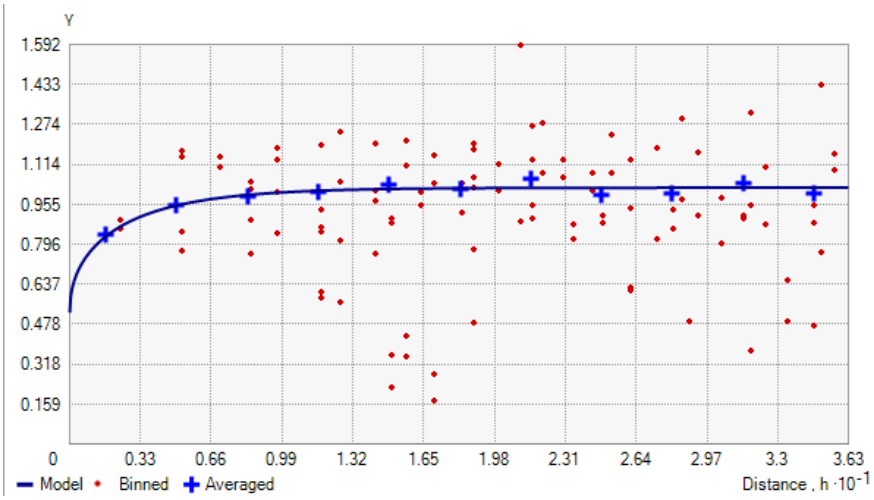

Figure J.8: Initial semi-variogram fit

J.4 Simple kriging

Initially, simple kriging was applied to the dataset, after normal-score transformation. Figure J.8 shows the initial semi-variogram model fit. The red dots show the binned points, while the blue crosses show the averages (which makes the point cloud easier to fit). Various semi-variogram models were tried to determine the best fit (Circular, Spherical, Tetraspherical, Pentaspherical, Exponential, Gaussian, Rational Quadratic, Hole-Effect, K-Bessel, J-Bessel, and stable. In this case, K-Bessel offered the most reasonable semi-variogram model fit. However, even when the data is kriged with the most reasonable semivariogram fit, the results are unreasonable due to oversmoothing. Therefore, after this analysis, inverse distance weighting was chosen as the interpolation method for data in this dissertation.

Appendix K

T-test results – comparison of methods

These results are referenced in Chapter 3 and detailed fully here. For these tests, the null hypothesis examined is that the two measurement results considered are statistically the same. For each t-test, alpha is applied as 0.025. This specific correction was applied because the values are examined in a familywise pattern, and thus, analysis errors introduced by autocorrelation must be accounted for. The strictest measure was chosen. The tables present results from two kinds of t-tests: (1) results assuming equal variance (AEV) and (2) results assuming unequal variance (AUV). P values are reported for each result, EVP and UVP, respectively. The calculations with the assumption of equal variance is preferred because the calculation has more degrees of freedom, which means the result has more statistical power.

Location	Result AEV	EVP	Result AUV	UVP	Variance: SBPVP	Variance: Piezo
1	Reject	2.29E-06	Reject	0.000963	0.00150	0
2	Reject	6.50E-05	Reject	6.50E-05	0.0114	0.0375
3	Reject	3.77E-05	Reject	0.00391	0.000	0.0375
4	Reject	0.00451	Reject	0.00450	0.216	0.668
5	Reject	4.84E-06	Reject	0.00140	0.0375	0
6	Reject	9.15E-05	Reject	0.00609	0.0240	0

Table K.1: SBPVP-Piezo T-tests

Location	Result AEV	EVP	Result AUV	UVP	Variance: SBPVP	Variance: Seepage
1	Reject	0.0141	Cannot Reject	0.0760	0.00150	0.794
2	Reject	0.000200	Reject	0.00900	0.0114	0.182
3	Reject	3.36E-05	Reject	0.00360	0.000	0.0634
4	Reject	0.00115	Reject	0.00120	0.216	0.631
5	Reject	7.98E-06	Reject	0.00180	0.0375	0.182
6	Reject	1.33E-05	Reject	0.00230	0.0240	0.182

Table K.2: SBPVP-Seepage T-tests

Location	Result AEV	EVP	Result AUV	UVP	Variance: SBPVP	Variance: Temperature
1	Reject	2.32E-06	Reject	0.000970	0.00150	3.75E-06
2	Reject	2.57E-06	Reject	0.00100	0.0114	6.00E-07
3	Reject	1.96E-09	Reject	2.82E-05	0.000	9.61E-06
4	Reject	5.34E-05	Reject	0.00470	0.216	3.75E-06
5	Reject	6.31E-07	Reject	0.000510	0.0375	7.36E-06
6	Reject	5.46E-07	Reject	0.000470	0.0240	1.22E-05

Table K.3: SBPVP-Temperature T-tests

Location	Result AEV	EVP	Result AUV	UVP	Variance: Piezometer	Variance: Seepage
1	Reject	0.00240	Cannot Reject	0.0311	0	0.794
2	Reject	0.0160	Cannot Reject	0.0811	0.0375	0.182
3	Reject	0.000710	Reject	0.000709	0.0375	0.0634
4	Reject	0.000770	Reject	0.000769	0.668	0.631
5	Reject	3.01E-05	Reject	0.00349	0.000	0.182
6	Reject	1.55E-05	Cannot Reject	0.00250	0	0.182

Table K.4: Piezo-Seepage T-tests

Location	Result AEV	EVP	Result AUV	UVP	Variance: Piezometer	Variance: Temperature
1	Reject	0.000234	Reject	0.00973	0	3.75E-06
2	Reject	2.46E-05	Reject	0.00316	0.0375	6.00E-07
3	Reject	2.53E-05	Reject	0.00320	0.0375	9.61E-06
4	Reject	0.000111	Reject	0.00671	0.668	3.75E-06
5	Reject	3.02E-10	Reject	1.1E-05	0.000	7.36E-06
6	Reject	3.25E-10	Reject	1.10E-05	0.000	1.22E-05

Table K.5: Piezo-Temperature T-tests

Location	Result AEV	EVP	Result AUV	UVP	Variance: Seepage	Variance: Temperature
1	Reject	0.00243	Reject	0.0314	0.794	3.75E-06
2	Reject	0.000145	Reject	0.00767	0.182	6.00E-07
3	Reject	8.98E-05	Reject	0.00603	0.0634	9.61E-06
4	Reject	0.000474	Reject	0.0139	0.631	3.75E-06
5	Reject	2.97E-05	Reject	0.00347	0.182	7.36E-06
6	Reject	2.50E-05	Reject	0.00318	0.182	1.22E-05

Table K.6: Seepage-Temperature T-tests

Appendix L

Raadvad preliminary data

As a side project through the Technical University of Denmark, a preliminary study of Raadvad, Denmark was conducted with the SBPVP. The primary objective of the study was to determine whether or not the SBPVP would function in such a complex geologic environment. The site features large engineered structures, directing the water, from its use as a factory site for manufacturing bread and cheese slicers. The manufacturing history of this site resulted in a significant amount of heavy metal contamination (in the soil and the water) as well as the contribution of several subsurface contaminant sources. This contamination affects the stream, which has a control structure on the eastern side, one engineered channel, and one natural channel. The streambed is affected significantly by debris (on the surface of the bed and beneath it). Therefore, the environment presents a new opportunity to try the SBPVP. The result is a preliminary report documented in this appendix.

The SBPVP was preliminarily tested across one transect at the Raadvad site, where temperature gradients (taken with temperature profiler made of an Ebro TFN-520 Type K handheld thermometer and a steel spear) suggested exchange zones were present. Three locations in that transect were measured and a soil core was also taken (Figure L.1). The soil core provides some insight into the stream bottom sediment, which had a fair mixture of sediment sizes (Figure L.2). Potentially,

this level of heterogeneity caused some issues for probe to sediment contact, resulting in non-ideal breakthrough curves (Figure L.3). For consistency in the data interpretation, all curves were fit using Method of Moments, which accounts for the bulk movement of the tracer. Location 1 had the highest velocity estimates, followed by location 3, and then location 2. Generally, while the curves are not as ideal as those from the sandy and organic environments presented in Chapters 2-5, the results seem preliminarily promising for the use of this device in complex sediment settings. The non-ideal breakthrough curve shapes likely occurred because the heterogeneity of the sediments was on a scale smaller than the SBPVP's scale of measurement. More testing would be needed to determine the utility of this tool in this setting, and this testing was undertaken by a master's student at the Technical University of Denmark starting in April 2017. The results from this study are documented in Schulz (2017).

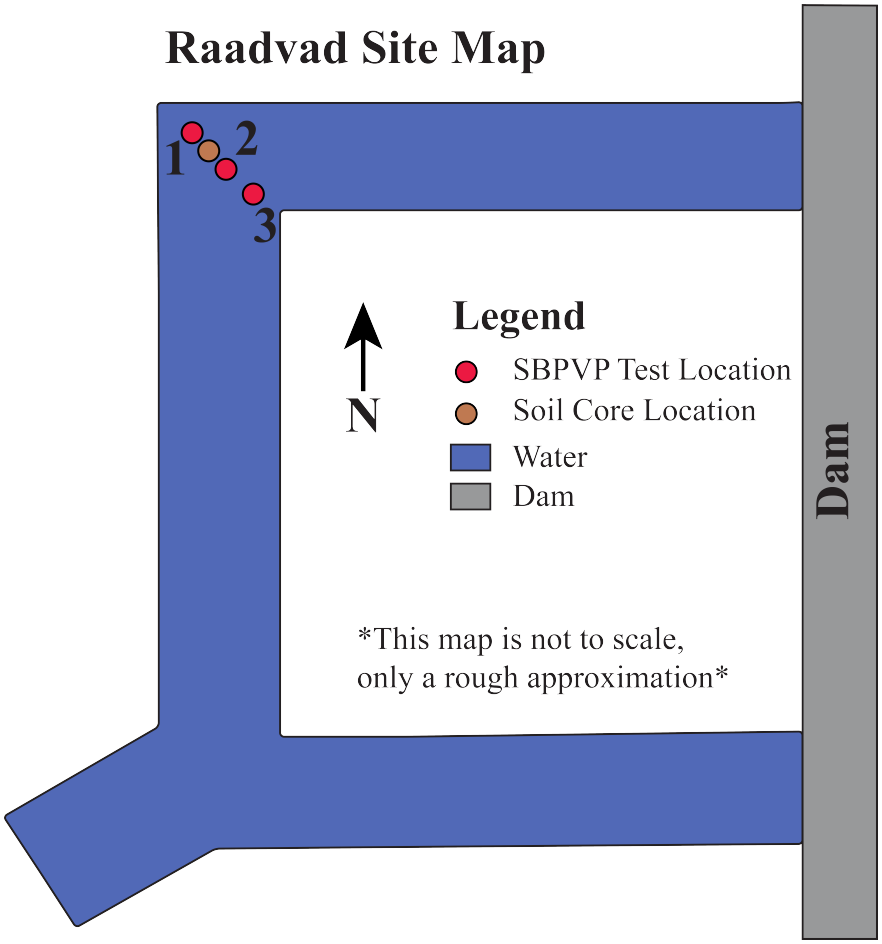

Figure L.1: A rough approximation of the Raadvad site showing the transect of interest with three SBPVP measurement locations and a soil core location.

Figure L.2: The soil core taken at the Raadvad site at the same time SBPVP testing was conducted.

Test 1
HB1: 356.61 cm/day
HB2: 314.82 cm/day

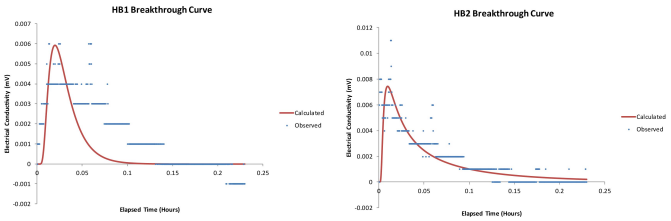

Test 2
HB1: 298.89 cm/day
HB2: 302.24 cm/day

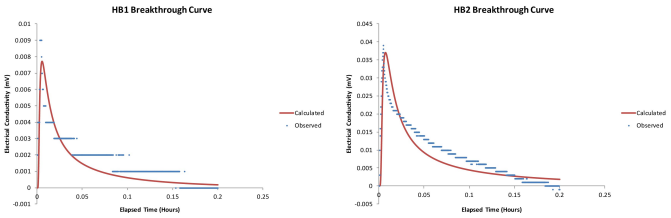

Test 3
HB1: 329.72 cm/day
HB2: 285.93 cm/day

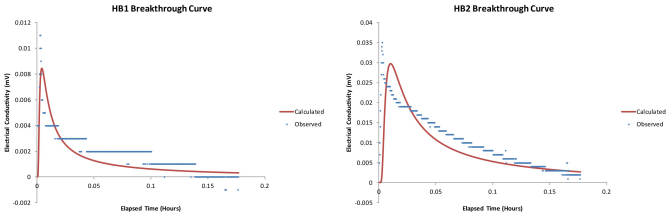

Figure L.3: The preliminary results from each location. Tests 1-3 were done at location 1.

Test 4
HB1: 34.15 cm/day
HB2: 33.52 cm/day

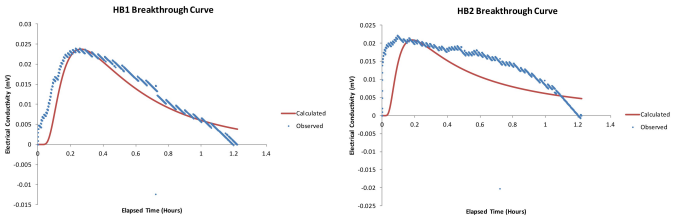

Test 5
HB1: 161.55 cm/day
HB2: 169.40 cm/day

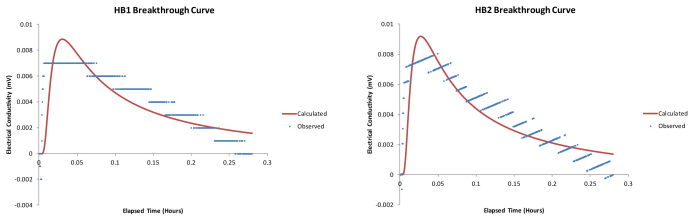

Test 6
HB1: 140.26 cm/day
HB2: 137.59 cm/day

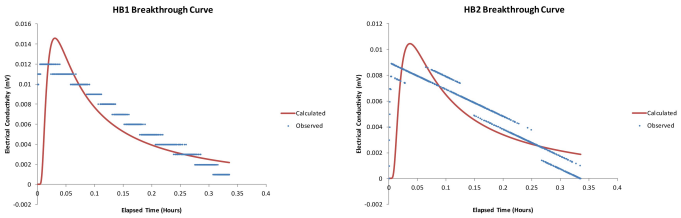

Figure L.4: The preliminary results from each location. Test 4 was at location 2, and tests 5-6 were at location 3.

References

D.J. Allen, C.D. Gooddy, D.J. Lapworth, A.J. Newell, A.T. Williams, D. Allen, and C. Abesser. Interaction between groundwater, the hyporheic zone and a chalk stream: a case study from the river lambourn, uk. *Journal of Hydrogeology*, 18(5):1125–1141, 2010. doi: 10.1007/s10040-010-0592-2.

M.P. Anderson. Heat as a ground water tracer. *Groundwater*, 43(6):951–968, 2005. doi: 10.1111/j.1745-6584.2005.00052.x.

C. Anibas, B. Verbeiren, K. Buis, J. Chormanski, L. De Doncker, T. Okruszko, P. Meire, and O. Batelaan. A hierarchical approach on groundwater-surface water interaction in wetlands along the upper biebrza river, poland. *Hydrology and Earth System Sciences*, 16(7):2329, 2012. doi: 10.5194/hess-16-2329-2012.

M. Arshadi, M.J. Amiri, and S. Mousavi. Kinetic, equilibrium and thermodynamic investigations of ni (ii), cd (ii), cu (ii) and co (ii) adsorption on barley straw ash. *Water Resources and Industry*, 6:1–17, 2014. doi: 10.1016/j.wri.2014.06.001.

N. Balbarini, W.M. Boon, E. Nicolajsen, J.M. Nordbotten, P.L. Bjerg, and P.J. Binning. A 3-d numerical model of the influence of meanders on groundwater discharge to a gaining stream in an unconfined sandy aquifer. *Journal of Hydrology*, 552:168–181, 2017. doi: 10.1016/j.jhydrol.2017.06.042.

S. Ballard. The in situ permeable flow sensor: A ground-water flow velocity meter. *Groundwater*, 34(2):231–240, 1996. doi: 10.1111/j.1745-6584.1996.tb01883.x.

K.K. Barnes, D.W. Kolpin, M.T. Meyer, E.M. Thurman, E.T. Furlong, S.D. Zaugg, and L.B. Barber. Water-quality data for pharmaceuticals, hormones, and other organic wastewater contaminants in us streams, 1999-2000. *US Geological Survey Open-File Report 02-94*, 2002.

J.R. Bartolino and R.G. Niswonger. *Numerical simulation of vertical ground-water flux of the Rio Grande from ground-water temperature profiles, central New Mexico*, volume 99. US Department of the Interior, US Geologcial Survey, 1999.

C.V. Baxter and F.R. Hauer. Geomorphology, hyporheic exchange, and selection of spawning habitat by bull trout (salvelinus confluentus). *Canadian Journal of Fisheries and Aquatic Sciences*, 57(7):1470–1481, 2000. doi: 10.1139/f00-056.

C.V. Baxter, F.R. Hauer, and W.W. Woessner. Measuring groundwater–stream water exchange: new techniques for installing minipiezometers and estimating hydraulic conductivity. *Transactions of the American Fisheries Society*, 132(3):493–502, 2003. doi: 10.1577/1548-8659(2003)132<0493:MGWENT>2.0.CO;2.

M.W. Becker, T. Georgian, H. Ambrose, J. Siniscalchi, and K. Fredrick. Estimating flow and flux of ground water discharge using water temperature and velocity. *Journal of Hydrology*, 296(1): 221–233, 2004. doi: 10.1016/j.jhydrol.2004.03.025.

C. Béland-Pelletier, M. Fraser, J. Barker, and T. Ptak. Estimating contaminant mass discharge: A field comparison of the multilevel point measurement and the integral pumping investigation approaches and their uncertainties. *Journal of contaminant hydrology*, 122(1-4):63–75, 2011. doi: 10.1016/j.jconhyd.2010.11.004.

S.J. Berg and R.W. Gillham. Studies of water velocity in the capillary fringe: The point velocity probe. *Groundwater*, 48(1):59–67, 2010. doi: 10.1111/j.1745-6584.2009.00606.x.

A. Bernstein, E. Adar, A. Yakirevich, and R. Nativ. Dilution tests in a low-permeability fractured aquifer: Matrix diffusion effect. *Groundwater*, 45(2):235–241, 2007. doi: 10.1111/j.1745-6584.2006.00268.x.

A.S. Bhaskar, J.W. Harvey, and E.J. Henry. Resolving hyporheic and groundwater components of streambed water flux using heat as a tracer. *Water Resources Research*, 48(8), 2012. doi: 10.1029/2011WR011784.

Thomas M Biksey and Elisa D Gross. The hyporheic zone: Linking groundwater and surface water—understanding the paradigm. *Remediation Journal*, 12(1):55–62, 2001. doi: 10.1002/rem.1025.

A. Binley, S. Ullah, A.L. Heathwaite, C. Heppell, P. Byrne, K. Lansdown, M. Trimmer, and H. Zhang. Revealing the spatial variability of water fluxes at the groundwater-surface water interface. *Water Resources Research*, 49(7):3978–3992, 2013. doi: 10.1002/wrcr.20214.

P.J. Blanchfield and M.S. Ridgway. Use of seepage meters to measure groundwater flow at brook trout redds. *Transactions of the American Fisheries Society*, 125(5):813–818, 1996. doi: 10.1577/1548-8659(1996)125<0813:UOSMTM>2.3.CO;2.

Fulvio Boano, Judson W Harvey, Andrea Marion, Aaron I Packman, Roberto Revelli, Luca Ridolfi, and Anders Wörman. Hyporheic flow and transport processes: Mechanisms, models, and biogeochemical implications. *Reviews of Geophysics*, 52(4):603–679, 2014.

H. Bokuniewicz, M. Pollock, J. Blum, and R. Wilson. Submarine ground water discharge and salt penetration across the sea floor. *Groundwater*, 42(7):983–989, 2004. doi: 10.1111/j.1745-6584.2004.tb02637.x.

I.R. Bowen, J.F. Devlin, and P.C. Schillig. Design and testing of a convenient benchtop sandbox for controlled flow experiments. *Groundwater Monitoring & Remediation*, 32(4):87–91, 2012. doi: 10.1111/j.1745-6592.2012.01400.x.

J.D. Bredehoeft and I.S. Papaopulos. Rates of vertical groundwater movement estimated from the earth's thermal profile. *Water Resources Research*, 1(2):325–328, 1965. doi: 10.1029/WR001i002p00325.

Martin A Briggs, Laura K Lautz, Jeffrey M McKenzie, Ryan P Gordon, and Danielle K Hare. Using high-resolution distributed temperature sensing to quantify spatial and temporal variability in vertical hyporheic flux. *Water Resources Research*, 48(2), 2012. doi: 10.1029/2011WR011227.

Martin A Briggs, Emily B Voytek, Frederick D Day-Lewis, Donald O Rosenberry, and John W Lane. Understanding water column and streambed thermal refugia for endangered mussels in the delaware river. *Environmental Science & Technology*, 47(20):11423–11431, 2013. doi: 10.1021/es4018893.

Martin A Briggs, Frederick D Day-Lewis, Jay P Zarnetske, and Judson W Harvey. A physical explanation for the development of redox microzones in hyporheic flow. *Geophysical Research Letters*, 42(11):4402–4410, 2015.

T.D. Brock, D.R. Lee, D. Janes, and D. Winek. Groundwater seepage as a nutrient source to a drainage lake; lake mendota, wisconsin. *Water Research*, 16(7):1255–1263, 1982. doi: 10.1016/0043-1354(82)90144-0.

Matthias Brunke and TOM Gonser. The ecological significance of exchange processes between rivers and groundwater. *Freshwater biology*, 37(1):1–33, 1997.

R.L. Burger and K. Belitz. Measurement of anisotropic hydraulic conductivity in unconsolidated sands: A case study from a shoreface deposit, oyster, virginia. *Water Resources Research*, 33 (6):1515–1522, 1997. doi: 10.1029/97WR00570.

J.J. Butler, J.M. Healey, G. McCall, E.J. Garnett, and S.P. Loheide. Hydraulic tests with direct-push equipment. *Groundwater*, 40(1):25–36, 2002. doi: 10.1111/j.1745-6584.2002.tb02488.x.

J.J. Butler Jr. *The Design, Performance, and Analysis of Slug Tests*. CRC press, 1997.

E.E. Cey, D.L. Rudolph, G.W. Parkin, and R. Aravena. Quantifying groundwater discharge to a small perennial stream in southern ontario, canada. *Journal of Hydrology*, 210(1):21–37, 1998. doi: 10.1016/S0022-1694(98)00172-3.

S.W. Chapman, B.L. Parker, J.A. Cherry, R. Aravena, and D. Hunkeler. Groundwater–surface water interaction and its role on tce groundwater plume attenuation. *Journal of Contaminant Hydrology*, 91(3):203–232, 2007. doi: 10.1016/j.jconhyd.2006.10.006.

B. Conant. Delineating and quantifying ground water discharge zones using streambed temperatures. *Ground water*, 42(2):243–257, 2004. doi: 10.1111/j.1745-6584.2004.tb02671.x.

P.G. Cook, G. Favreau, J.C. Dighton, and S. Tickell. Determining natural groundwater influx to a tropical river using radon, chlorofluorocarbons and ionic environmental tracers. *Journal of Hydrology*, 277(1):74–88, 2003. doi: 10.1016/S0022-1694(03)00087-8.

M.M. Cremeans and J.F. Devlin. Validation of a new device to quantify groundwater-surface water exchange. *Journal of Contaminant Hydrology*, 206:75–80, 2017. doi: 10.1016/j.jconhyd.2017.08.005.

M.M. Cremeans, J.F. Devlin, U.S. McKnight, and P.L. Bjerg. Application of new point measurement device to quantify groundwater-surface water interactions. *Journal of Contaminant Hydrology*, 2018.

J.P. Dakin, D.J. Pratt, G.W. Bibby, and J.N. Ross. Distributed optical fibre raman temperature sensor using a semiconductor light source and detector. *Electronics letters*, 21(13):569–570, 1985. doi: 10.1049/el:19850402.

F. De Smedt. Analytical solution for the catchment zone of a well located near a groundwater divide in a recharged semi-confined aquifer. *Journal of Hydrology*, 519:1271–1277, 2014. doi: 10.1016/j.jhydrol.2014.08.054.

E.L. de Souza, P. Galvão, R. de Almeida, C. Pinheiro, M. Baessa, and M. Cabral. Stable isotopes studies in the urucu oil province, amazon region, brazil. *Journal of Water Resource and Protection*, 7(3):131, 2015. doi: 10.4236/jwarp.2015.73011.

J. Derx, A.P. Blaschke, and G. Blöschl. Three-dimensional flow patterns at the river–aquifer interface—a case study at the danube. *Advances in Water Resources*, 33(11):1375–1387, 2010. doi: 10.1016/j.advwatres.2010.04.013.

J.F. Devlin and C.D. McElwee. Effects of measurement error on horizontal hydraulic gradient estimates. *Groundwater*, 45(1):62–73, 2007. doi: 10.1111/j.1745-6584.2006.00249.x.

J.F. Devlin, G. Tsoflias, M. McGlashan, and P.C. Schillig. An inexpensive multilevel array of sensors for direct ground water velocity measurement. *Groundwater Monitoring & Remediation*, 29(2):73–77, 2009. doi: 10.1111/j.1745-6592.2009.01233.x.

J.F. Devlin, P.C. Schillig, I.R. Bowen, C.E. Critchley, D.L. Rudolph, N.R. Thomson, G.P. Tsoflias, and J.A. Roberts. Applications and implications of direct groundwater velocity measurement at the centimetre scale. *Journal of Contaminant Hydrology*, 127(1):3–14, 2012. doi: 10.1016/j.jconhyd.2011.06.007.

W. Drost, D. Klotz, A. Koch, H. Moser, F. Neumaier, and W. Rauert. Point dilution methods of investigating ground water flow by means of radioisotopes. *Water Resources Research*, 4(1): 125–146, 1968. doi: 10.1029/WR004i001p00125.

P.A. Ellis and M.O. Rivett. Assessing the impact of voc-contaminated groundwater on surface water at the city scale. *Journal of Contaminant Hydrology*, 91(1):107–127, 2007. doi: 10.1016/j.jconhyd.2006.08.015.

D.R. Erickson. *The hydrogeology of Williams Lake, Minnesota with special emphasis on quantification of littoral ground water contributions using seepage meters and wells*. PhD thesis, MS thesis, Department of Geology and Geophysics, University of Minnesota, 1981.

ESRI. Arcmap documentation. *Online resources*, Version 10.4.1, 2017. URL `http://desktop.arcgis.com/en/documentation/`.

C.W. Fetter. *Applied hydrogeology*. Prentice Hall, 2000.

J.H. Fleckenstein, R.G. Niswonger, and G.E. Fogg. River-aquifer interactions, geologic heterogeneity, and low-flow management. *Groundwater*, 44(6):837–852, 2006. doi: 10.1111/j.1745-6584.2006.00190.x.

J.H. Fleckenstein, S. Krause, D.M. Hannah, and F. Boano. Groundwater-surface water interactions: New methods and models to improve understanding of processes and dynamics. *Advances in Water Resources*, 33(11):1291–1295, 2010. doi: 10.1016/j.advwatres.2010.09.011.

N. Flipo, A. Mouhri, B. Labarthe, S. Biancamaria, A. Rivière, and P. Weill. Continental hydrosystem modelling: the concept of nested stream–aquifer interfaces. *Hydrology and Earth System Sciences*, 18(8):3121–3149, 2014. doi: 10.5194/hess-18-3121-2014.

W.J. Flipse, B.G. Katz, J.B Lindner, and R. Markel. Sources of nitrate in ground water in a sewered housing development, central long island, new york. *Groundwater*, 22(4):418–426, 1984. doi: 10.1111/j.1745-6584.1984.tb01412.x.

R.A. Freeze and J.A. Cherry. *Groundwater*. 0-13-365312-9. Prentice-Hall, 1979. ISBN 9780133653120. URL `https://books.google.com/books?id=8P7kFowKnGUC`.

J.G. Freitas, M.O. Rivett, R.S. Roche, M. Durrant, C. Walker, and J.H. Tellam. Heterogeneous hyporheic zone dechlorination of a tce groundwater plume discharging to an urban river reach. *Science of the Total Environment*, 505:236–252, 2015. doi: 10.1016/j.scitotenv.2014.09.083.

D.L. Freyberg. A natural gradient experiment on solute transport in a sand aquifer: 2. spatial moments and the advection and dispersion of nonreactive tracers. *Water Resources Research*, 22(13):2031–2046, 1986. doi: 10.1029/WR022i013p02031.

T.V. Fusillo, J.J. Hochreiter, and D.G. Lord. Distribution of volatile organic compounds in a new jersey coastal plain aquifer system. *Groundwater*, 23(3):354–360, 1985. doi: 10.1111/j.1745-6584.1985.tb00780.x.

Pierre Goovaerts. *Geostatistics for Natural Resources Characterization*. Oxford University Press New York, 1997.

E. Halevy, H. Moser, O. Zellhofer, and A. Zuber. Borehole dilution techniques: A critical review. In *Isotopes in hydrology. Proceedings of a symposium*, 1967.

A.H. Haria, P. Shand, C. Soulsby, and S. Noorduijn. Spatial delineation of groundwater–surface water interactions through intensive in-stream profiling. *Hydrological Processes*, 27(4):628–634, 2013. doi: 10.1002/hyp.9551.

P.T. Harte and R.G. Kiah. Measured river leakages using conventional streamflow techniques: the case of souhegan river, new hampshire, usa. *Hydrogeology Journal*, 17(2):409–424, 2009. doi: 10.1007/s10040-008-0359-1.

J.W. Harvey and K.E. Bencala. The effect of streambed topography on surface-subsurface water exchange in mountain catchments. *Water Resources Research*, 29(1):89–98, 1993. doi: 10.1029/92WR01960.

J.W. Harvey, B.J. Wagner, and K.E. Bencala. Evaluating the reliability of the stream tracer approach to characterize stream-subsurface water exchange. *Water Resources Research*, 32(8):2441–2451, 1996. doi: 10.1029/96WR01268.

J.W. Harvey, J.K. Böhlke, M.A. Voytek, D. Scott, and C.R. Tobias. Hyporheic zone denitrification: Controls on effective reaction depth and contribution to whole-stream mass balance. *Water Resources Research*, 49(10):6298–6316, 2013. doi: 10.1002/wrcr.20492.

C.E. Hatch, A.T. Fisher, J.S. Revenaugh, J. Constantz, and C. Ruehl. Quantifying surface water–groundwater interactions using time series analysis of streambed thermal records: Method development. *Water Resources Research*, 42(10), 2006. doi: 10.1029/2005WR004787.

M.B. Hausner, F. Suárez, K.E. Glander, N. van de Giesen, J.S. Selker, and S.W. Tyler. Calibrating

single-ended fiber-optic raman spectra distributed temperature sensing data. *Sensors*, 11(11): 10859–10879, 2011. doi: 10.3390/s111110859.

G. Heron, P.L. Bjerg, P. Gravesen, L. Ludvigsen, and T.H. Christensen. Geology and sediment geochemistry of a landfill leachate contaminated aquifer (grindsted, denmark). *Journal of Contaminant Hydrology*, 29(4):301–317, 1998. doi: 10.1016/S0169-7722(97)00028-4.

K.M. Hiscock and V.F. Bense. *Hydrogeology: Principles and Practice*. Wiley, 2014. ISBN 9780470656631. URL `https://books.google.pn/books?id=_tnjAgAAQBAJ`.

J.V. Holm, K. Ruegge, P.L. Bjerg, and T.H. Christensen. Occurrence and distribution of pharmaceutical organic compounds in the groundwater downgradient of a landfill (grindsted, denmark). *Environmental Science and Technology*, 29(5):1415–1420, 1995. doi: 10.1021/es00005a036.

R.M. Holmes. The importance of ground water to stream ecosystem function. In J.B. Jones and P.J. Mulholland, editors, *Streams and Ground Waters*, chapter 5. Elsevier, 2000.

J.W. Hopmans, J. Šimunek, and K.L. Bristow. Indirect estimation of soil thermal properties and water flux using heat pulse probe measurements: Geometry and dispersion effects. *Water Resources Research*, 38(1), 2002. doi: 10.1029/2000WR000071.

P. Huggenberger, E. Hoehn, R. Beschta, and W. Woessner. Groundwater control on riparian/fluvial systems. *Freshwater Biology*, 40:407–425, 1998. doi: 10.1046/j.1365-2427.1998.00371.x.

D. Hunkeler, Y. Abe, M.M. Broholm, S. Jeannottat, C. Westergaard, C.S. Jacobsen, R. Aravena, and P.L. Bjerg. Assessing chlorinated ethene degradation in a large scale contaminant plume by dual carbon–chlorine isotope analysis and quantitative pcr. *Journal of Contaminant Hydrology*, 119(1-4):69–79, 2011. doi: 10.1016/j.jconhyd.2010.09.009.

J.P. Hurley, D.E. Armstrong, G.J. Kenoyer, and C.J. Bowser. Ground water as a silica source for diatom production in a precipitation-dominated lake. *Science*, 227:1576–1579, 1985. doi: 10.1126/science.227.4694.1576.

P.A. Hutchinson and I.T. Webster. Solute uptake in aquatic sediments due to current-obstacle interactions. *Journal of Environmental Engineering*, 124(5):419–426, 1998. doi: 10.1061/(ASCE)0733-9372(1998)124:5(419).

M.J. Hvorslev. Time lag and soil permeability in ground-water observations. *Waterways Experiment Station*, 36, 1951.

HydroSOLVE Inc. Aqtesolv. *Online resources*, Demo Version, 2016.

D.J. Irvine, I. Cartwright, V.E.A. Post, C.T. Simmons, and E.W. Banks. Uncertainties in vertical groundwater fluxes from 1-d steady state heat transport analyses caused by heterogeneity, multidimensional flow, and climate change. *Water Resources Research*, 2016. doi: 10.1002/2015WR017702.

D.J. Irvine, M.A. Briggs, L.K. Lautz, R.P. Gordon, J.M. McKenzie, and I. Cartwright. Using diurnal temperature signals to infer vertical groundwater-surface water exchange. *Groundwater*, 55(1):10–26, 2017. doi: 10.1111/gwat.12459.

S.A. Isiorho and J.H. Meyer. The effects of bag type and meter size on seepage meter measurements. *Groundwater*, 37(3):411–413, 1999. doi: 10.1111/j.1745-6584.1999.tb01119.x.

O.W. Israelsen and R.C. Reeve. Canal lining experiments in the delta area, utah. *Utah Agriculture*, 1944.

K.M. Ivkovic. A top–down approach to characterise aquifer–river interaction processes. *Journal of Hydrology*, 365(3):145–155, 2009. doi: 10.1016/j.jhydrol.2008.11.021.

A.I. Johnson. Filter pack and well screen design. Technical report, US Geological Survey, Hydrologic Laboratory, 1963.

Jeremy B Jones and Patrick J Mulholland. *Streams and ground waters*. academic press, 2000.

A.G. Journel. Geostatistics for conditional simulation of ore bodies. *Economic Geology*, 69(5):673–687, 1974. doi: 10.2113/gsecongeo.69.5.6.

E. Kalbus, F. Reinstorf, and M. Schirmer. Measuring methods for groundwater? surface water interactions: a review. *Hydrology and Earth System Sciences Discussions*, 10(6):873–887, 2006. doi: hess-10-873-2006.

D.H. Käser, A. Binley, A.L. Heathwaite, and S. Krause. Spatio-temporal variations of hyporheic flow in a riffle-step-pool sequence. *Hydrological Processes*, 23(15):2138–2149, 2009. doi: 10.1002/hyp.7317.

P.M. Kearl. Observations of particle movement in a monitoring well using the colloidal borescope. *Journal of Hydrology*, 200(1-4):323–344, 1997. doi: 10.1016/S0022-1694(97)00026-7.

J. Keery, A. Binley, N. Crook, and J.W.N. Smith. Temporal and spatial variability of groundwater–surface water fluxes: development and application of an analytical method using temperature time series. *Journal of Hydrology*, 336(1):1–16, 2007. doi: 10.1016/j.jhydrol.2006.12.003.

A. Kempf, C.E. Divine, G. Leone, S. Holland, and J. Mikac. Field performance of point velocity probes at a tidally influenced site. *Remediation Journal*, 23(1):37–61, 2013. doi: 10.1002/rem.21337.

C.D. Kennedy, L.C. Murdoch, D.P. Genereux, D.R. Corbett, K. Stone, P. Pham, and H. Mitasova. Comparison of darcian flux calculations and seepage meter measurements in a sandy streambed in north carolina, united states. *Water Resources Research*, 46(9), 2010. doi: 10.1029/2009WR008342.

W.B. Kerfoot and V.A. Massard. Monitoring well screen influences on direct flowmeter measurements. *Groundwater Monitoring & Remediation*, 5(4):74–77, 1985. doi: 10.1111/j.1745-6592.1985.tb00942.x.

H. Kim and H.F. Hemond. Natural discharge of volatile organic compounds from contaminated aquifer to surface waters. *Journal of environmental engineering*, 124(8):744–751, 1998. doi: 10.1061/(ASCE)0733-9372(1998)124:8(744).

P. Kjeldsen, A. Grundtvig, P. Winther, and J.S. Andersen. Characterization of an old municipal landfill as a groundwater pollution source: landfill history and leachate composition. *Waste Management and Research*, 16(1):3–13, 1998. doi: 10.1177/0734242X9801600102.

S. Krause and T. Blume. Impact of seasonal variability and monitoring mode on the adequacy of fiber-optic distributed temperature sensing at aquifer-river interfaces. *Water Resources Research*, 49(5):2408–2423, 2013. doi: 10.1002/wrcr.20232.

S. Krause, A. Bronstert, and E. Zehe. Seasonal variability of groundwater—surface exchange and its implications for riparian groundwater nitrate retention at the havel river. *International Journal of River Basin Management*, 7(4):329–343, 2009. doi: 10.1080/15715124.2009.9635392.

S. Krause, D.M. Hannah, J.H. Fleckenstein, C.M. Heppell, D. Kaeser, R. Pickup, G. Pinay, A.L. Robertson, and P.J. Wood. Inter-disciplinary perspectives on processes in the hyporheic zone. *Ecohydrology*, 4(4):481–499, 2011. doi: 10.1002/eco.176.

S. Krause, T. Blume, and N.J. Cassidy. Investigating patterns and controls of groundwater upwelling in a lowland river by combining fibre-optic distributed temperature sensing with observations of vertical hydraulic gradients. *Hydrology and Earth System Sciences*, 16(6):1775–1792, 2012. doi: 10.5194/hess-16-1775-2012.

S. Krause, F. Boano, M.O. Cuthbert, J.H. Fleckenstein, and J. Lewandowski. Understanding process dynamics at aquifer-surface water interfaces: An introduction to the special section on new modeling approaches and novel experimental technologies. *Water Resources Research*, 50(2): 1847–1855, 2014. doi: 10.1002/2013WR014755.

D.G. Krige. A statistical approach to some basic miine valuation problems on the witwatersrand. *Journal of the Southern African Institute of Mining and Metallurgy*, 52(6):119–139, 1951.

W. Labaky, J.F. Devlin, and R.W. Gillham. Probe for measuring groundwater velocity at the centimeter scale. *Environmental Science & Technology*, 41(24):8453–8458, 2007. doi: 10.1021/es0716047.

W. Labaky, J.F. Devlin, and R.W. Gillham. Field comparison of the point velocity probe with other groundwater velocity measurement methods. *Water Resources Research*, 45(4), 2009. doi: 10.1029/2008WR007066.

J.A. LaBar and R.W. Nairn. Impact of naso4 dominated ionic strength on trace metal removal products in vertical flow bioreactors. *Applied Geochemistry*, 73:24–34, 2016.

J.A. LaBar and R.W. Nairn. Characterization of trace metal removal products in vertical flow bioreactor substrates at the mayer ranch passive treatment system in the tar creek superfund site. *Chemosphere*, 199:107–113, 2018. doi: 10.1016/j.chemosphere.2018.01.134.

J.W. LaBaugh, D.O. Rosenberry, and T.C. Winter. Groundwater contribution to the water and chemical budgets of williams lake, minnesota, 1980–1991. *Canadian Journal of Fisheries and Aquatic Sciences*, 52(4):754–767, 1995. doi: 10.1139/f95-075.

D.J. Lapworth, N. Baran, M.E. Stuart, and R.S. Ward. Emerging organic contaminants in groundwater: a review of sources, fate and occurrence. *Environmental pollution*, 163:287–303, 2012. doi: 10.1016/j.envpol.2011.12.034.

R.G. Larkin and J.M. Sharp. On the relationship between river-basin geomorphology, aquifer hydraulics, and ground-water flow direction in alluvial aquifers. *Geological Society of America Bulletin*, 104(12):1608–1620, 1992. doi: 10.1130/0016-7606(1992)104<1608:OTRBRB>2.3.CO;2.

D.M. LaSage, A.E. Fryar, A. Mukherjee, N.C. Sturchio, and L.J. Heraty. Groundwater-derived contaminant fluxes along a channelized coastal plain stream. *Journal of Hydrology*, 360(1): 265–280, 2008. doi: 10.1016/j.jhydrol.2008.07.026.

L.K. Lautz. Impacts of nonideal field conditions on vertical water velocity estimates from streambed temperature time series. *Water Resources Research*, 46(1), 2010. doi: 10.1029/2009WR007917.

D.R. Lee. A device for measuring seepage flux in lakes and estuaries. *Limnology and Oceanography*, 22(1):140–147, 1977. doi: 10.4319/lo.1977.22.1.0140.

D.R. Lee and J.A. Cherry. A field exercise on groundwater flow using seepage meters and mini-piezometers. *Journal of Geological Education*, 27(1):6–10, 1979. doi: 10.5408/0022-1368-27.1.6.

J. Lewandowski, L. Angermann, G. Nützmann, and J.H. Fleckenstein. A heat pulse technique for the determination of small-scale flow directions and flow velocities in the streambed of sand-bed streams. *Hydrological Processes*, 25(20):3244–3255, 2011. doi: 10.1002/hyp.8062.

M.J. Lønborg, P. Engesgaard, P.L. Bjerg, and D. Rosbjerg. A steady state redox zone approach for modeling the transport and degradation of xenobiotic organic compounds from a landfill site. *Journal of Contaminant Hydrology*, 87(3):191–210, 2006. doi: 10.1016/j.jconhyd.2006.05.004.

M.M. Lorah and L.D. Olsen. Degradation of 1, 1, 2, 2-tetrachloroethane in a freshwater tidal wetland: field and laboratory evidence. *Environmental Science & Technology*, 33(2):227–234, 1999a. doi: 10.1021/es980503t.

M.M. Lorah and L.D. Olsen. Natural attenuation of chlorinated volatile organic compounds in a freshwater tidal wetland: Field evidence of anaerobic biodegradation. *Water Resources Research*, 35(12):3811–3827, 1999b. doi: 10.1029/1999WR900116.

C. Lu, S. Chen, Y. Zhang, X. Su, and G. Chen. Heat tracing to determine spatial patterns of hyporheic exchange across a river transect. *Hydrogeology Journal*, pages 1–14, 2017. doi: 10.1007/s10040-017-1553-9.

D.M. Mackay, D.L. Freyberg, P.V. Roberts, and J.A. Cherry. A natural gradient experiment on solute transport in a sand aquifer: 1. approach and overview of plume movement. *Water Resources Research*, 22(13):2017–2029, 1986. doi: 10.1029/WR022i013p02017.

K. Mahmud, G. Mariethoz, J. Caers, P. Tahmasebi, and A. Baker. Simulation of earth textures by conditional image quilting. *Water Resources Research*, 50(4):3088–3107, 2014.

G. Matheron. The theory of regionalized variables and their applications: Ecole des mines. *Fontainbleau, France*, 1971.

G. Matheron. The intrinsic random functions and their applications. *Advances in Applied Probability*, 5(3):439–468, 1973.

K. Matheswaran, M. Blemmer, D. Rosbjerg, and E. Boegh. Seasonal variations in groundwater upwelling zones in a danish lowland stream analyzed using distributed temperature sensing (dts). *Hydrological Processes*, 28(3):1422–1435, 2014. doi: 10.1002/hyp.9690.

J.L. McCallum, P.G. Cook, D. Berhane, C. Rumpf, and G.A. McMahon. Quantifying groundwater flows to streams using differential flow gaugings and water chemistry. *Journal of Hydrology*, 416:118–132, 2012. doi: 10.1016/j.jhydrol.2011.11.040.

M.E. McClain, E.W. Boyer, C.L. Dent, S.E. Gergel, N.B. Grimm, P.M. Groffman, S.C. Hart, J.W. Harvey, C.A. Johnston, E. Mayorga, W.H. McDowell, and G. Pinay. Biogeochemical hot spots and hot moments at the interface of terrestrial and aquatic ecosystems. *Ecosystems*, 6(4):301–312, 2003. doi: 10.1007/s10021-003-0161-9.

U.S. McKnight, S.G. Funder, J.J. Rasmussen, M. Finkel, P.J. Binning, and P.L. Bjerg. An integrated model for assessing the risk of tce groundwater contamination to human receptors and surface water ecosystems. *Ecological Engineering*, 36(9):1126–1137, 2010. doi: 10.1016/j.ecoleng.2010.01.004.

U.S. McKnight, J.J. Rasmussen, B. Kronvang, P.L. Bjerg, and P.J. Binning. Integrated assessment of the impact of chemical stressors on surface water ecosystems. *Science of the Total Environment*, 427:319–331, 2012. doi: 10.1016/j.scitotenv.2012.04.011.

R.S. McLeod. Evaluation of superfund sites for control of leachate and contaminant migration. In *Proceedings*, pages 114–121, 1984.

F.J. Molz, R.H. Morin, A.E. Hess, J.G. Melville, and O. Güven. The impeller meter for measuring aquifer permeability variations: evaluation and comparison with other tests. *Water Resources Research*, 25(7):1677–1683, 1989. doi: 10.1029/WR025i007p01677.

W.S. Moore. The subterranean estuary: a reaction zone of ground water and sea water. *Marine Chemistry*, 65(1):111–125, 1999. doi: 10.1016/S0304-4203(99)00014-6.

M. Munz, S.E. Oswald, and C. Schmidt. Analysis of riverbed temperatures to determine the geometry of subsurface water flow around in-stream geomorphological structures. *Journal of Hydrology*, 539:74–87, 2016. doi: 10.1016/j.jhydrol.2016.05.012.

L.C. Murdoch and S.E. Kelly. Factors affecting the performance of conventional seepage meters. *Water Resources Research*, 39(6), 2003. doi: 10.1029/2002WR001347.

R.W. Nairn, T. Beisel, R.C. Thomas, J.A. LaBar, K.A. Strevett, D. Fuller, W.H. Strosnider, W.J. Andrews, J. Bays, and R.C. Knox. Challenges in design and construction of a large multi-cell passive treatment system for ferruginous lead-zinc mine waters. In *Proceedings of the 26th National Meeting of the American Society of Mining and Reclamation. Billings, MT, May*, pages 871–892, 2009.

R.W. Nairn, J.A. LaBar, K.A. Strevett, W.H. Strosnider, D. Morris, A.E. Garrido, C.A. Neely, and K. Kauk. Initial evaluation of a large multi-cell passive treatment system for net-alkaline ferruginous lead-zinc mine waters. *Proceedings America Society of Mining and Reclamation*, pages 635–649, 2010.

R.W. Nairn, J.A. LaBar, and K.A. Strevett. Passive treatment opportunities in a drastically disturbed watershed: Reversing the irreversible. In *28th National Conference of the American Society of Mining and Reclamation, Bismarck, ND, USA*, pages 450–468, 2011.

ES Nicolajsen. *Local scale modelling of temporal and spatial variations in groundwater -surface water interaction at Grindsted, Denmark*. PhD thesis, Master's thesis, Technical University of Denmark, Kongens Lyngby, Denmark, 2014.

S.S. Nielsen, N. Tuxen, O.F. Pedersen, P.L. Bjerg, A.Th. Sonne, P.J. Binning, A.S. Fjordbøge, and J. Aabling. Risikovurdering af overfladevand, som er påvirket af punktkildeforurenet grundvand. 2014.

D.P. Oliveira and N. Sitar. Ground water contamination from underground solvent storage tanks santa clara. In *California Proceedings of the Fifth National Symposium on Aquifer Restoration and Groundwater Monitoring Natl. Water Well Assoc. Columbus, Ohio May*, pages 21–24, 1985.

B.J. Page. *Quantifying Hydraulic Conductivity in Mine Drainage Passive Treatment System Vertical Flow Bioreactors*. PhD thesis, Master's thesis, University of Oklahoma, 2016.

M.F. Petersen. *Quantification and risk assessment of continuous micropollutant mass discharges from multiple sources to a gaining stream at the catchment scale*. PhD thesis, Master's thesis, Technical University of Denmark, Kongens Lyngby, Denmark, 2012.

V.E.A. Post and J.R. von Asmuth. Review: Hydraulic head measurements—new technologies, classic pitfalls. *Hydrogeology Journal*, 21(4):737–750, 2013. doi: 10.1007/s10040-013-0969-0.

J.J. Rasmussen, U.S. McKnight, A.Th. Sonne, P. Wiberg-Larsen, and P.L. Bjerg. Legacy of a chemical factory site: Contaminated groundwater impacts stream macroinvertebrates. *Archives of Environmental Contamination and Toxicology*, 70(2):219–230, 2016. doi: 10.1007/s00244-015-0211-2.

C.M. Richards and C. Pallud. Kinetics of sulfate reduction and sulfide precipitation rates in sediments of a bar-built estuary (pescadero, california). *Water research*, 94:86–102, 2016. doi: 10.1016/j.watres.2016.01.044.

S.D. Richardson and T.A. Ternes. Water analysis: emerging contaminants and current issues. *Analytical chemistry*, 83(12):4614–4648, 2018. doi: 10.1021/acs.analchem.7b04577.

M.O. Rivett, R.J. Turner, P. Glibbery, and M.O. Cuthbert. The legacy of chlorinated solvents in the birmingham aquifer, uk: Observations spanning three decades and the challenge of future urban groundwater development. *Journal of Contaminant Hydrology*, 140:107–123, 2012. doi: 10.1016/j.jconhyd.2012.08.006.

W.D. Robertson and J.A. Cherry. Tritium as an indicator of recharge and dispersion in a groundwater system in central ontario. *Water Resources Research*, 25(6):1097–1109, 1989. doi: 10.1029/WR025i006p01097.

M. Robinson, D. Gallagher, and W. Reay. Field observations of tidal and seasonal variations in ground water discharge to tidal estuarine surface water. *Groundwater Monitoring & Remediation*, 18(1):83–92, 1998. doi: 10.1111/j.1745-6592.1998.tb00605.x.

V.K. Rønde, U.S. McKnight, A.Th. Sonne, J.F. Devin, and P.L. Bjerg. Contaminant mass discharge to streams: comparing direct groundwater velocity measurements and multi-level groundwater sampling with an in-stream approach. *Journal of Contaminant Hydrology*, 2017. doi: 10.1016/j.jconhyd.2017.09.010.

M.I. Rorabaugh. Estimating changes in bank storage and ground-water contribution to streamflow. *International Association of Scientific Hydrology*, 63(1):432–441, 1964.

L. Rose, S. Krause, and N.J. Cassidy. Capabilities and limitations of tracing spatial temperature patterns by fiber-optic distributed temperature sensing. *Water Resources Research*, 49(3):1741–1745, 2013. doi: 10.1002/wrcr.20144.

D.O. Rosenberry. Integrating seepage heterogeneity with the use of ganged seepage meters. *Limnology and Oceanography: Methods*, 3(2005):131–142, 2005. doi: 10.4319/lom.2005.3.131.

D.O. Rosenberry. A seepage meter designed for use in flowing water. *Journal of Hydrology*, 359 (1):118–130, 2008. doi: 10.1016/j.jhydrol.2008.06.029.

D.O. Rosenberry and J.W. LaBaugh. Field techniques for estimating water fluxes between surface water and ground water. *Techniques and Methods*, 4-D2, 2008.

D.O. Rosenberry and R.H. Morin. Use of an electromagnetic seepage meter to investigate temporal variability in lake seepage. *Ground water*, 42(1):68–77, 2004. doi: 10.1111/j.1745-6584.2004.tb02451.x.

D.O. Rosenberry and J. Pitlick. Effects of sediment transport and seepage direction on hydraulic properties at the sediment–water interface of hyporheic settings. *Journal of Hydrology*, 373(3): 377–391, 2009. doi: 10.1016/j.jhydrol.2009.04.030.

D.O. Rosenberry, J.W. LaBaugh, and R.J. Hunt. Use of monitoring wells, portable piezometers, and seepage meters to quantify flow between surface water and ground water. *Field Techniques for estimating water fluxes between surface water and ground water*, 4-D2:43–67, 2008.

D.O. Rosenberry, R.W. Sheibley, S.E. Cox, F.W. Simonds, and D.L. Naftz. Temporal variability of exchange between groundwater and surface water based on high-frequency direct measurements of seepage at the sediment-water interface. *Water Resources Research*, 49(5):2975–2986, 2013. doi: 10.1002/wrcr.20198.

E.R. Rothschild, R.J. Manser, and M.P. Anderson. Investigation of aldicarb in ground water in selected areas of the central sand plain of wisconsin. *Groundwater*, 20(4):437–445, 1982. doi: 10.1111/j.1745-6584.1982.tb02764.x.

K. Rügge, P.L. Bjerg, J.K. Pedersen, H. Mosbæk, and T.H. Christensen. An anaerobic field injection experiment in a landfill leachate plume, grindsted, denmark: 1. experimental setup, tracer movement, and fate of aromatic and chlorinated compounds. *Water Resources Research*, 35(4): 1231–1246, 1999. doi: 10.1029/1998WR900101.

P.C. Schillig. Velprobepe: An automated spreadsheet program for interpreting point velocity probe breakthrough curves. *Computers and Geosciences*, 39:161–170, 2012. doi: 10.1016/j.cageo.2011.06.007.

P.C. Schillig, J.F. Devlin, J.A. Roberts, G.P. Tsoflias, and M.A. McGlashan. Transient heterogeneity in an aquifer undergoing bioremediation of hydrocarbons. *Groundwater*, 49(2):184–196, 2011. doi: 10.1111/j.1745-6584.2010.00682.x.

P.C. Schillig, J.F. Devlin, C.D. McElwee, K. Walter, and B. Gibson. Assessment of density-induced tracer movement in groundwater velocity measurements with point velocity probes (pvps). *Groundwater Monitoring & Remediation*, 34(4):44–50, 2014. doi: 10.1111/gwmr.12075.

P.C. Schillig, J.F. Devlin, and D. Rudolph. Upscaling point velocity measurements to characterize a glacial outwash aquifer. *Groundwater*, 54(3):394–405, 2016. doi: 10.1111/gwat.12357.

C. Schmidt, M. Bayer-Raich, and M. Schirmer. Characterization of spatial heterogeneity of groundwater-stream water interactions using multiple depth streambed temperature measurements at the reach scale. *Hydrology and Earth System Sciences Discussions*, 3(4):1419–1446, 2006. doi: 10.5194/hess-10-849-2006.

C. Schmidt, B. Conant, M. Bayer-Raich, and M. Schirmer. Evaluation and field-scale application of an analytical method to quantify groundwater discharge using mapped streambed temperatures. *Journal of Hydrology*, 347(3):292–307, 2007. doi: 10.1016/j.jhydrol.2007.08.022.

H. Schulz. *Application of the streambed point velocity probe for investigating contaminant mass discharge to streams*. PhD thesis, Master's thesis, Technical University of Denmark, Kongens Lyngby, Denmark, 2017.

F.W. Schwartz and D.N. Gallup. Some factors controlling the major ion chemistry of small lakes: Examples from the prairie parkland of canada. *Hydrobiologia*, 58(1):65–81, 1978. doi: 10.1007/BF00018896.

J.S. Selker, L. Thévenaz, H. Huwald, A. Mallet, W. Luxemburg, N. van de Giesen, M. Stejskal, J. Zeman, M. Westhoff, and M.B. Parlange. Distributed fiber-optic temperature sensing for hydrologic systems. *Water Resources Research*, 42(12), 2006a. doi: 10.1029/2006WR005326.

J.S. Selker, N. van de Giesen, M. Westhoff, W. Luxemburg, and M.B. Parlange. Fiber optics opens window on stream dynamics. *Geophysical Research Letters*, 33(24), 2006b. doi: 10.1029/2006GL027979.

R.D. Shaw and E.E. Prepas. Groundwater-lake interactions: Ii. nearshore seepage patterns and the contribution of ground water to lakes in central alberta. *Journal of Hydrology*, 119(1-4): 121–136, 1990.

I.A. Shiklomanov. World fresh water resources. In P.H. Gleick, editor, *Water in Crisis: A Guide to the World's Fresh Water Resources*, chapter 2. Oxford University Press, 1993.

E.A. Shinn, C.D. Reich, and T.D. Hickey. Seepage meters and bernoulli's revenge. *Estuaries and Coasts*, 25(1):126–132, 2002. doi: 10.1007/BF02696056.

W.W. Simpkins. A multiscale investigation of ground water flow at clear lake, iowa. *Groundwater*, 44(1):35–46, 2006. doi: 10.1111/j.1745-6584.2005.00084.x.

C.S. Slichter. The motions of underground waters. Technical Report USGS Report 67, 1902.

C.S. Slichter. Field measurements of the rate of movement of underground waters. Technical Report Water Supply Paper 140, Government Printing Office, 1905.

J.E. Solder, T.E. Gilmore, D.P. Genereux, and D.K. Solomon. A tube seepage meter for in situ measurement of seepage rate and groundwater sampling. *Groundwater*, 54(4):588–595, 2016. doi: 10.1111/gwat.12388.

A.Th. Sonne, U.S. McKnight, V.K. Rønde, and P.L. Bjerg. Assessing the chemical contamination dynamics in a mixed land use stream system. *Water Research*, 125:141–151, 2017. doi: 10.1016/j.watres.2017.08.031.

M. Sophocleous. Interactions between groundwater and surface water: the state of the science. *Hydrogeology journal*, 10(1):52–67, 2002. doi: 10.1007/s10040-001-0170-8.

R.W. Stallman. Steady one-dimensional fluid flow in a semi-infinite porous medium with sinusoidal surface temperature. *Journal of Geophysical Research*, 70(12):2821–2827, 1965. doi: 10.1029/JZ070i012p02821.

G.W. Su, B.M. Freifeld, C.M. Oldenburg, P.D. Jordan, and P.F. Daley. Interpreting velocities from heat-based flow sensors by numerical simulation. *Groundwater*, 44(3):386–393, 2006. doi: 10.1111/j.1745-6584.2005.00147.x.

C.V. Theis. The effect of a well on the flow of a nearby stream. *Eos, Transactions American Geophysical Union*, 22(3):734–738, 1941.

A. Thiem. Verfahren für natürliche grundwassergeschwindigkeiten [methods to evaluate natural groundwater velocities]. *Polyt Notizblatt*, 42:229, 1887.

G. Tomassoni. A federal statutory/regulatory/policy perspective on remedial decision-making with respect to ground-water/surface-water interaction. In *Surface-Water Interactions Workshop*, page 13, 2000.

D.L. Turcotte and G. Schubert. *Geodynamics: Applications of continuum mechanics to geological problems*. Wiley, New York, 1982.

S.W. Tyler, J.S. Selker, M.B. Hausner, C.E. Hatch, T. Torgersen, C.E. Thodal, and S.G. Schladow. Environmental temperature sensing using raman spectra dts fiber-optic methods. *Water Resources Research*, 45(4), 2009. doi: 10.1029/2008WR007052.

N. van de Giesen, S.C. Steele-Dunne, J. Jansen, O. Hoes, M.B. Hausner, S. Tyler, and J.S. Selker. Double-ended calibration of fiber-optic raman spectra distributed temperature sensing data. *Sensors*, 12(5):5471–5485, 2012. doi: 10.3390/s120505471.

G. van der Kamp, L.D. Luba, J.A. Cherry, and H. Maathuis. Field study of a long and very narrow contaminant plume. *Groundwater*, 32(6):1008–1016, 1994. doi: 10.1111/j.1745-6584.1994.tb00940.x.

A. Verruijt. A local groundwater divide in a regional system. *Engineering Geology*, 91(1):78–83, 2007. doi: 10.1016/j.enggeo.2006.12.015.

T. Vogt, P. Schneider, L. Hahn-Woernle, and O.A. Cirpka. Estimation of seepage rates in a losing stream by means of fiber-optic high-resolution vertical temperature profiling. *Journal of Hydrology*, 380(1):154–164, 2010. doi: 10.1016/j.jhydrol.2009.10.033.

K. Walter and J.F. Devlin. Application of 3d printing to the manufacturing of groundwater velocity probes. *Groundwater Monitoring & Remediation*, 37(2):71–77, 2017. doi: 10.1111/gwmr.12210.

C.C. Warnick. *Methods of measuring seepage loss in irrigation canals*. Engineering Experiment Station, University of Idaho, 1951.

G.R. Watzlaf, K.T. Schroeder, R.L.P. Kleinmann, C.L. Kairies, and R.W. Nairn. The passive treatment of coal mine drainage. *United States Department of Energy National Energy Technology Laboratory Internal Publication*, 2004.

J. Weatherill, S. Krause, K. Voyce, F. Drijfhout, A. Levy, and N. Cassidy. Nested monitoring approaches to delineate groundwater trichloroethene discharge to a uk lowland stream at multiple spatial scales. *Journal of Contaminant Hydrology*, 158:38–54, 2014. doi: 10.1016/j.jconhyd.2013.12.001.

M.C. Westhoff, M.N. Gooseff, T.A. Bogaard, and H.H.G. Savenije. Quantifying hyporheic exchange at high spatial resolution using natural temperature variations along a first-order stream. *Water Resources Research*, 47(10), 2011. doi: 10.1029/2010WR009767.

T.H. Wiedemeier. *Natural attenuation of fuels and chlorinated solvents in the subsurface*. John Wiley & Sons, 1999. ISBN 9780471197492.

T.C. Winter, J.W. LaBaugh, and D.O. Rosenberry. The design and use of a hydraulic potentiomanometer for direct measurement of differences in hydraulic head between groundwater and surface water. *Limnology and Oceanography*, 33(5):1209–1214, 1988.

T.C. Winter, J.W. Harvey, O.L. Franke, and W.M. Alley. *Ground Water and Surface Water: A Single Resource*. Number Circular 1139. United States Geological Survey, 1998.

T.C. Winter, D.O. Rosenberry, and J.W. LaBaugh. Where does the ground water in small watersheds come from? *Groundwater*, 41(7):989–1000, 2003. doi: 10.1111/j.1745-6584.2003.tb02440.x.

S.L. Winters and D.R. Lee. In situ retardation of trace organics in groundwater discharge to a sandy stream bed. *Environmental Science & Technology*, 21(12):1182–1186, 1987.

W.W. Woessner. Stream and fluvial plain ground water interactions: Rescaling hydrogeologic thought. *Groundwater*, 38(3):423–429, 2000.

W.W. Woessner and K.E. Sullivan. Results of seepage meter and mini-piezometer study, lake mead, nevada. *Groundwater*, 22(5):561–568, 1984.

K. Yamamoto, M. Fukushima, N. Kakutani, and K. Tsuruho. Contamination of vinyl chloride in shallow urban rivers in osaka, japan. *Water Research*, 35(2):561–566, 2001. doi: 10.1016/S0043-1354(00)00278-5.

C. Zamora. Estimating rates of exchange across the sediment/water interface in the lower merced river, ca. *Unpublished MS thesis. California State University, Sacramento*, 2006.

G.W. Zellweger. Testing and comparison of four ionic tracers to measure stream flow loss by multiple tracer injection. *Hydrological Processes*, 8(2):155–165, 1994. doi: 10.1002/hyp.3360080206.

G.M. Zemansky and C.D. McElwee. High-resolution slug testing. *Groundwater*, 43(2):222–230, 2005. doi: 10.1111/j.1745-6584.2005.0008.x.